



PRECISION MEDICINE IN METASTATIC PROSTATE CANCER

THE CHALLENGES AND CLINICAL IMPACT

MINKE SMITS

PRECISION MEDICINE IN METASTATIC PROSTATE CANCER

THE CHALLENGES AND CLINICAL IMPACT

Minke Smits

Provided by thesis specialist Ridderprint, [ridderprint.nl](https://www.ridderprint.nl)

ISBN:	978-94-6483-572-4
Layout and design:	Marilou Maes, persoonlijkproefschrift.nl
Printing:	Ridderprint

© Copyright 2024. Minke Smits

All rights reserved. No part of this thesis may be reproduced, stored or transmitted in any way or by means without the written permission of the author or by the publishers of the publication.

PRECISION MEDICINE IN METASTATIC PROSTATE CANCER

The challenges and clinical impact

Proefschrift ter verkrijging van de graad van doctor
aan de Radboud Universiteit Nijmegen
op gezag van de rector magnificus prof. dr. J.M. Sanders,
volgens besluit van het college voor promoties
in het openbaar te verdedigen op

woensdag 10 januari 2024
om 10.30 uur precies

door

Minke Smits
geboren op 10 mei 1988
te Arnhem

Promotoren:

Prof. dr. J.A. Schalken

Prof. dr. W.R. Gerritsen

Dr. N. Mehra

Copromotor:

Dr. J.P.M. Sedelaar

Manuscriptcommissie:

Prof. dr. P.H. van Erp

Prof. dr. S. Heskamp

Prof. dr. H. van der Poel (Antoni van Leeuwenhoek)

TABLE OF CONTENTS

Chapter 1	General introduction & Outline of this thesis	9
PART I	THE TECHNICAL CHALLENGES OF MOLECULAR ANALYSES IN METASTATIC PROSTATE CANCER	
Chapter 2	⁶⁸ Ga-PSMA-guided bone biopsies for molecular diagnostics in patients with metastatic prostate cancer <i>Journal of Nuclear Medicine. 2020;61(11):1607-14</i>	29
Chapter 3	Prior PSMA-PET/CT imaging and Hounsfield unit impact on tumor yield and success of molecular analyses from bone biopsies in metastatic prostate cancer <i>Cancers (Basel). 2020;12(12)</i>	49
PART II	IMPROVING THE SUCCESS RATE OF MOLECULAR ANALYSES IN BONE METASTATIC PROSTATE CANCER	
Chapter 4	⁶⁸ Ga-PSMA-PET/CT and diffusion MRI targeting for cone-beam CT-guided bone biopsies of castration-resistant prostate cancer patients <i>Cardiovascular and Interventional Radiology. 2020;43(1):147-54</i>	71
PART III	THE POTENTIAL CLINICAL IMPACT OF MOLECULAR ANALYSES IN METASTATIC PROSTATE CANCER	
Chapter 5	The genomic landscape of metastatic castration-resistant prostate cancers reveals multiple distinct genotypes with potential clinical impact <i>Nature Communications. 2019;10(1):5251</i>	85
Chapter 6	Responsiveness to immune checkpoint inhibitors is associated with a peripheral blood T-cell signature in metastatic castration-resistant prostate cancer <i>JCO Precision Oncology. 2020;4:1374-85</i>	117
PART IV	EPILOGUE	
Chapter 7	Summary	139
Chapter 8	Discussion & Future perspectives	145
PART V	APPENDICES	
	List of abbreviations	172
	List of publications	173
	Research data management	174
	PhD portfolio	175
	Curriculum vitae	176
	Nederlandse samenvatting	177
	Dankwoord	182

ACKNOWLEDGEMENTS

The research presented in this thesis was performed at the Department of Urology/ Radboud Institute for Molecular Innovation and the Department of Medical Oncology, Radboudumc, Nijmegen, the Netherlands. The studies described in this thesis were supported by MDxHealth, Center for Personalized Cancer Treatment (CPCT) and the Hartwig Medical Foundation (HMF).



CHAPTER 1

GENERAL INTRODUCTION & OUTLINE OF THIS THESIS

GENERAL INTRODUCTION

(Adapted from 'Future therapeutic strategies for metastatic prostate cancer' by Smits et al and 'Molecular biomarkers to guide precision medicine in localized prostate cancer' by Smits et al)

Treatment of metastatic prostate cancer in a historic perspective

On April 12 1853 an article was published in The Lancet about the first case of 'scirrhus of the prostate gland' by Dr John Adams, surgeon in the London Hospital (1). It was, at that time, described as a very rare disease. Nowadays, according to the GLOBOCAN 2020, prostate cancer is the fourth most commonly diagnosed cancer and is responsible for 6.8% of all cancer related deaths in men (2). Although the first case in the Western world was reported in 1853, it was not until 1941 before Dr Charles Huggins discovered that prostate cancer responded to androgen ablation therapy. This led to the introduction of oral estrogens and orchidectomy, which was the beginning of systemic treatment for metastatic prostate cancer (3).

Despite the fact that inhibition of androgen receptor signaling by the use of anti-androgens or an orchidectomy led to a prolonged duration of disease control, progressive disease was eventually inevitable. Huggins and Scott hypothesized that this progression of prostate cancer was caused by resistance driven by the production of extragonadal androgens. They performed in 1945 a bilateral adrenalectomy in four patients following positive results seen in animal studies (4). In these patients urinary 17-ketosteroids were increased prior to orchidectomy, decreased following this surgery and slowly increased again up to their bilateral adrenalectomy. Although two patients died one day after the bilateral adrenalectomy of post-operative complications, in the other two patients urinary 17-ketosteroids decreased and in one patient alkaline phosphatase decreased considerably. This small study led to the idea of extragonadal androgen production and androgen-independent prostate cancer and encouraged investigators to search for the alternative of the risky bilateral adrenalectomy.

It was Dr Andrew Schally who discovered the structure of luteinizing releasing hormone (LHRH) in the 1970s (5), which normally activates the pituitary to produce luteinizing hormone (LH). LH binds to the receptor on the adrenal glands, activating the production of testosterone. By creating a synthesized peptide of LHRH (6) he was able to block the negative feedback loop of LHRH, causing a downregulation of LHRH receptors, which led to the inhibition of LH release by the pituitary and eventually causing a decrease of production of testosterone by the adrenal glands (7). Testosterone is converted to dihydrotestosterone, which both can bind to the androgen receptor (AR) on the prostate

cancer cell, promoting cancer cell proliferation. Dr Ferdinand Labrie proposed in the 1980s the idea of combining the two mechanisms of treatment to overcome the initial flare of LHRH agonists and saw a clinical response in patients with advanced prostate cancer (8, 9). Although the combination of dual blockage did show some prolongation until progression, disease progression always occurred. The distinction between hormone sensitive and castration resistant prostate cancer was now made and new treatment modalities were investigated for metastatic castration resistant prostate cancer (mCRPC) in the early 2000s.

The first cytotoxic treatment registered for mCRPC was mitoxantrone. It was investigated in a phase 3 trial by Berry et al compared to prednisolone (10). Its introduction led to a prolonged time to progression of four months, however no significant differences were seen in median survival. In 2004 docetaxel was compared to mitoxantrone in two larger phase 3 trials (11, 12) and besides a significant biochemical response and prolongation of median survival, a significantly better quality of life and reduction of pain was seen in the group that received docetaxel. Another taxane-based chemotherapy was introduced in 2010. A randomized controlled phase 3 trial comparing cabazitaxel versus mitoxantrone in patients progressing after docetaxel was conducted by the Bono et al (13). Cabazitaxel was registered based on a prolonged median overall survival (OS) of 15.1 months versus 12.7 months in the mitoxantrone group.

The development from hormone-sensitive to castration resistance during androgen deprivation therapy (ADT) is explained by several mechanisms involving androgen biosynthesis/steroidogenesis (14, 15) and overexpression of or mutations in the AR gene (16, 17). These mechanisms have led to the development of new second generation androgen receptor signaling inhibitors (ARSI), abiraterone acetate (18) and enzalutamide (19), in respectively 2011 and 2012. Abiraterone blocks the CYP450 CYP17A1 enzyme, which has an important role in the testosterone synthesis, consequently leading to a decrease in the androgen synthesis intratumorally, in the testes and in the adrenal glands (20). Abiraterone with prednisolone was investigated in a randomized placebo-controlled phase 3 trial in patients with progression of mCRPC after treatment with docetaxel. Treatment with abiraterone and prednisolone significantly improved median OS and progressive-free survival (PFS). Enzalutamide has a high affinity for binding to AR and interferes with the AR signaling pathway, suppressing tumor growth even in the castration resistant prostate cancer cells (21). After promising results in a phase 1 / 2 trial (22) enzalutamide was investigated in the AFFIRM trial, a randomized placebo-controlled phase 3 trial for patients with progression after docetaxel, and showed a similar reduction in the risk of death as abiraterone (19). Enzalutamide also improved median OS and PFS and was therefore next to abiraterone registered as second line treatment for mCRPC.

With the registration of three new treatment options in mere two years, all as second line options following docetaxel, the optimal agent or sequence of these novel drugs remained unclear. Although abiraterone showed some advantage over enzalutamide with regard to time until biochemical progression, a phase 2 crossover trial presented also evidence for cross-resistance between both anti-androgens (23). The phase 3 CARD trial strengthened this hypothesis by showing an advantage of cabazitaxel over an anti-androgen after progression on both docetaxel and an anti-androgen with regard to PFS and OS in patients with a duration of response to anti-androgens of less than a year (24).

Since both chemotherapy and the new second generation ARSIs have led to great improvement of OS in mCRPC patients, trials were designed to investigate whether the introduction of these treatments in an earlier stage, in metastatic hormone sensitive prostate cancer (mHSPC), could lead to an even greater overall survival benefit. Although the first phase 3 trial (GETUG-15) investigating the role of docetaxel in mHSPC failed to present an improvement of OS compared to ADT alone (25), two other landmark trials, the CHAARTED trial (26) and the first analysis of the multigroup multistage STAMPEDE trial (27) were able to show an improved OS when docetaxel was added to ADT, which was for both trials confirmed in long-term follow up analyses (28, 29). Since docetaxel is not suitable for every mHSPC patient due to for example performance status, comorbidity and patient preferences, trials were designed to investigate the recently registered second generation anti-androgens in mHSPC patients. The role of abiraterone in mHSPC was first analyzed in the STAMPEDE trial by randomly assigning locally advanced non-metastatic and mHSPC patients to abiraterone plus ADT versus ADT alone (30). Significant improvement of median OS was seen for the addition of abiraterone to ADT with in the updated long-term analysis a median OS of 79 months versus 46 months in patients with ADT alone (31). The phase 3 LATITUDE trial presented their data on the intensification of abiraterone in mHSPC patients at the same time and showed similar results with respect to the improvement of OS (32). The overall survival in mHSPC patients with enzalutamide was investigated in the ENZAMET trial, but in contrast to the previous trials in mHSPC enzalutamide was compared to ADT plus a standard nonsteroidal anti-androgen drug and addition of docetaxel was allowed (33). Median OS was especially improved with enzalutamide in patients with low volume disease (according to CHAARTED criteria) in the updated OS outcomes (34). The meaningful addition of enzalutamide in mHSPC patients was also found by the ARCHES trial (35), however their primary endpoint was radiographic progression free survival (rPFS). The role of the new second generation anti-androgen, apalutamide, was analyzed in the phase 3 TITAN trial (36). When compared to ADT alone, apalutamide improved both rPFS as well as OS (although median survival in both groups not yet reached), independent of high volume or low volume disease and previous docetaxel use.

Since the above four new treatment options displayed their advantage when added to ADT alone in the mHSPC setting, the question arose whether patients with mHSPC would benefit more from chemotherapy or anti-androgens. Therefore the STAMPEDE trial compared abiraterone and docetaxel, both in addition to ADT in mHSPC patients, with death from any cause as primary outcome measure (37). Although not formally pre-powered the study did not show any evidence of difference in OS with both treatments. A recent quality of life study in these patients however reported clinically meaningful higher quality of life scores in patients treated with abiraterone, especially in the first year of treatment (38). Recently several clinical trials provided evidence for triplet combination therapy in mHSPC. The ENZAMET trial (34) was not initially designed to compare ADT plus docetaxel and an anti-androgen and therefore not powered to make this analysis, but the addition of an anti-androgen tend to show improvement in radiographic progression of disease and OS when compared to ADT plus docetaxel alone. The PEACE-1 trial is a multi-arm phase 3 trial for mHSPC patients and compares standard of care (ADT alone and later on after an amendment based on the results of the CHAARTED trial docetaxel plus ADT) with docetaxel plus ADT plus abiraterone (39). In the cohort of patients with docetaxel plus ADT (n=710) the addition of abiraterone led to a significant improvement of OS compared to docetaxel plus ADT (not yet reached vs 4.4 years). This improvement of OS is however only seen in high volume mHSPC, in low volume disease median OS is for both groups not yet reached and updated analyses will show whether triplet therapy improves outcome in low volume mHSPC (39). The international ARASENS trial investigated the addition of darolutamide to ADT plus docetaxel in mHSPC patients and showed at 4 years an OS of 62.7% versus 50.4% for treatment with or without darolutamide respectively (40). Results of correlation of response with volume of disease at baseline were not presented.

In conclusion, during the last decade several new treatment options have been developed for metastatic prostate cancer, for both hormone sensitive and castration resistant disease, which had led to a great impact on the overall survival of men with metastatic prostate cancer. However, the optimal sequence of these agents remains unclear, and many studies investigating combinatory strategies are underway, as well as the development of new precision medicine strategies based on recurrent molecular aberrations.

Molecular analyses/targets in metastatic prostate cancer

During the last decade several next generation sequencing (NGS) studies (41-45) have given us a comprehensive insight regarding the genomic landscape of metastatic prostate cancer. Results show both commonalities as heterogeneity between patients, regarding genetic alterations in key signaling pathways such as AR signaling, PI3K-Akt-

mTOR and DNA repair. In this thesis, results from a whole genome sequencing (WGS) study from a Dutch patient cohort, comprising 197 mCRPC patients from the CPCT-02 study (NCT01855477), are presented and support the use of NGS in metastatic prostate cancer patients. In the era of precision medicine, this molecular profiling is becoming paramount for the identification of patients that may benefit from specific targeted therapies, but it could also guide us in selecting a choice of routine treatment strategies, such as chemotherapy regimen or hormonal agent.

AR alterations

AR alterations, such as AR mutation, amplification, and genomic structural rearrangements, are the second most frequent aberration (aside from ERG fusion) in mCRPC, which is associated with ADT resistance (41). In addition, diverse AR variant species have been described, with certain variant species lacking the ligand-binding domain and making them constitutively active; these AR splice variants (AR-Vs) drive prostate cancer growth in a ligand-independent way (46). One such AR-V is AR-V7 that contains exon 2 and 3 encoding but lacks the ligand-binding domain and is the most commonly expressed splice variant in mCRPC. In the presence of AR gain or AR-V7, which appear to be associated with resistance to second generation anti-androgens (47, 48), taxane-based chemotherapy might be preferred (48-50).

PIK3CA/Akt pathway and PTEN

Approximately 35–60% of patients with metastatic prostate cancer (41, 43) show inactivation of *PTEN*, an important tumor suppressor and guardian of the genome, through loss of function mutations or through (focal) loss. Inactivation of *PTEN* leads to hyperactivation of the PI3K-Akt-mTOR pathway (41). This is of importance, as there is clinically relevant cross-talk between AR signaling and the PI3K-Akt-mTOR pathway; when targeting AR signaling, for example by enzalutamide or abiraterone, activation of the PI3K-Akt-mTOR overrides the inhibitory effects of these agents through downstream activation of androgen responsive genes (51). Inhibition of the PI3K-Akt-mTOR pathway therefore has received remarkable interest as a novel target in prostate cancer. After promising results of combining an Akt-inhibitor with abiraterone in a phase 2 trial demonstrating a prolonged rPFS and trend towards PSA PFS and OS (52), the phase 3 trial with the addition of ipatasertib to abiraterone showed improved rPFS in mCRPC patients with *PTEN* loss, but not in the intention-to-treat population. They concluded that the addition of ipatasertib to abiraterone could be a potential treatment for mCRPC patients with *PTEN* loss (53).

DNA damage repair deficiency

In about 25-27% of the patients with mCRPC DNA repair deficiencies, mutations or deletions in DNA repair genes such as *BRCA1/2*, *ATM*, *CHEK1/2*, *RAD51B*, *CDK12* and the Fanconi anemia genes, can be found (41, 54, 55). When a single-strand break occurs in DNA, PARP 1 and 2 bind to this break and by generating PAR polymers (PARylation) on itself and target proteins, PARP is able to recruit repair proteins that have roles in different aspects of DNA damage repair (56, 57). PARP-1 is also able to repair double-strand breaks in DNA (56, 57). Cumulative PARylation ultimately leads to dissociation of PARP from the DNA. PARP inhibition results in accumulation of unrepaired DNA breaks and trapping of PARP on DNA. When single strand breaks accumulate, replication-induced double-strand DNA breaks arise, in part through stalled replication forks. Error-free reparation of these breaks requires key DNA repair genes from the homologous repair (HR) pathway. However, if these key DNA repair genes, such as *BRCA1/2*, are mutated and a PARP inhibitor is administered, an enormous accumulation of both single and double strand breaks arise leading to apoptosis of the cell. The phase 3 randomized controlled ProFOUND trial compared the PARP inhibitor olaparib to abiraterone or enzalutamide in men with a qualifying alteration in prespecified genes with a role an (in)direct role in homologous recombination repair mechanism who had disease progression while receiving abiraterone or enzalutamide (58). The trial endpoints were powered on cohort A, with qualifying alteration in *BRCA1/2* and *ATM*, while an exploratory cohort of less common DNA damage repair (DDR) alterations was included in cohort B. In cohort A, both PFS as OS was significantly improved by olaparib compared to the comparator arm. Nevertheless, the European Medicine Agency (EMA) approved olaparib only for patients with *BRCA1/2* alterations, excluding *ATM* due to lack of clear efficacy from subgroups analysis. Since the end of 2020, olaparib has been registered for *BRCA1/2* mutated mCRPC patients after treatment with abiraterone or enzalutamide. In the US, rucaparib also was approved by the Food and Drug Administration (FDA) following results of the TRITON-2 trial (59) in May of 2020, for patients with a germline/somatic *BRCA1/2* alteration.

There is also evidence that AR signaling is associated with DNA damage. A feedback loop was discovered whereby DNA repair genes activate the AR upon DNA damage and subsequently promote DNA repair (60). Further, AR has itself been shown to induce double stranded breaks via topoisomerase IIb (61). Polkinghorn et al. was also able to demonstrate that AR signaling increases the expression of DNA repair genes from the HR pathway (62). As discussed earlier HR is necessary for error-free repair of double-strand breaks in DNA. It was hypothesized that ADT would decrease the AR-regulated transcriptional program leading to reduced activity of HR, thereby inhibiting repair of double-strand breaks, which would lead to an increase of PARP activity. This was indeed

proven by Asim et al (63) leading to the hypothesis that the combination of ADT and a PARP inhibitor would be more effective than ADT alone. This implies that PARP inhibitors may also be effective in DDR proficient patients. Due to promising results from a phase 2 trial (64), suggesting that the rPFS benefit of the combination of abiraterone and olaparib was independent of DDR deficient or DDR proficient status, a large phase 3 PROpel trial was conducted to compare abiraterone with or without olaparib, regardless of homologous recombination repair (HRR) gene mutation status. The results of the planned primary analysis were recently published (65) and showed a significantly longer rPFS in all mCRPC patients treated with the combination of abiraterone and olaparib, although more pronounced in patients with mutations in HRR genes. Simultaneously, the first results of the phase 3 MAGNITUDE trial (66) were presented, comparing abiraterone with or without niraparib in patients in two pre-specified cohorts; one with and one without DNA damage repair alterations (in)directly associated with HRR. The study demonstrated rPFS benefit of the combination niraparib with abiraterone for those mCRPC patients with HRR mutated disease while no benefit was seen in the cohort of patients without an HRR mutation (66).

Platinum-based chemotherapy causes intra- or interstrand DNA crosslinks which are repaired by a combination of enzymes and other factors from the nucleotide excision repair pathway, HR and the base excision repair pathway (67). When key DNA damage genes are mutated, such as those of the HR pathway, the resulting double-strand breaks accumulate and lead to cell death. Platinum-based chemotherapy shows some efficacy in DDR deficient mCRPC patients in several retrospective studies (68-71) and is a promising addition to the current taxane-based chemotherapy. Results from prospective studies are lacking thus far. The lack of evidence is partly due to the introduction and registration of PARP inhibitors for patients harboring DDR alterations. The place of platinum-based therapy in the sequence of mCRPC treatment options is yet unknown, but several phase 2 studies are conducted to investigate the role and position of platinum-based chemotherapy and PARP inhibition or the combination of both in DDR deficient mCRPC patients (NCT04038502 and NCT03442556). In DDR deficient patients, besides PARP inhibitors and platinum chemotherapy, additional options could also provide better outcomes. For example, checkpoint inhibitors show higher responses in DDR deficient patients compared to DDR proficient patients due to a higher mutational burden witnessed in DDR deficient patients, putatively resulting in more neoantigens that can be presented to the immune system (41, 72). Two phase 2 trials (NCT03431350 and NCT03248570) are investigating the effectiveness of PDL1 inhibition in DDR deficient mCRPC patients, of which the results are eagerly awaited. The phase 3 KEYLINK-010 trial investigated whether the combination of pembrolizumab and olaparib would improve rPFS and OS when compared to abiraterone or enzalutamide in previously treated

molecular unselected mCRPC patients (73). Although no improvement in both rPFS and OS was seen with pembrolizumab plus olaparib in the total group, an exploratory analysis of the subgroup with HRR gene alterations suggested an improvement of rPFS with pembrolizumab plus olaparib. However, the trial was not designed for this analysis and further prospective research is warranted for this particular subgroup.

Biallelic inactivation of CDK12, a key player in the DNA repair pathway, results in a distinct genetic fingerprint, comprising focal tandem duplications and gene fusions across the genome, and is identified as a novel molecular subtype by Wu et al (72). CDK12 inactivation is present in about 7% of mCRPC patients (72) and this tumor subtype appears to be very immunogenic due to a high neoantigen burden resulting from the genetic rearrangements and focal amplifications. This is accompanied by higher T cell infiltration compared to wildtype patients, which led to the study by Wu et al evaluating whether these patients were good responders to immune checkpoint inhibition (72). These results have led to a phase 2 IMPACT trial in which mCRPC patients with CDK12 inactivation or function aberrations were treated with ipilimumab/nivolumab. First preliminary results show a PSA decline of at least 30% in 21% of the patients (74).

Microsatellite instability

Mismatch repair (MMR) deficiency leading to microsatellite instability (MSI) results in a high tumor mutational burden with corresponding high neoantigen load. MSI and/or MMR deficiency are therefore an ideal tumor-agnostic and predictive biomarker for checkpoint immunotherapy. The prevalence of MSI in mCRPC is between 3–7% (41, 75-77). A small retrospective study (n= 11 MSI/MMR deficient patients) presented by Abida et al. showed impressive and durable responses to anti-PD1 therapy; 54.5% had a PSA decline of >50% of whom 67.7% had also a radiologic response (75). The Drug Rediscovery Program (DRUP) study in the Netherlands has used this tumor-agnostic biomarker as selection criteria for a checkpoint inhibitor cohort, and was able to confirm the impressive response rates published before (78). These data have led to the approval of nivolumab for pan-cancer MSI high or MMR loss by the Zorginstituut Nederland in 2022 and support the use of routine MSI testing and/or next-generation sequencing in all patients with metastatic prostate cancer.

To summarize, our understanding and knowledge about metastatic prostate cancer has improved dramatically over the last ten years, partly due to advances in molecular characterization technologies and the systematic and comprehensive exploration of the genetic and epigenetic landscape of prostate cancer. This had already led to an extensive number of clinical trials with new targeted therapies and helped identify the subgroup of patients with metastatic prostate cancer that would particularly benefit from

these specific treatments. Based on the results of these clinical trials, guidelines of the European Association of Urology (EAU) (79) and European Society for Medical Oncology (ESMO) (80) have been updated and recommend testing for HRR and MRR deficiencies (or MSI) in every metastatic prostate cancer patient. Furthermore, it is recommended that patients with pathogenic mutations in cancer-risk genes should be referred to the for germline testing based on studies showing a relatively high incidence of germline mutations in metastatic prostate cancer patients (41, 81, 82).

The technical challenges of molecular analyses in metastatic prostate cancer

Although these new palliative therapies have had great clinical impact on patient quality of life and outcome, optimal sequencing and the introduction of new targeted treatment strategies that may deliver long-term disease stabilization are still lacking. This is partly due to technical challenges in molecular analyses. Even though, as mentioned earlier, several NGS studies have been conducted and showed its added predictive and prognostic value in metastatic prostate cancer patients, a large subgroup of prostate cancer patients is underrepresented in these studies (41-43). Bone-only (43%) and bone-predominant (73%) metastatic disease are most frequently reported in prostate cancer (83, 84). Since molecular analysis of a metastasis is the first step in individualizing patient care, a biopsy with sufficient and high quality tumor material is necessary. However, previous studies (85-87) have described that the success rate for molecular analyses on a bone biopsies is significantly lower than biopsies from soft tissue (lymph node or visceral), mainly due to technical difficulties in identifying bone lesions with predominant tumor tissue and regarding the biopsy procedure from sclerotic bone lesions. A relatively high failure of NGS was also presented in the precision medicine phase 3 ProFOUND study, showing a success rate of 69% in all samples with lowest success rate in bone metastases (43%) (88), which are comparable results with previously mentioned pivotal NGS studies. In addition, both archival and fresh tumor tissue can be used for NGS for precision medicine as shown in this study (88). However, an association was found between age of the sample and generating a NGS result with significantly lower chance for samples of more than 10 years old, compared to samples less than 1 year old. Furthermore, genomic evolution occurs when progressing from mHSPC towards mCRPC and therefore new oncogenic drivers, which are often actionable alterations, can be missed in archival tissue. Consequently, there is a rationale for obtaining fresh frozen biopsies of new or progressive metastases to determine the most optimal treatment for the individual patient.

In conclusion, due to several technical challenges in obtaining sufficient tumor yield for NGS there is still a gap in knowledge about the genomic landscape and its potential clinical impact for a large group of metastatic prostate cancer patients. To expand individualized

care for all metastatic prostate cancer patients, research about the technical challenges in performing molecular analyses is warranted.

OUTLINE OF THIS THESIS

This thesis aims to improve our knowledge of the genomic landscape of metastatic castration-resistant prostate cancer. Stratification of prostate cancer into actionable genomic subgroups could contribute, in the current era of precision medicine, to the introduction of more individualized treatment strategies.

For that, in **part I** we initiated our research on obtaining a representative biopsy. We investigated and improved both clinical and technical factors contributing to the relatively low success rate of bone biopsies in metastatic prostate cancer patients in **chapter 2** and **3**. The introduction of the prostate-specific membrane antigen (PSMA) positron-emission tomography (PET) improved care for patients with localized prostate cancer and biochemical recurrence and but might also be a useful clinical tool in selecting a PSMA expressing bone metastasis to improve the yield of bone biopsies for molecular analyses in prostate cancer patients.

In **part II, chapter 4** we take the next step and aimed to improve the success rate of molecular analyses in bone biopsies by designing a pilot study investigating the added value of the combination of PSMA-PET and a diffusion MRI followed by a cone-beam CT guided biopsy and evaluating the feasibility of incorporating this advanced target planning.

The potential clinical impact of molecular analyses in metastatic prostate cancer patients is described in **part III**. In **chapter 5** we will elaborate about the eight distinct genomic clusters that have been found in a Dutch cohort of metastatic castration resistant prostate cancer (mCRPC) patients by unsupervised clustering based on genomic features. Furthermore, the response to immune checkpoint inhibitors (ICIs) in patients with mCRPC, treated in the Radboud University Medical Center, is evaluated in **chapter 6**. Using next-generation T-cell repertoire sequencing in peripheral blood of a small cohort with both microsatellite stable (MSS) and MSI high mCRPC patients, immune signatures were explored.

In **part IV** we summarize the main findings of this thesis in **chapter 7**. The implications of our research are discussed in **chapter 8** as well as our perspective on and recommendations for further research in the near future are presented.

REFERENCES

1. Adams J. The case of scirrhus of the prostate gland with corresponding affliction of the lymphatic glands in the lumbar region and in the pelvis. *Lancet*. 1853.
2. Sung H, Ferlay J, Siegel RL, Laversanne M, Soerjomataram I, Jemal A, et al. Global Cancer Statistics 2020: GLOBOCAN Estimates of Incidence and Mortality Worldwide for 36 Cancers in 185 Countries. *CA Cancer J Clin*. 2021;71(3):209-49.
3. Huggins C, Hodges CV. Studies on prostatic cancer. I. The effect of castration, of estrogen and of androgen injection on serum phosphatases in metastatic carcinoma of the prostate. 1941. *J Urol*. 2002;167(2 Pt 2):948-51; discussion 52.
4. Huggins C, Scott WW. Bilateral Adrenalectomy in Prostatic Cancer: Clinical Features and Urinary Excretion of 17-Ketosteroids and Estrogen. *Ann Surg*. 1945;122(6):1031-41.
5. Schally AV, Kastin AJ, Arimura A. Hypothalamic follicle-stimulating hormone (FSH) and luteinizing hormone (LH)-regulating hormone: structure, physiology, and clinical studies. *Fertil Steril*. 1971;22(11):703-21.
6. Schally AV, Coy DH, Arimura A. LH-RH agonists and antagonists. *Int J Gynaecol Obstet*. 1980;18(5):318-24.
7. Schally AV, Redding TW, Comaru-Schally AM. Inhibition of prostate tumors by agonistic and antagonistic analogs of LH-RH. *Prostate*. 1983;4(6):545-52.
8. Labrie F, Dupont A, Belanger A, Cusan L, Lacourciere Y, Monfette G, et al. New hormonal therapy in prostatic carcinoma: combined treatment with an LHRH agonist and an antiandrogen. *Clin Invest Med*. 1982;5(4):267-75.
9. Labrie F, Dupont A, Belanger A, Lacourciere Y, Monfette JE, Monfette G. [Combined antiandrogen treatment in adenocarcinoma of the prostate: first use of a new therapeutically efficacious principle in hormone-dependent cancer]. *Ann Urol (Paris)*. 1986;20(2):98-106.
10. Berry W, Dakhil S, Modiano M, Gregurich M, Asmar L. Phase III study of mitoxantrone plus low dose prednisone versus low dose prednisone alone in patients with asymptomatic hormone refractory prostate cancer. *J Urol*. 2002;168(6):2439-43.
11. Petrylak DP, Tangen CM, Hussain MH, Lara PN, Jr., Jones JA, Taplin ME, et al. Docetaxel and estramustine compared with mitoxantrone and prednisone for advanced refractory prostate cancer. *N Engl J Med*. 2004;351(15):1513-20.
12. Tannock IF, de Wit R, Berry WR, Horti J, Pluzanska A, Chi KN, et al. Docetaxel plus prednisone or mitoxantrone plus prednisone for advanced prostate cancer. *N Engl J Med*. 2004;351(15):1502-12.
13. de Bono JS, Oudard S, Ozguroglu M, Hansen S, Machiels JP, Kocak I, et al. Prednisone plus cabazitaxel or mitoxantrone for metastatic castration-resistant prostate cancer progressing after docetaxel treatment: a randomised open-label trial. *Lancet*. 2010;376(9747):1147-54.
14. Stanbrough M, Bubley GJ, Ross K, Golub TR, Rubin MA, Penning TM, et al. Increased expression of genes converting adrenal androgens to testosterone in androgen-independent prostate cancer. *Cancer Res*. 2006;66(5):2815-25.

15. Holzbeierlein J, Lal P, LaTulippe E, Smith A, Satagopan J, Zhang L, et al. Gene expression analysis of human prostate carcinoma during hormonal therapy identifies androgen-responsive genes and mechanisms of therapy resistance. *Am J Pathol.* 2004;164(1):217-27.
16. Linja MJ, Savinainen KJ, Saramaki OR, Tammela TL, Vessella RL, Visakorpi T. Amplification and overexpression of androgen receptor gene in hormone-refractory prostate cancer. *Cancer Res.* 2001;61(9):3550-5.
17. Taplin ME, Bubley GJ, Ko YJ, Small EJ, Upton M, Rajeshkumar B, et al. Selection for androgen receptor mutations in prostate cancers treated with androgen antagonist. *Cancer Res.* 1999;59(11):2511-5.
18. de Bono JS, Logothetis CJ, Molina A, Fizazi K, North S, Chu L, et al. Abiraterone and increased survival in metastatic prostate cancer. *N Engl J Med.* 2011;364(21):1995-2005.
19. Scher HI, Fizazi K, Saad F, Taplin ME, Sternberg CN, Miller K, et al. Increased survival with enzalutamide in prostate cancer after chemotherapy. *N Engl J Med.* 2012;367(13):1187-97.
20. Attard G, Belldegrun AS, de Bono JS. Selective blockade of androgenic steroid synthesis by novel lyase inhibitors as a therapeutic strategy for treating metastatic prostate cancer. *BJU Int.* 2005;96(9):1241-6.
21. Tran C, Ouk S, Clegg NJ, Chen Y, Watson PA, Arora V, et al. Development of a second-generation antiandrogen for treatment of advanced prostate cancer. *Science.* 2009;324(5928):787-90.
22. Scher HI, Beer TM, Higano CS, Anand A, Taplin ME, Efstathiou E, et al. Antitumour activity of MDV3100 in castration-resistant prostate cancer: a phase 1-2 study. *Lancet.* 2010;375(9724):1437-46.
23. Khalaf DJ, Annala M, Taavitsainen S, Finch DL, Oja C, Vergidis J, et al. Optimal sequencing of enzalutamide and abiraterone acetate plus prednisone in metastatic castration-resistant prostate cancer: a multicentre, randomised, open-label, phase 2, crossover trial. *Lancet Oncol.* 2019;20(12):1730-9.
24. de Wit R, de Bono J, Sternberg CN, Fizazi K, Tombal B, Wulfing C, et al. Cabazitaxel versus Abiraterone or Enzalutamide in Metastatic Prostate Cancer. *N Engl J Med.* 2019;381(26):2506-18.
25. Gravis G, Fizazi K, Joly F, Oudard S, Priou F, Esterni B, et al. Androgen-deprivation therapy alone or with docetaxel in non-castrate metastatic prostate cancer (GETUG-AFU 15): a randomised, open-label, phase 3 trial. *Lancet Oncol.* 2013;14(2):149-58.
26. Sweeney CJ, Chen YH, Carducci M, Liu G, Jarrard DF, Eisenberger M, et al. Chemohormonal Therapy in Metastatic Hormone-Sensitive Prostate Cancer. *N Engl J Med.* 2015;373(8):737-46.
27. James ND, Sydes MR, Clarke NW, Mason MD, Dearnaley DP, Spears MR, et al. Addition of docetaxel, zoledronic acid, or both to first-line long-term hormone therapy in prostate cancer (STAMPEDE): survival results from an adaptive, multiarm, multistage, platform randomised controlled trial. *Lancet.* 2016;387(10024):1163-77.
28. Kyriakopoulos CE, Chen YH, Carducci MA, Liu G, Jarrard DF, Hahn NM, et al. Chemohormonal Therapy in Metastatic Hormone-Sensitive Prostate Cancer: Long-Term Survival Analysis of the Randomized Phase III E3805 CHAARTED Trial. *J Clin Oncol.* 2018;36(11):1080-7.
29. Clarke NW, Ali A, Ingleby FC, Hoyle A, Amos CL, Attard G, et al. Addition of docetaxel to hormonal therapy in low- and high-burden metastatic hormone sensitive prostate cancer: long-term survival results from the STAMPEDE trial. *Ann Oncol.* 2019;30(12):1992-2003.

30. James ND, de Bono JS, Spears MR, Clarke NW, Mason MD, Dearnaley DP, et al. Abiraterone for Prostate Cancer Not Previously Treated with Hormone Therapy. *N Engl J Med*. 2017;377(4):338-51.
31. James ND, Clarke NW, Cook A, Ali A, Hoyle AP, Attard G, et al. Abiraterone acetate plus prednisolone for metastatic patients starting hormone therapy: 5-year follow-up results from the STAMPEDE randomised trial (NCT00268476). *Int J Cancer*. 2022;151(3):422-34.
32. Fizazi K, Tran N, Fein L, Matsubara N, Rodriguez-Antolin A, Alekseev BY, et al. Abiraterone plus Prednisone in Metastatic, Castration-Sensitive Prostate Cancer. *N Engl J Med*. 2017;377(4):352-60.
33. Davis ID, Martin AJ, Stockler MR, Begbie S, Chi KN, Chowdhury S, et al. Enzalutamide with Standard First-Line Therapy in Metastatic Prostate Cancer. *N Engl J Med*. 2019;381(2):121-31.
34. Davis ID. Updated overall survival outcomes in ENZAMET (ANZUP 1304), an international, cooperative group trial of enzalutamide in metastatic hormone-sensitive prostate cancer (mHSPC). *Journal of Clinical Oncology*. 2022;40.
35. Armstrong AJ, Szmulewitz RZ, Petrylak DP, Holzbeierlein J, Villers A, Azad A, et al. ARCHES: A Randomized, Phase III Study of Androgen Deprivation Therapy With Enzalutamide or Placebo in Men With Metastatic Hormone-Sensitive Prostate Cancer. *J Clin Oncol*. 2019;37(32):2974-86.
36. Chi KN, Agarwal N, Bjartell A, Chung BH, Pereira de Santana Gomes AJ, Given R, et al. Apalutamide for Metastatic, Castration-Sensitive Prostate Cancer. *N Engl J Med*. 2019;381(1):13-24.
37. Sydes MR, Spears MR, Mason MD, Clarke NW, Dearnaley DP, de Bono JS, et al. Adding abiraterone or docetaxel to long-term hormone therapy for prostate cancer: directly randomised data from the STAMPEDE multi-arm, multi-stage platform protocol. *Ann Oncol*. 2018;29(5):1235-48.
38. Rush HL, Murphy L, Morgans AK, Clarke NW, Cook AD, Attard G, et al. Quality of Life in Men With Prostate Cancer Randomly Allocated to Receive Docetaxel or Abiraterone in the STAMPEDE Trial. *J Clin Oncol*. 2022;40(8):825-36.
39. Fizazi K, Foulon S, Carles J, Roubaud G, McDermott R, Flechon A, et al. Abiraterone plus prednisone added to androgen deprivation therapy and docetaxel in de novo metastatic castration-sensitive prostate cancer (PEACE-1): a multicentre, open-label, randomised, phase 3 study with a 2 x 2 factorial design. *Lancet*. 2022;399(10336):1695-707.
40. Smith MR, Hussain M, Saad F, Fizazi K, Sternberg CN, Crawford ED, et al. Darolutamide and Survival in Metastatic, Hormone-Sensitive Prostate Cancer. *N Engl J Med*. 2022;386(12):1132-42.
41. Robinson D, Van Allen EM, Wu YM, Schultz N, Lonigro RJ, Mosquera JM, et al. Integrative clinical genomics of advanced prostate cancer. *Cell*. 2015;161(5):1215-28.
42. Viswanathan SR, Ha G, Hoff AM, Wala JA, Carrot-Zhang J, Whelan CW, et al. Structural Alterations Driving Castration-Resistant Prostate Cancer Revealed by Linked-Read Genome Sequencing. *Cell*. 2018;174(2):433-47 e19.
43. Quigley DA, Dang HX, Zhao SG, Lloyd P, Aggarwal R, Alumkal JJ, et al. Genomic Hallmarks and Structural Variation in Metastatic Prostate Cancer. *Cell*. 2018;174(3):758-69 e9.
44. Gundem G, Van Loo P, Kremeyer B, Alexandrov LB, Tubio JMC, Papaemmanuil E, et al. The evolutionary history of lethal metastatic prostate cancer. *Nature*. 2015;520(7547):353-7.

45. Beltran H, Prandi D, Mosquera JM, Benelli M, Puca L, Cyrta J, et al. Divergent clonal evolution of castration-resistant neuroendocrine prostate cancer. *Nat Med.* 2016;22(3):298-305.
46. Cancer Genome Atlas Research N. The Molecular Taxonomy of Primary Prostate Cancer. *Cell.* 2015;163(4):1011-25.
47. Armstrong AJ, Halabi S, Luo J, Nanus DM, Giannakakou P, Szmulewitz RZ, et al. Prospective Multicenter Validation of Androgen Receptor Splice Variant 7 and Hormone Therapy Resistance in High-Risk Castration-Resistant Prostate Cancer: The PROPHECY Study. *J Clin Oncol.* 2019;37(13):1120-9.
48. Armstrong AJ, Luo J, Nanus DM, Giannakakou P, Szmulewitz RZ, Danila DC, et al. Prospective Multicenter Study of Circulating Tumor Cell AR-V7 and Taxane Versus Hormonal Treatment Outcomes in Metastatic Castration-Resistant Prostate Cancer. *JCO Precis Oncol.* 2020;4.
49. Scher HI, Lu D, Schreiber NA, Louw J, Graf RP, Vargas HA, et al. Association of AR-V7 on Circulating Tumor Cells as a Treatment-Specific Biomarker With Outcomes and Survival in Castration-Resistant Prostate Cancer. *JAMA Oncol.* 2016;2(11):1441-9.
50. Antonarakis ES, Lu C, Luber B, Wang H, Chen Y, Nakazawa M, et al. Androgen Receptor Splice Variant 7 and Efficacy of Taxane Chemotherapy in Patients With Metastatic Castration-Resistant Prostate Cancer. *JAMA Oncol.* 2015;1(5):582-91.
51. Carver BS, Chapinski C, Wongvipat J, Hieronymus H, Chen Y, Chandarlapaty S, et al. Reciprocal feedback regulation of PI3K and androgen receptor signaling in PTEN-deficient prostate cancer. *Cancer Cell.* 2011;19(5):575-86.
52. de Bono JS, De Giorgi U, Rodrigues DN, Massard C, Bracarda S, Font A, et al. Randomized Phase II Study Evaluating Akt Blockade with Ipatasertib, in Combination with Abiraterone, in Patients with Metastatic Prostate Cancer with and without PTEN Loss. *Clin Cancer Res.* 2019;25(3):928-36.
53. Sweeney C, Bracarda S, Sternberg CN, Chi KN, Olmos D, Sandhu S, et al. Ipatasertib plus abiraterone and prednisolone in metastatic castration-resistant prostate cancer (IPATential150): a multicentre, randomised, double-blind, phase 3 trial. *Lancet.* 2021;398(10295):131-42.
54. Abida W, Armenia J, Gopalan A, Brennan R, Walsh M, Barron D, et al. Prospective Genomic Profiling of Prostate Cancer Across Disease States Reveals Germline and Somatic Alterations That May Affect Clinical Decision Making. *JCO Precis Oncol.* 2017;2017.
55. Armenia J, Wankowicz SAM, Liu D, Gao J, Kundra R, Reznik E, et al. The long tail of oncogenic drivers in prostate cancer. *Nat Genet.* 2018;50(5):645-51.
56. Pommier Y, O'Connor MJ, de Bono J. Laying a trap to kill cancer cells: PARP inhibitors and their mechanisms of action. *Sci Transl Med.* 2016;8(362):362ps17.
57. Ray Chaudhuri A, Nussenzweig A. The multifaceted roles of PARP1 in DNA repair and chromatin remodelling. *Nat Rev Mol Cell Biol.* 2017;18(10):610-21.
58. de Bono J, Mateo J, Fizazi K, Saad F, Shore N, Sandhu S, et al. Olaparib for Metastatic Castration-Resistant Prostate Cancer. *N Engl J Med.* 2020;382(22):2091-102.
59. Abida W, Patnaik A, Campbell D, Shapiro J, Bryce AH, McDermott R, et al. Rucaparib in Men With Metastatic Castration-Resistant Prostate Cancer Harboring a BRCA1 or BRCA2 Gene Alteration. *J Clin Oncol.* 2020;38(32):3763-72.

60. Goodwin JF, Schiewer MJ, Dean JL, Schrecengost RS, de Leeuw R, Han S, et al. A hormone-DNA repair circuit governs the response to genotoxic insult. *Cancer Discov.* 2013;3(11):1254-71.
61. Haffner MC, Aryee MJ, Toubaji A, Esopi DM, Albadine R, Gurel B, et al. Androgen-induced TOP2B-mediated double-strand breaks and prostate cancer gene rearrangements. *Nat Genet.* 2010;42(8):668-75.
62. Polkinghorn WR, Parker JS, Lee MX, Kass EM, Spratt DE, laquinta PJ, et al. Androgen receptor signaling regulates DNA repair in prostate cancers. *Cancer Discov.* 2013;3(11):1245-53.
63. Asim M, Tarish F, Zecchini HI, Sanjiv K, Gelali E, Massie CE, et al. Synthetic lethality between androgen receptor signalling and the PARP pathway in prostate cancer. *Nat Commun.* 2017;8(1):374.
64. Clarke N, Wiechno P, Alekseev B, Sala N, Jones R, Kocak I, et al. Olaparib combined with abiraterone in patients with metastatic castration-resistant prostate cancer: a randomised, double-blind, placebo-controlled, phase 2 trial. *Lancet Oncol.* 2018;19(7):975-86.
65. Clarke N. Abiraterone and Olaparib for Metastatic Castration-Resistant Prostate Cancer. *New England Journal of Medicine Evidence.* 2022.
66. Chi K. Phase 3 MAGNITUDE study: First results of niraparib (NIRA) with abiraterone acetate and prednisone (AAP) as first-line therapy in patients (pts) with metastatic castration-resistant prostate cancer (mCRPC) with and without homologous recombination repair (HRR) gene alterations. *Journal of Clinical Oncology.* 2022.
67. McHugh PJ, Spanswick VJ, Hartley JA. Repair of DNA interstrand crosslinks: molecular mechanisms and clinical relevance. *Lancet Oncol.* 2001;2(8):483-90.
68. Slootbeek PHJ, Duizer ML, van der Doelen MJ, Kloots ISH, Kuppen MCP, Westgeest HM, et al. Impact of DNA damage repair defects and aggressive variant features on response to carboplatin-based chemotherapy in metastatic castration-resistant prostate cancer. *Int J Cancer.* 2021;148(2):385-95.
69. Pomerantz MM, Spisak S, Jia L, Cronin AM, Csabai I, Ledet E, et al. The association between germline BRCA2 variants and sensitivity to platinum-based chemotherapy among men with metastatic prostate cancer. *Cancer.* 2017;123(18):3532-9.
70. Cheng HH, Pritchard CC, Boyd T, Nelson PS, Montgomery B. Biallelic Inactivation of BRCA2 in Platinum-sensitive Metastatic Castration-resistant Prostate Cancer. *Eur Urol.* 2016;69(6):992-5.
71. Mota JM, Barnett E, Nauseef JT, Nguyen B, Stopsack KH, Wibmer A, et al. Platinum-Based Chemotherapy in Metastatic Prostate Cancer With DNA Repair Gene Alterations. *JCO Precis Oncol.* 2020;4:355-66.
72. Wu YM, Cieslik M, Lonigro RJ, Vats P, Reimers MA, Cao X, et al. Inactivation of CDK12 Delineates a Distinct Immunogenic Class of Advanced Prostate Cancer. *Cell.* 2018;173(7):1770-82 e14.
73. Yu EY. Pembrolizumab + olaparib vs abiraterone (abi) or enzalutamide (enza) for patients (pts) with previously treated metastatic castration-resistant prostate cancer (mCRPC): Randomized open-label phase III KEYLYNK-010 study. *Ann Oncol.* 2022.
74. Alva AS. Phase 2 trial of immunotherapy in tumors with CDK12 inactivation (IMPACT): Results from cohort A of patients (pts) with metastatic castration resistant prostate cancer (mCRPC) receiving dual immune checkpoint inhibition (ICI). *Journal of Clinical Oncology.* 2022.

75. Abida W, Cheng ML, Armenia J, Middha S, Autio KA, Vargas HA, et al. Analysis of the Prevalence of Microsatellite Instability in Prostate Cancer and Response to Immune Checkpoint Blockade. *JAMA Oncol.* 2019;5(4):471-8.
76. Le DT, Uram JN, Wang H, Bartlett BR, Kemberling H, Eyring AD, et al. PD-1 Blockade in Tumors with Mismatch-Repair Deficiency. *N Engl J Med.* 2015;372(26):2509-20.
77. Le DT, Durham JN, Smith KN, Wang H, Bartlett BR, Aulakh LK, et al. Mismatch repair deficiency predicts response of solid tumors to PD-1 blockade. *Science.* 2017;357(6349):409-13.
78. van der Velden DL, Hoes LR, van der Wijngaart H, van Berge Henegouwen JM, van Werkhoven E, Roepman P, et al. The Drug Rediscovery protocol facilitates the expanded use of existing anticancer drugs. *Nature.* 2019;574(7776):127-31.
79. Mottet N. EAU-EANM-ESTRO-ESUR-ISUP-SIOG Guidelines on prostate cancer. European Association of Urology. 2022.
80. Parker C, Castro E, Fizazi K, Heidenreich A, Ost P, Procopio G, et al. Prostate cancer: ESMO Clinical Practice Guidelines for diagnosis, treatment and follow-up. *Ann Oncol.* 2020;31(9):1119-34.
81. Pritchard CC, Mateo J, Walsh MF, De Sarkar N, Abida W, Beltran H, et al. Inherited DNA-Repair Gene Mutations in Men with Metastatic Prostate Cancer. *N Engl J Med.* 2016;375(5):443-53.
82. Castro E, Romero-Laorden N, Del Pozo A, Lozano R, Medina A, Puente J, et al. PROREPAIR-B: A Prospective Cohort Study of the Impact of Germline DNA Repair Mutations on the Outcomes of Patients With Metastatic Castration-Resistant Prostate Cancer. *J Clin Oncol.* 2019;37(6):490-503.
83. Halabi S, Kelly WK, Ma H, Zhou H, Solomon NC, Fizazi K, et al. Meta-Analysis Evaluating the Impact of Site of Metastasis on Overall Survival in Men With Castration-Resistant Prostate Cancer. *J Clin Oncol.* 2016;34(14):1652-9.
84. Bubendorf L, Schopfer A, Wagner U, Sauter G, Moch H, Willi N, et al. Metastatic patterns of prostate cancer: an autopsy study of 1,589 patients. *Hum Pathol.* 2000;31(5):578-83.
85. Suprun H, Rywlin AM. Metastatic carcinoma in histologic sections of aspirated bone marrow: a comparative autopsy study. *South Med J.* 1976;69(4):438-9.
86. McKay RR, Zukotynski KA, Werner L, Voznesensky O, Wu JS, Smith SE, et al. Imaging, procedural and clinical variables associated with tumor yield on bone biopsy in metastatic castration-resistant prostate cancer. *Prostate Cancer Prostatic Dis.* 2014;17(4):325-31.
87. Mehra R, Kumar-Sinha C, Shankar S, Lonigro RJ, Jing X, Philips NE, et al. Characterization of bone metastases from rapid autopsies of prostate cancer patients. *Clin Cancer Res.* 2011;17(12):3924-32.
88. Hussain M, Corcoran C, Sibilla C, Fizazi K, Saad F, Shore N, et al. Tumor Genomic Testing for >4,000 Men with Metastatic Castration-resistant Prostate Cancer in the Phase III Trial PROfound (Olaparib). *Clin Cancer Res.* 2022;28(8):1518-30.



PART I

**THE TECHNICAL CHALLENGES OF MOLECULAR
ANALYSES IN METASTATIC PROSTATE CANCER**



CHAPTER 2

⁶⁸GA-PSMA-GUIDED BONE BIOPSIES FOR MOLECULAR DIAGNOSTICS IN PATIENTS WITH METASTATIC PROSTATE CANCER

Anouk C. de Jong*

Job van Riet

Tessa Brabander

Inge M. van Oort

Martijn P. Lolkema

Marcel Segbers

Minke Smits*

Jurgen J. Fütterer

Paul Hamberg

Ronald de Wit

Niven Mehra

Astrid A.M. van der Veldt

* These authors contributed equally to this work.

Journal of Nuclear Medicine. 2020;61(11):1607-14.

ABSTRACT

For individual treatment decisions in patients with metastatic prostate cancer (mPC), molecular diagnostics are increasingly used. Bone metastases are frequently the only source for obtaining metastatic tumor tissue. However, the success rate of CT-guided bone biopsies for molecular analyses in mPC patients is only 40%. PET using Gallium-68 prostate specific membrane antigen (^{68}Ga -PSMA) is a promising tool to improve the harvest rate of bone biopsies for molecular analyses. Aim of this study was to determine the success rate of ^{68}Ga -PSMA guided bone biopsies for molecular diagnostics in mPC patients.

Methods

Within a prospective multicenter whole-genome sequencing trial (NCT01855477), 69 mPC patients underwent ^{68}Ga -PSMA PET/CT before bone biopsy. The primary endpoint was success rate (tumor percentage $\geq 30\%$) of ^{68}Ga -PSMA guided bone biopsies. At biopsy sites, ^{68}Ga -PSMA uptake was quantified using rigid body image registration of ^{68}Ga -PSMA PET/CT and interventional CT. Actionable somatic alterations were identified.

Results

The success rate of ^{68}Ga -PSMA guided biopsies for molecular analyses was 70%. At biopsy sites categorized as positive, inconclusive, or negative for ^{68}Ga -PSMA uptake, 70%, 64%, and 36% of biopsies were tumor-positive ($\geq 30\%$), respectively ($p=0.0610$). In tumor-positive biopsies, ^{68}Ga -PSMA uptake was significantly higher ($p=0.008$), whereas radiodensity was significantly lower ($p=0.006$). With an area under the curve of 0.84 and 0.70, both ^{68}Ga -PSMA uptake (SUV_{max}) and radiodensity (HU_{mean}) were strong predictors for a positive biopsy. Actionable somatic alterations were detected in 73% of the sequenced biopsies.

Conclusion

In patients with mPC, ^{68}Ga -PSMA PET/CT improves the success rate of CT-guided bone biopsies for molecular analyses, thereby identifying actionable somatic alterations in more patients. Therefore, ^{68}Ga -PSMA PET/CT may be considered for guidance of bone biopsies in both clinical practice and clinical trials.

INTRODUCTION

With more than 350.000 men dying of prostate cancer in 2018, prostate cancer is not only one of the most common malignancies in men, but also the fifth leading cause of cancer-related death worldwide [1]. To improve treatment planning for individual patients with metastatic prostate cancer (mPC), molecular analyses are increasingly used to predict treatment response, guide clinical decision making and identify additional targets for targeted therapy [2-4]. Because of tumor evolution and genetic adaption following castration resistance and subsequent treatment resistance, tumor DNA for molecular analyses is preferably obtained from a biopsy of a metastatic lesion. Because bone-only and bone predominant disease are most frequently reported in patients with mPC, bone metastases are usually the only source for molecular analyses [5,6].

In men with mPC, 67-77% of bone biopsies have sufficient quality for diagnostic histopathological examination [7-9]. However, molecular analyses on CT-guided bone biopsies from prostate cancer are less feasible, as the success rate is only 39-44% and 36.5% for RNA analysis and whole exome sequencing, respectively [7,8,10]. This poor success rate of bone biopsies might be due to the predominantly osteoblastic character of these metastases. Because bone metastases of prostate cancer have a dense sclerotic matrix and decreased tumor cellularity, these lesions are difficult to distinguish from non-malignant osteosclerosis on CT [11].

In clinical practice, most bone biopsies are guided by computed tomography (CT). Since the yield of CT-guided bone biopsies for molecular analyses is rather low, the use of molecular diagnostics for personalized treatment in prostate cancer patients is limited. To improve the yield of bone biopsies in mPC patients, biopsies could be obtained from bone metastases, which express prostate specific membrane antigen (PSMA). In the apical region of normal prostate cells, PSMA shows physiological expression, whereas it is usually 100-1000x overexpressed in prostate cancer cells [12]. To visualize and quantify PSMA expression *in vivo*, positron emission tomography (PET) using Gallium-68 PSMA (⁶⁸Ga-PSMA) can be performed. Nowadays, ⁶⁸Ga-PSMA PET/CT is increasingly used in the setting of biochemical recurrence, as it has a high sensitivity and specificity for early detection of prostate cancer [13]. Recently, fused images of ⁶⁸Ga-PSMA PET/CT and diffusion weighted MRI, in combination with cone-beam CT guidance, have been applied to guide bone biopsies in patients with prostate cancer. Although this pilot study was performed on only a small number of patients (N=10), it showed a success rate of 80% [14]. Therefore, ⁶⁸Ga-PSMA PET/CT is a promising technique to increase the success rate of bone biopsies for molecular analyses in prostate cancer patients.

Within a prospective multicenter whole-genome sequencing (WGS) trial, we determined the success rate of ^{68}Ga -PSMA guided bone biopsies for molecular diagnostics in metastatic prostate cancer patients. In addition, we evaluated the potential impact of these molecular analyses on clinical decision making in mPC patients.

MATERIALS AND METHODS

Design

In this comprehensive PET study, mPC patients, who had a ^{68}Ga -PSMA guided bone biopsy within the prospective multicenter nationwide CPCT-02 study (NCT01855477), were included [15]. CPCT-02 aims to improve selection of patients for experimental therapy by WGS of tumor DNA, which is obtained by image-guided biopsies. For the current study, informed consent was obtained within CPCT-02, and additional approval was provided by the institutional review boards of two academic institutes in the Netherlands: Erasmus Medical Center in Rotterdam and Radboud University Medical Center in Nijmegen.

Patients

Between December 2014 and July 2018, all mPC patients, who underwent ^{68}Ga -PSMA PET/CT within 12 weeks before a completed bone biopsy procedure within CPCT-02, were included. Full in- and exclusion criteria of CPCT-02 were described previously [15]. Tumor tissue was obtained from a metastatic lesion to fully capture the genomic tumor evolution. Patients could be included at multiple time points in their treatment course, resulting in repeated biopsies for some patients. Biopsies were always obtained prior to the start of a new systemic treatment. Clinical data were collected in an electronic case report form (ALEA Clinical).

Primary and Secondary Endpoints

The primary endpoint was the success rate of ^{68}Ga -PSMA guided bone biopsies in patients with mPC, with success defined as $\geq 30\%$ tumor cells in at least one biopsy core (i.e. the minimal amount of tissue required for DNA isolation for WGS), as assessed by a dedicated pathologist. Exploratory endpoints included the correlation between biopsy success and imaging (standardized uptake value [SUV] and Hounsfield Units [HU]) and laboratory variables (haemoglobin [Hb], alkaline phosphatase [ALP], prostate specific antigen [PSA], and lactate dehydrogenase [LDH]). In addition, the potential impact of molecular analyses on clinical decision making was evaluated.

Image Acquisition

Before the biopsy procedure, ⁶⁸Ga-PSMA PET/CT was performed to identify a biopsy site with high ⁶⁸Ga-PSMA uptake. During the procedure, biopsies were performed with or without CT, or ultrasound guidance, as decided by the interventional radiologist.

⁶⁸Ga-PSMA PET and Low Dose CT

On-site, PSMA-N,N9-bis [2- hydroxy-5-(carboxyethyl)benzyl]ethylenediamine-N,N9-diacetic acid was labeled with ⁶⁸Ga and administered intravenously with a mean (±SD) single bolus of 133.6 ± 35 MBq. At 60 min after injection, images were acquired from head to mid thigh on a Biograph mCT PET/CT scanner (Siemens Healthineers). A low-dose CT was acquired with 120kV and 40 reference mAs (Erasmus Medical Center) or 50 reference mAs (Radboud University Medical Center). All PET data were obtained during 3 minutes per bed position, except for images with 4 minutes per bed position for patients with weight more than 70 kg at Erasmus Medical Center. For quantitative analyses of ⁶⁸Ga-PSMA uptake, data were reconstructed according to Evaluation and Report Language [16].

Interventional CT

Before CT acquisition for CT-guided biopsy, the field of view was determined by acquiring an overview image. Next, subsequent CT scans with a smaller field of view were acquired to visualize the biopsy needle until the biopsy site was reached.

Biopsy Procedure

Bone biopsies were performed according to local institutional guidelines. The biopsy site was selected by the interventional radiologist based on clinical judgement, safety, and prior imaging including ⁶⁸Ga-PSMA PET/CT.

Image Analyses

Rigid Body Image Registration

In order to evaluate whether biopsies were accurately obtained from a ⁶⁸Ga-PSMA positive lesion, co-registration of ⁶⁸Ga-PSMA PET/CT and the interventional CT was retrospectively performed using rigid body image registration. This analysis, which was performed with the Elastix Toolbox [17,18], enables measurement of ⁶⁸Ga-PSMA uptake at the exact position of the biopsy site. When the image quality of ⁶⁸Ga-PSMA PET, low-dose CT and interventional CT was sufficient for rigid body image registration, patients were included for this exploratory analysis. Rigid body image registration merges ⁶⁸Ga-PSMA PET/CT and the interventional CT within two steps. To exclude soft tissues in both image registration steps, bone masks were obtained by applying a region growing algorithm that included CT voxels greater than 150 HU. In the first co-registration step, patient

motion on interventional CT is corrected by co-registration of the overview image and the image acquired during biopsy. Next, the overview image of the interventional CT was co-registered with the low-dose CT of the ^{68}Ga -PSMA PET/CT image. Combining rotation calculations from both image registration steps with interventional CT enabled fusion of ^{68}Ga -PSMA PET with the interventional CT, thereby visualizing the biopsy needle.

^{68}Ga -PSMA Uptake and Radiodensity at Biopsy Site

An experienced nuclear medicine physician (T.B.), who was blinded for the biopsy results, determined visually whether the biopsy was accurately taken from a ^{68}Ga -PSMA positive lesion, using a three-point scale categorized as hit, borderline or miss. Besides these qualitative analyses, quantitative analyses consisted of SUV and HU measurements. To measure ^{68}Ga -PSMA uptake (SUV) and radiodensity (HU) at the exact biopsy location, a cylindrical volume of interest (VOI) with a length of 2 cm and a diameter of 1 cm was drawn at the site of the biopsy as visualized on rigid body co-registration images of ^{68}Ga -PSMA PET and interventional CT. VOIs were defined in Python using in-house developed scripts, based on SimpleITK framework for medical imaging [19]. The SUV_{max} and SUV_{mean} of ^{68}Ga -PSMA uptake were calculated using the injected radioactivity, body weight and the amount of radioactivity within a VOI. To assess radiodensity in bone metastases, HUs were determined on CT images. For CT measurements, if necessary, VOIs were minimally moved or reduced in size to avoid overlap with cortical bone.

Molecular Analyses

Alterations in genes described in OncoKB, a precision oncology knowledge base, were extracted from the genomic data of all successfully sequenced biopsies and categorized as level 1, 2, 3, or 4 alterations, based on available (clinical) evidence [20]. In addition, PTEN deletions were extracted because these might also be actionable with protein kinase B inhibitors [2].

Processing and Analysis of WGS

We requested the WGS data from the Hartwig Medical Foundation for prostate cancer patients (Erasmus MC and Radboud UMC) with bone metastasis who had successfully undergone a ^{68}Ga -PSMA-guided biopsy and passed all pre- and post-WGS quality metrics ($n=40$). These quality metrics consisted of a minimum tumor-cell percentage ($\geq 30\%$) as estimated by an expert pathologist, sufficient DNA yield, and an estimated in silico tumor-cell purity of at least 15%. Sample acquisition, library preparations, sequencing protocols, and processing (alignment, quality control, mutational calling, and others) were performed as part of the CPCT-02 study and have been described previously (21,22). In addition, GISTIC2 (version 2.0.23) (23) was performed to determine recurrent and high-level amplifications or deletions of chromosomal regions: `gistic2 -b <output> -seg`

```
<segments> -refgene <hg19 UCSC> -genegistic 1 -gcm extreme -maxseg 4000 -broad 1
-brlen 0.98 -conf 0.95 -rx 0 -cap 3 -saveseg 0 -armpeel 1 -smallmem 0 -res 0.01 -ta 0.1
-td 0.1 -savedata 0 -savegene 1 -qvt 0.1.
```

Furthermore, we reannotated the somatic single-nucleotide, insertion/deletion, and multiple nucleotide variants with a variant-effect predictor using ENSEMBL annotations (ensembl-vep 95.1) (24) for GRCh37 and determined the overlap of genomic annotations based on GENCODE (version 30) (25) on copy-number alterations (GISTIC2) and structural variants. Per the somatic variant (at a nucleotide level), we selected the most deleterious coding effect per overlapping transcript; if a transcript had 2 or more coding mutations, these were summarized as “multiple mutations.”

Identification of Driver Genes and Clinically Actionable Somatic Events.

Potential driver genes were determined by unbiased selection using dndscv (0.0.1.0) (26), which detected genes under negative or positive mutational selection (qglobal_cv or qallsubs_cv ≤ 0.1) and by GISTIC2 (23) focal copynumber-peak discovery on cohortwide copy-number alterations (q ≤ 0.1) with GENCODE (version 30) annotations (25). This list of potential driver genes was complemented with detected driver genes based on the CPCT-02 pan-cancer study (21). Structural variants potentially leading to known gene fusions involving TMPRSS2, ETV, ERG, or FLI1 were summarized as ETS fusions. Somatic events (coding mutations, MSI, deep gain/deletions, and structural variants) were reviewed in OncoKB (20) (version of June 21, 2019) to assess any clinically actionable events. All molecular analyses were performed with the statistical language platform R (version 3.6.1) (27)

Statistical Analyses

Depending on normality distribution, the unpaired t-test or Mann-Whitney U test was used to test for differences between clinical variables (age, Gleason score, haemoglobin, ALP, LDH, and PSA), imaging variables (HU_{mean} , HU_{max} , SUV_{mean} , and SUV_{max}), and primary outcome of biopsy (≥30% tumor). To test for differences between the summed Gleason score (<8 and ≥8) and primary outcome, a Chi-square test was used. The three ⁶⁸Ga-PSMA uptake categories (hit, borderline, miss) were compared for tumor positivity (≥30% tumor) using the Chi-square for trend test. For SUV at the biopsy location, the three biopsy outcome groups were compared using the Kruskal-Wallis test in combination with Dunn’s multiple comparisons test. Univariate and multivariate regression analyses were performed to evaluate relations between variables and primary outcome. For these analyses all non-normal distributed variables were log-transformed prior to testing. Since normal distribution was not reached for LDH by log-transformation, LDH was categorized in normal LDH (<250) and elevated (≥250) and a Chi-square test was

used to test for an association with biopsy outcome. Univariate logistic regression analysis tested for any association between continuous variables and primary outcome. Subsequently, significantly associated variables were selected for multivariate logistic regression analysis. Due to the relatively small sample size, the most significant variables of HU (mean or max) and SUV (mean or max) were selected for multivariate testing. No correction was set for multiplicity of secondary endpoints. Odds for a positive biopsy were calculated by logistic regression for SUV and HU. For the area under the curve and receiver operating characteristic curve, the logarithm of odds was calculated. Receiver operating characteristic curves were calculated for HU_{mean} and SUV_{max}. All statistical tests were performed two-sided. A p-value of ≤ 0.05 was considered statistically significant.

RESULTS

Biopsy Selection

Between December 2014 and June 2018, 115 bone biopsies from 103 patients with mPC were obtained within CPCT-02 in Erasmus Medical Center and Radboud University Medical Center. For 71 biopsies (62%), ^{68}Ga -PSMA PET/CT was performed beforehand to identify bone metastases, whereas 44 biopsies (38%) within CPCT-02 were preceded by other imaging modalities. Two out of 71 ^{68}Ga -PSMA guided biopsies (3%) were not eligible because of a failed biopsy procedure and more than 12 weeks between imaging and biopsy. In total, 69 ^{68}Ga -PSMA guided biopsies, from 60 individual patients, were eligible for primary analysis to determine the success rate of ^{68}Ga -PSMA guided bone biopsies (Fig. 1). Seven patients underwent two ^{68}Ga -PSMA guided bone biopsies. One patient underwent three ^{68}Ga -PSMA guided bone biopsies. Median time between ^{68}Ga -PSMA PET/CT and the biopsy procedure was nine days (interquartile range 3-22).

Clinical Characteristics and Success Rate of ^{68}Ga -PSMA Guided Biopsies

The clinical characteristics of patients and biopsies are described in Table 1. Biopsies were primarily performed in the castration resistant setting (97%, N=67) and most commonly obtained from the pelvis (N=57, 83%). During the procedure, biopsies were performed unguided (N=5, 7%), or guided by ultrasound (N=1, 1%), or CT (N=63, 91%), based on the interventional radiologist's decision. During one biopsy procedure (1%), excessive bleeding, which was directly controlled by manual pressure, occurred.

On the basis of tumor percentage ($\geq 30\%$) in at least one core, 48 out of 69 (70%) ^{68}Ga -PSMA guided biopsies (44 out of 60 individual patients (73%)) were eligible for molecular analyses. No significant differences were found in age ($p=0.42$), Gleason score ($p=0.46$) and baseline laboratory findings (Hb $p=0.54$, PSA $p=0.36$, ALP $p=0.56$) between biopsies

with tumor percentage <30% and ≥30%, although elevated LDH levels were seen with borderline significance in the group with a successful biopsy ($p=0.05$). In the univariate logistic regression analysis, none of these variables were associated with biopsy outcome (data not shown). The success rate of biopsies obtained from pelvis ($N=57$, 83%), spine ($N=6$, 9%), and other locations ($N=6$, 9%) was 65%, 100% and 83%, respectively.

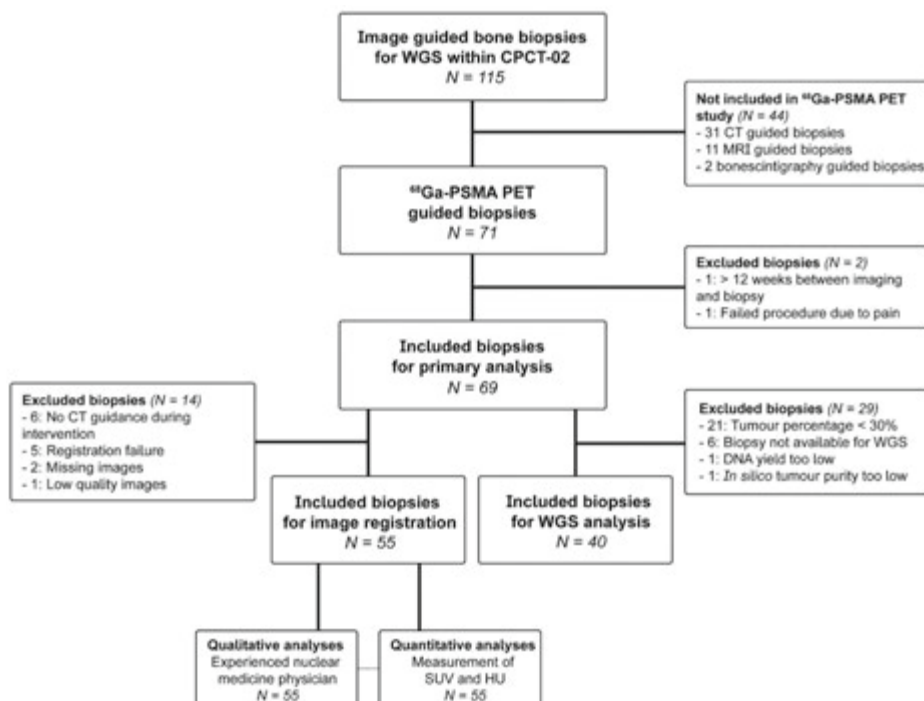


Figure 1. Flowchart of included ⁶⁸Ga-PSMA guided bone biopsies for primary and secondary analyses of the current PET study within CPCT-02. WGS: whole genome sequencing, SUV: standardized uptake value, HU: Hounsfield Units

Table 1. Clinical characteristics at time of ⁶⁸Ga-PSMA-guided bone biopsy

Characteristic	⁶⁸ Ga-PSMA guided bone biopsies (n= 69)
Location of bone biopsy	
Pelvis	57 (82.6%)
Spine	6 (8.7%)
Rib	3 (4.3%)
Extremity	3 (4.3%)
Location of bone biopsy irradiated	3 (4.3%)
Age at biopsy (y) (mean ± SD)	68.5 ± 8.3
Gleason score at primary diagnosis	
8	22 (31.9%)
≥8	39 (56.5%)
Unknown	8 (11.6%)
Prior local treatment (n,%)	
Radical prostatectomy	15 (21.7%)
External radiotherapy prostate	16 (32.2%)
Brachytherapy	1 (1.4%)
Hormone status at time of biopsy (n,%)	
mHSPC	2 (2.9%)
mCRPC	67 (97.1%)
Prior second generation ADT (n,%)	
Abiraterone	23 (33.3%)
Enzalutamide	34 (49.2%)
Prior chemotherapy (n,%)	
Docetaxel	49 (71%)
Cabazitaxel	19 (27.5%)
Estramustine	1 (1.4%)
Prior radiotherapy (n,%)	
²²³ Radium	5 (7.2%)
External radiotherapy metastatic site	21 (30.4%)
Laboratory values at time of biopsy	
Hemoglobin (mmol/L) (n=67)	8.0 (5.3 - 9.5)
Leukocytes (x10 ⁹ /L) (n=62)	6.5 (3.6 - 13.2)
Thrombocytes (x10 ⁹ /L) (n=65)	232 (122 – 576)
Alkaline phosphatase (U/L) (n=59)	123 (43 – 4598)
LDH (U/L) (n=53)	233 (152 – 2718)
PSA (ug/L) (n=63)	96 (0.14 – 2375)

mHSPC: metastatic hormone sensitive prostate cancer; mCRPC: metastatic castration resistant prostate cancer; ADT: androgen deprivation therapy; LDH: lactate dehydrogenase; PSA: prostate-specific antigen.

Qualitative data are numbers followed by percentages in parentheses; continuous data are median followed by range in parentheses or mean ± SD

⁶⁸Ga-PSMA Uptake and Radiodensity at Biopsy Site

To evaluate whether biopsies were accurately obtained from lesions with high ⁶⁸Ga-PSMA uptake, ⁶⁸Ga-PSMA PET/CT was co-registered with interventional CT (Fig. 2a-d) for qualitative and quantitative analyses (Fig. 1). For 55 biopsies, rigid body image registration could be performed adequately (Fig. 1). Based on the rigid body image registrations, 33 biopsies were categorized as hit, 11 biopsies as borderline, and 11 biopsies as miss (Fig. 3a). As expected, biopsy sites categorized as hit had higher SUV_{max} and SUV_{mean} compared with biopsy sites categorized as miss ($p < 0.001$ for both) (Fig. 3b-c). Subsequently, the correlation between ⁶⁸Ga-PSMA uptake and biopsy outcome was evaluated. At biopsy sites categorized as hit, borderline or miss for ⁶⁸Ga-PSMA uptake, 70%, 64%, and 36% of biopsies were tumor positive ($\geq 30\%$), respectively ($p = 0.0610$, Fig. 3a).

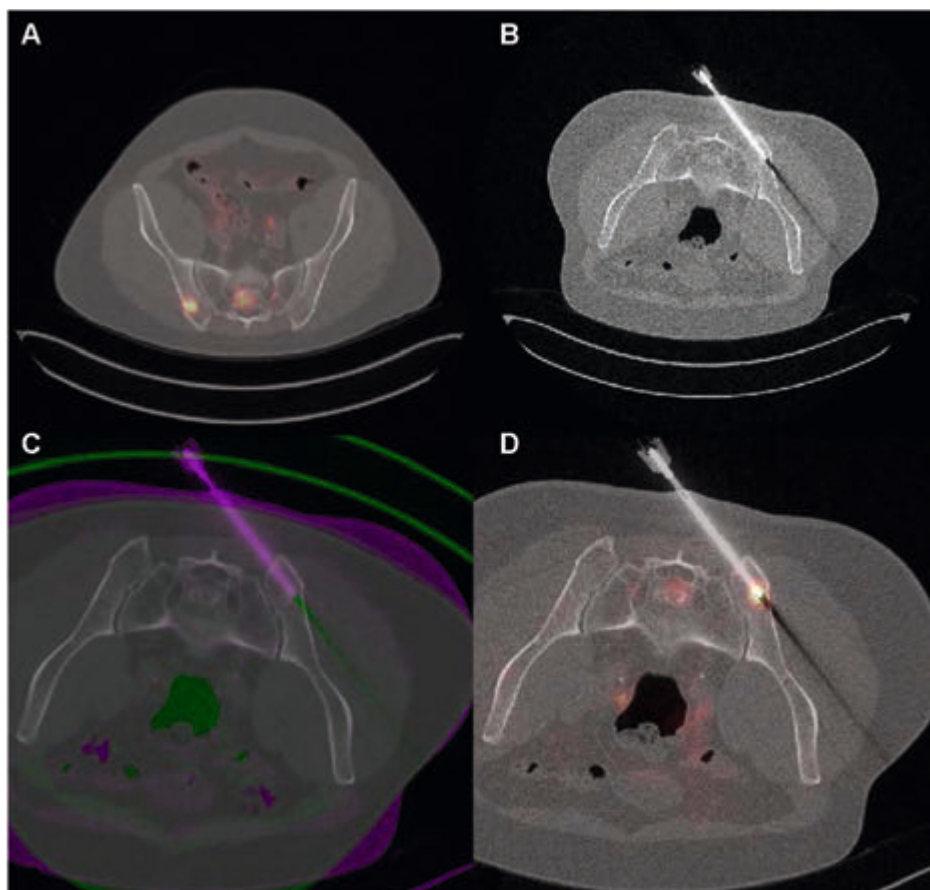


Figure 2. Rigid-body image registration of ⁶⁸Ga-PSMA PET/CT and interventional CT visualizes biopsy needle on ⁶⁸Ga-PSMA PET and enables measurement of ⁶⁸Ga-PSMA uptake and radiodensity at biopsy site. (A) ⁶⁸Ga-PSMA PET/CT, before biopsy. (B) CT, acquired during biopsy procedure. (C) Coregistration of ⁶⁸Ga-PSMA PET/CT and interventional CT. (D) Visualization of biopsy needle on ⁶⁸Ga-PSMA PET/CT.

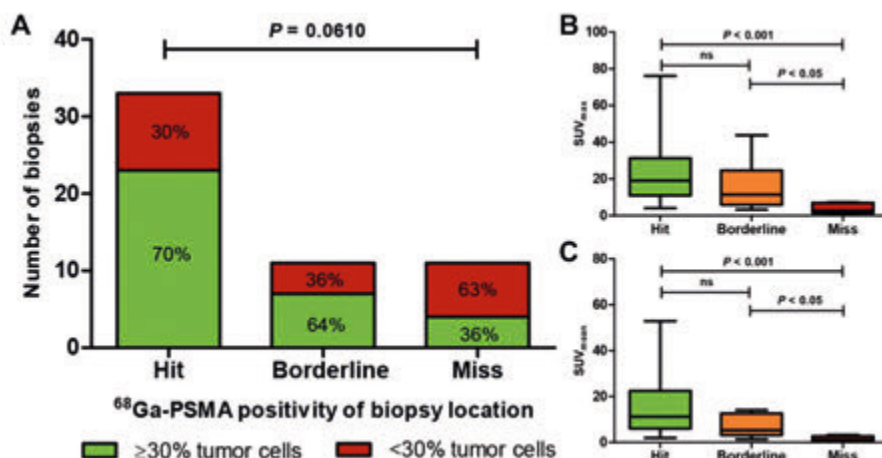


Figure 3. ^{68}Ga -PSMA uptake at biopsy sites (A) Biopsy sites were categorized as hit (^{68}Ga -PSMA positive), borderline or miss (^{68}Ga -PSMA negative) by masked nuclear medicine physician and correlated to tumor percentage ($\geq 30\%$ vs $< 30\%$). There were 55 biopsies and Chi-square for trend test was performed. (B) SUV_{max} at biopsy site, categorized by ^{68}Ga -PSMA uptake score. There were 55 biopsies and Kruskal-Wallis was performed in combination with Dunn multiple comparisons test. (C) SUV_{mean} at biopsy site, categorized by ^{68}Ga -PSMA uptake score. There were 55 biopsies and Kruskal-Wallis was performed in combination with Dunn multiple comparisons test. ns= not statistically significant.

At biopsy sites with tumor percentage $\geq 30\%$, median ^{68}Ga -PSMA uptake was significantly higher (SUV_{max} 20.9, inter quartile range [IQR] 10.0-32.1; SUV_{mean} 10.3, IQR 3.4-18.7), whereas median ^{68}Ga -PSMA uptake was lower at biopsy sites with tumor percentage $< 30\%$ (SUV_{max} 6.7, IQR 3.7-14.2; SUV_{mean} 3.4, IQR, 1.8-9.1; $p=0.0021$ and $p=0.0123$, respectively) (Figs. 4a-b). In contrast, median radiodensity on CT was significantly lower at biopsy sites with tumor percentage $\geq 30\%$ (HU_{max} 786, IQR 600-977; HU_{mean} 294, IQR 184-473) as compared to biopsy sites with tumor percentage $< 30\%$ (HU_{max} 1019, IQR 780-1132; HU_{mean} 524, IQR 296-738; $p=0.0266$ and $p=0.0064$, respectively) (Figs. 4c-d). In univariate logistic regression analysis, SUV and HU values were also significantly associated with biopsy outcome (SUV_{max} $p=0.008$, SUV_{mean} $p=0.016$, HU_{mean} $p=0.006$, and HU_{max} $p=0.037$) (Supplemental Table 1a). After stepwise multivariate analysis, HU_{mean} and SUV_{max} resulted in an odds ratio of 0.995 (95%CI 0.992-0.998, $p=0.003$) and 11.737 (95%CI 2.258-60.996, $p=0.003$), respectively (Supplemental Table 1b). Receiver operating characteristic curves of HU_{mean} and SUV_{max} for successful biopsies had an area under the curve of 0.70 and 0.84, respectively (Supplemental Fig. 1).

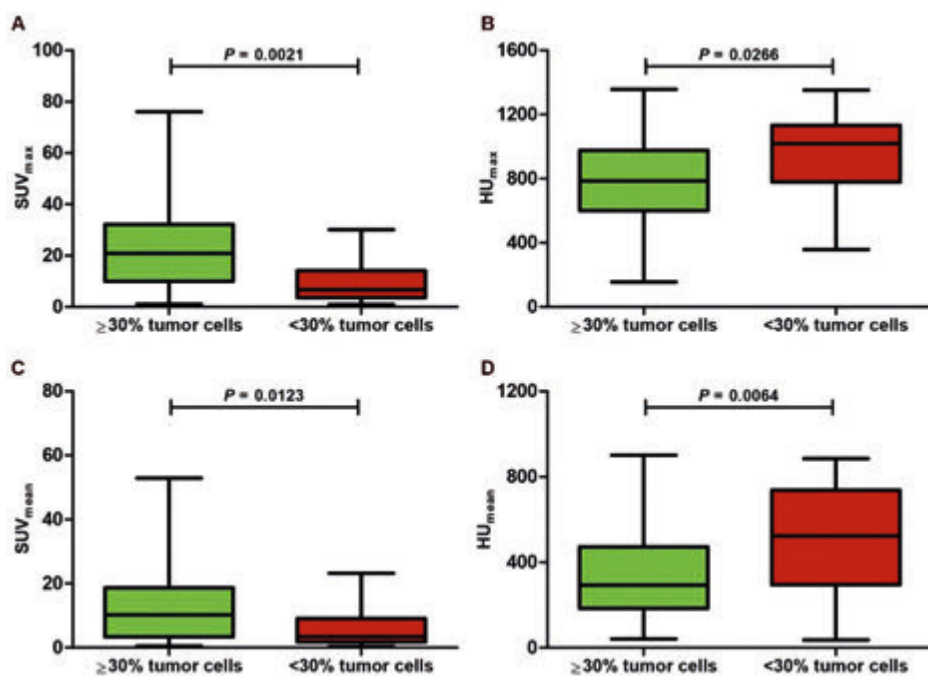


Figure 4. ⁶⁸Ga-PSMA uptake (SUV) and radiodensity (HU) in biopsies with tumor percentage ≥30% and <30%. (A) SUV_{max}, (B) SUV_{mean}, (C) HU_{max}, (D) HU_{mean}. There were 55 biopsies and Mann Whitney test was performed for all parameters. SUV: standardized uptake values, HU: Hounsfield Units.

Clinical Impact of ⁶⁸Ga-PSMA Guided Bone Biopsies for Molecular Analyses

Forty out of 48 positive biopsies (83%) were successfully used for WGS (Fig. 1). Median *in silico* tumor purity of the successfully sequenced samples was 55% (range 17-94%) (Supplemental Fig. 2) [20-27]. In total, 53 actionable somatic alterations were detected in 73% (n=29) of the successfully sequenced biopsies (Fig. 5). Forty-one actionable somatic alterations, detected in 21 biopsies, were described in the OncoKB database as level 1 (n=9, 22%), level 2 (n=4, 10%), level 3 (n=13, 32%), and level 4 (n=15, 37%) [20]. Twelve biopsies (30%) contained a deep *PTEN* deletion, which is not (yet) included in the OncoKB database, but might be actionable with protein kinase B inhibitors [2]. The genomic landscape of metastatic castration resistant prostate cancer, including this subset of biopsies, has been described in detail by Van Dessel et al.[22].

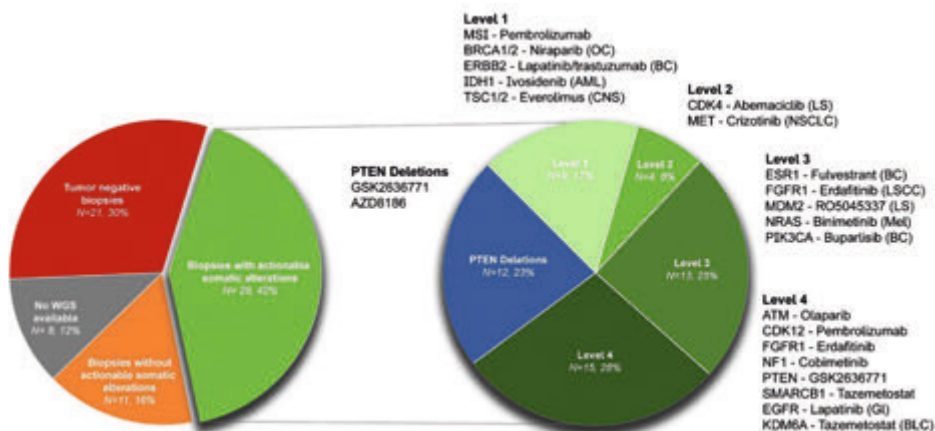


Figure 5 Actionable somatic alterations, detected by WGS, in ^{68}Ga -PSMA PET-guided bone biopsies from metastatic prostate cancer patients. Genes with actionable somatic alterations are categorized by level of evidence for targeted therapy as described in the OncoKB database. Evidence for both prostate cancer and other malignancies was combined within one category. Level 1: Food and Drug Administration (FDA)-recognized biomarker predictive of response to FDA-approved drug. Level 2: Standard-care biomarker predictive of response to FDA-approved drug. Level 3: Compelling clinical evidence supports the biomarker as being predictive of response to a drug. Level 4: Compelling biological evidence supporting biomarker as being predictive of response to drug. For every altered gene, example of targeted therapy suitable for specific alteration was described. WGS= whole genome sequencing, OC= ovarian cancer, BC= breast cancer, AML= acute myeloid leukemia, CNS= central nervous system cancer, LS= liposarcoma, NSCLC= non-small cell lung cancer, LSCC= lung squamous cell carcinoma, Mel= melanoma, GI= glioma, BLC= bladder cancer.

DISCUSSION

In this comprehensive PET study, we show that 70% of ^{68}Ga -PSMA guided bone biopsies provide sufficient quality for molecular analyses. Our findings indicate that ^{68}Ga -PSMA guided bone biopsies are more successful than bone biopsies with CT-guidance only, that have a reported success rate for molecular analysis of only 36.5-44% in patients with mPC [7,8,10]. With 70% of the biopsies being successful for molecular analyses, the success rate approximates the overall success rate of 76.5% for 3655 biopsies within the CPCT-02 study, which mainly included non-skeletal biopsies [21]. For objective analyses of the success rate of ^{68}Ga -PSMA guided bone biopsies, we applied rigid body image registration, which confirmed that the majority of biopsies was accurately obtained from a lesion with high ^{68}Ga -PSMA uptake. In addition, there was a trend towards a higher percentage of tumor positive biopsies in the hit group. For biopsies with a tumor percentage of $\geq 30\%$, ^{68}Ga -PSMA uptake was significantly higher than for biopsies with a tumor percentage of $< 30\%$. In contrast, HU values on CT were lower for biopsies with a tumor percentage of $\geq 30\%$ than for biopsies with a tumor percentage of $< 30\%$. The higher success rate of biopsies from bone lesions with lower HU values has also been

reported by two other studies [7,8], indicating that osteosclerotic lesions with high HU values contain less viable tumor cells. With an area under the curve of 0.84 and 0.70, both SUV_{max} and HU_{mean} were strong predictors for a positive biopsy. In the absence of ⁶⁸Ga-PSMA PET/CT, it might therefore be advisable to obtain biopsies from less sclerotic lesions with lower HU. The high frequency of actionable alterations, found in this study, emphasizes the medical need for a high success rate of bone biopsies. Within the CPCT-02 trial, potentially actionable alterations, identified by WGS of the tumor biopsy, were shared with the patient to enable targeted treatment in, for example, the Drug Rediscovery Protocol (NCT02925234). According to this protocol, patients are treated with approved, off-label targeted agents based on the molecular characteristics of the tumor. First results are promising with clinical benefit for multiple treatment cohorts [28].

Because ⁶⁸Ga-PSMA PET is becoming increasingly widely available in current clinical practice, it can be easily implemented to improve the success rate of bone biopsies. By optimizing the first step of the pipeline for molecular diagnostics, ⁶⁸Ga-PSMA PET significantly contributes to improved genomic characterization of mPC. Although the current study shows a high success rate, there are a few limitations of ⁶⁸Ga-PSMA guided bone biopsies for molecular diagnostics. First, tumor heterogeneity might be better reflected by molecular analyses of liquid biopsies than by WGS of tumor tissue from a single lesion. However, techniques for detailed molecular analyses of liquid biopsies are still under development, whereas WGS of tissue biopsies is currently more feasible. Second, PSMA expression has high inter- and intra-patient heterogeneity [29]. High PSMA expression is associated with defective DNA damage repair and PTEN loss, whereas patients with low ⁶⁸Ga-PSMA expression have poor survival [29-31]. Since bone biopsies in this study were not obtained from metastases with low ⁶⁸Ga-PSMA uptake, these sites are underrepresented in the current study. In addition, there were some notable results. First, four biopsies that were scored as miss (⁶⁸Ga-PSMA negative) did contain $\geq 30\%$ tumor cells (false negative). As these biopsies were all close to a ⁶⁸Ga-PSMA positive lesion, these false negative results may be due to patients' movements and/or different spatial resolution between scans. Although most biopsies were accurately obtained from lesions with high ⁶⁸Ga-PSMA uptake, guidance might be further optimized by real-time visualization of ⁶⁸Ga-PSMA uptake, though this is technically and logistically more challenging. Second, in five biopsies, all of which were obtained from spine or ribs, image registration failed. This image registration failure at non-pelvic sites may be explained by the rigid body algorithm, which relies on the assumption that the spine and rib cage are rigid bodies. As the rigid body algorithm was only applied for image analyses in this study, this limitation will not impact the feasibility of ⁶⁸Ga-PSMA guided biopsies from non-pelvic sites in clinical practice.

CONCLUSION

^{68}Ga -PSMA guided bone biopsies have a 70% success rate for molecular analyses in mPC patients, indicating that ^{68}Ga -PSMA PET/CT has added value to increase the success rate of CT-guided bone biopsies. In successful ^{68}Ga -PSMA guided biopsies, whole genome sequencing identified numerous targetable mutations, emphasizing the potential clinical impact of ^{68}Ga -PSMA guided bone biopsies in mPC patients.

SUPPLEMENTARY INFORMATION

Supplemental materials are available at <https://doi.org/10.2967/jnumed.119.241109>

REFERENCES

1. Bray F, Ferlay J, Soerjomataram I, Siegel RL, Torre LA, Jemal A. Global cancer statistics 2018: GLOBOCAN estimates of incidence and mortality worldwide for 36 cancers in 185 countries. *CA Cancer J Clin*. 2018;68:394-424.
2. de Bono JS, De Giorgi U, Rodrigues DN, et al. Randomized phase II study evaluating AKT Blockade with ipatasertib, in combination with abiraterone, in patients with metastatic prostate cancer with and without PTEN Loss. *Clin Cancer Res*. 2019;25:928-936.
3. Mateo J, Carreira S, Sandhu S, et al. DNA-repair defects and olaparib in metastatic prostate cancer. *N Engl J Med*. 2015;373:1697-1708.
4. Abida W, Cheng ML, Armenia J, et al. Analysis of the prevalence of microsatellite instability in prostate cancer and response to immune checkpoint blockade. *JAMA Oncol*. 2019;5:471-478.
5. Halabi S, Kelly WK, Ma H, et al. Meta-analysis evaluating the impact of site of metastasis on overall survival in men with castration-resistant prostate cancer. *J Clin Oncol*. 2016;34:1652-1659.
6. Bubendorf L, Schopfer A, Wagner U, et al. Metastatic patterns of prostate cancer: an autopsy study of 1,589 patients. *Hum Pathol*. 2000;31:578-583.
7. Holmes MG, Foss E, Joseph G, et al. CT-guided bone biopsies in metastatic castration-resistant prostate cancer: factors predictive of maximum tumor yield. *J Vasc Interv Radiol*. 2017;28:1073-1081.
8. Spritzer CE, Afonso PD, Vinson EN, et al. Bone marrow biopsy: RNA isolation with expression profiling in men with metastatic castration-resistant prostate cancer--factors affecting diagnostic success. *Radiology*. 2013;269:816-823.
9. McKay RR, Zukotynski KA, Werner L, et al. Imaging, procedural and clinical variables associated with tumor yield on bone biopsy in metastatic castration-resistant prostate cancer. *Prostate Cancer Prostatic Dis*. 2014;17:325-331.
10. Sailer V, Schiffman MH, Kossai M, et al. Bone biopsy protocol for advanced prostate cancer in the era of precision medicine. *Cancer*. 2018;124:1008-1015
11. Coleman RE. Clinical features of metastatic bone disease and risk of skeletal morbidity. *Clin Cancer Res*. 2006;12:6243s-6249s.
12. Perera M, Papa N, Christidis D, et al. Sensitivity, specificity, and predictors of positive (68) Ga-prostate-specific membrane antigen positron emission tomography in advanced prostate cancer: a systematic review and meta-analysis. *Eur Urol*. 2016;70:926-937.
13. Lecouvet FE, Oprea-Lager DE, Liu Y, et al. Use of modern imaging methods to facilitate trials of metastasis-directed therapy for oligometastatic disease in prostate cancer: a consensus recommendation from the EORTC Imaging Group. *Lancet Oncol*. 2018;19:e534-e545.
14. van Steenbergen TRF, Smits M, Scheenen TWJ, et al. (68)Ga-PSMA-PET/CT and diffusion MRI targeting for cone-beam CT-guided bone biopsies of castration-resistant prostate cancer patients. *Cardiovasc Intervent Radiol*. 2020;43:147-154.
15. Bins S, Cirkel GA, Gadellaa-Van Hooijdonk CG, et al. Implementation of a multicenter bio-banking collaboration for next-generation sequencing-based biomarker discovery based on fresh frozen pretreatment tumor tissue biopsies. *Oncologist*. 2017;22:33-40.

16. Boellaard R, Oyen WJG, Giammarile F, et al. FDG PET/CT: EANM procedure guidelines for tumour imaging: version 2.0. *Eur J Nucl Med Mol Imaging*. 2015;42:328-354.
17. Shamonin DP, Bron EE, Lelieveldt BP, et al. Fast parallel image registration on CPU and GPU for diagnostic classification of Alzheimer's disease. *Front Neuroinform*. 2014;7:50.
18. Klein S, Staring M, Murphy K, Viergever MA, Pluim JP. Elastix: a toolbox for intensity based medical image registration. *IEEE Trans Med Imaging*. 2010;29:196-205
19. Lowekamp BC, Chen DT, Ibáñez L, Blezek D. The design of SimpleITK. *Front Neuroinform*. 2013;7:45.
20. Chakravarty D, Gao J, Phillips SM, et al. OncoKB: A precision oncology knowledge base. *JCO Precis Oncol*. 2017;2017.
21. Priestley P, Baber J, Lolkema MP, et al. Pan-cancer whole-genome analyses of metastatic solid tumours. *Nature*. 2019;575:210-216.
22. Van Dessel LF, van Riet J, Smits M, et al. The genomic landscape of metastatic castration-resistant prostate cancers using whole genome sequencing reveals multiple distinct genotypes with potential clinical impact. *Nat Commun*. 2019;10:5251.
23. Mermel CH, Schumacher SE, Hill B, Meyerson ML, Beroukhi R, Getz G. GISTIC2.0 facilitates sensitive and confident localization of the targets of focal somatic copy-number alteration in human cancers. *Genome Biol*. 2011;12:R41.
24. McLaren W, Gil L, Hunt SE, et al. The Ensembl Variant Effect Predictor. *Genome Biol*. 2016;17:122.
25. Harrow J, Frankish A, Gonzalez JM, et al. GENCODE: the reference human genome annotation for The ENCODE Project. *Genome Res*. 2012;22:1760-1774.
26. Martincorena I, Raine KM, Gerstung M, et al. Universal patterns of selection in cancer and somatic tissues. *Cell*. 2017;171:1029-1041.
27. R Core Team. R: A language and environment for statistical computing [computer program]. 2017. <http://www.R-project.org/>
28. Van der Velden DL, Hoes LR, Van der Wijngaart H, et al. The drug rediscovery protocol facilitates the expanded use of existing anticancer drugs. *Nature*. 2019;574: 127–131.
29. Paschalis A, Sheehan B, Riisnaes R, et al. Prostate-specific membrane antigen heterogeneity and DNA repair defects in prostate cancer. *Eur Urol*. 2019;76:469-478.
30. Wang B, Gao J, Zhang Q, et al. Diagnostic value of ⁶⁸Ga-PSMA PET/CT for detection of PTEN expression in prostate cancer: a pilot study. *J Nucl Med*. 2019; Epub ahead of print.
31. Thang S, Violet J, Sandhu S, et al. Poor outcomes for patients with metastatic castration-resistant prostate cancer with low prostate-specific membrane antigen (PSMA) expression deemed ineligible for ¹⁷⁷Lu-labelled PSMA radioligand therapy. *Eur Urol Oncol*. 2019;2:670-676



CHAPTER 3

PRIOR PSMA PET-CT IMAGING AND HOUNSFIELD UNIT IMPACT ON TUMOR YIELD AND SUCCESS OF MOLECULAR ANALYSES FROM BONE BIOPSIES IN METASTATIC PROSTATE CANCER

Minke Smits *
Samhita Pamidimarri Naga
Michiel J. P. Sedelaar
James Nagarajah
Winald R. Gerritsen
Niven Mehra

Kamer Ekici *
Inge M. van Oort
Jack A. Schalken
Tom W. J. Scheenen
Jurgen J. Fütterer

* These authors contributed equally to this work.

Cancers (Basel). 2020;12(12)

ABSTRACT

Developing and optimizing targeted therapies in metastatic castration-resistant prostate cancer (mCRPC) necessitates molecular characterization. Obtaining sufficient tumor material for molecular characterization has been challenging. We aimed to identify clinical and imaging variables of imaging-guided bone biopsies in metastatic prostate cancer patients that associate with tumor yield and success in obtaining molecular results, and to design a predictive model. Clinical and imaging data were collected retrospectively from patients with prostate cancer who underwent a bone biopsy for histological and molecular characterization. Clinical characteristics, imaging modalities and imaging variables, were associated with successful biopsy results. In our study, we included a total of 110 bone biopsies. Histological conformation was possible in 84 of all biopsies, of which in 73 of 84 successful molecular characterization was performed. Prior use of PSMA-PET/CT resulted in higher success rates in histological and molecular successful biopsies compared to CT or MRI. Evaluation of spine biopsies showed more often successful results compared to other locations for both histological and molecular biopsies ($p=0.027$ and $p=0.012$, respectively). Low Hounsfield Units (HU) and Deviation (Dev), taken at CT-guidance, were associated with histological successful biopsies ($p=0.025$ and $p=0.023$, respectively) and with molecular successful biopsies ($p=0.010$ and $p=0.006$, respectively). A prediction tool combining low HU and low Dev resulted in significantly more successful biopsies, histological and molecular ($p=0.023$ and $p=0.007$, respectively). Based on these results we concluded that site selection for metastatic tissue biopsies with prior PSMA-PET/CT imaging improves the chance of a successful biopsy. Further optimization can be achieved at CT-guidance, by selection of low HU and low Dev lesions. A prediction tool is provided to increase the success rate of bone biopsies in mCRPC patients, which can easily be implemented in daily practice.

INTRODUCTION

Prostate cancer is currently the most common cancer in developed countries and the fifth leading cause of death in men worldwide [1]. Despite optimal initial treatment of the primary prostate cancer, men still will develop metastatic prostate cancer [2,3], currently an incurable disease. Following resistance to androgen-deprivation therapy, metastatic castration-resistant prostate cancer (mCRPC) develops, a heterogeneous disease state showing substantial inter-individual genomic diversity [4,5]. Validated molecular biomarkers to help personalize and guide treatment selection are therefore of major importance [6]. Determination of druggable aberrations and pathways in metastatic prostate cancer include DNA repair, e.g. genes involved in DNA damage sensing, homologous recombination, mismatch repair, as well as the PI3K pathway. Molecular characterization of mCRPC moreover contributes to the understanding of treatment resistance and includes assessment of androgen receptor (AR) splice variants, AR structural variants and mutations. Currently, tissue-based techniques like immunohistochemistry (IHC), RNA in situ hybridization (RNAish), and next-generation sequencing (NGS) are current tools to personalize and optimize treatment for patients with mCRPC.

To individualize patient care through profiling of a fresh prostate cancer metastasis, the first step is to obtain sufficient and high quality tumor material for IHC and molecular studies. Prostate cancer often metastasizes to the bones solely (43%) or predominantly (73%) [7,8]. Although a biopsy from soft tissue (nodal and visceral metastases) often provides a sufficient tumor yield [9], obtaining enough tumor cells from a bone biopsy proves more challenging, in part due to technical difficulties regarding biopsy procedure from sclerotic bone metastases, and in identifying bone lesions containing predominant cancerous tissue [10,11]. This is one of the reasons that bone metastatic prostate cancer has been underrepresented in most genomic landscape manuscripts [12-14], and underrepresented in biomarker-selected clinical trials, mandating fresh tissue biopsies. Previous studies indicated success rates, defined as any tumor cells found, between 25.5% and 85.7% and have aimed to assess factors influencing tumor yield from bone biopsies [9,15-20]. These variables include level of prostate specific antigen (PSA), lactate dehydrogenase (LDH), and Hounsfield units derived from pre-biopsy computed tomography (CT).

Optimal bone-biopsy site selection is deterministic of a successful outcome. The osseous site of choice is commonly determined by visual inspection of pre-biopsy CT, bone scintigraphy, MRI scan and since recently the prostate-specific membrane antigen (PSMA) positron-emission tomography (PET). In our institute, patients referred for a

biopsy are discussed in a weekly multidisciplinary meeting, where a radiologist and/or nuclear physician determine optimal biopsy site. We observed that since the introduction of PSMA-PET/CT imaging, rates of successful bone biopsies increased, with higher yields of adequate tissue.

In a recently published multicenter study [21] a high success rate of 70% for molecular analyses of Gallium-68 (^{68}Ga) PSMA-PET selected bone lesions in metastatic prostate cancer patients was showed. The SUV was found to be a predictive variable. One of the limitations of this study was that no comparisons were made with a group of patients that received a bone biopsy pre-biopsy selected by alternative imaging modalities.

This retrospective study was performed to compare the success rate of ^{68}Ga -PSMA-PET for biopsy site selection, in comparison to other imaging modalities, and to identify additional predictors that may strongly associate with tumor yield in bone biopsies. This included additional pre-biopsy and biopsy variables, including Hounsfield and deviation, extracted from the CT-guidance biopsy. Based on these data we aimed to design a simple prediction model that could be used in daily clinical practice.

RESULTS

Study population

A total of 99 patients with a total number of 114 biopsies were considered for selection in this retrospective study. After exclusion a total number of 110 biopsies from 96 patients were included for this study (figure 1). 29 out of 62 bone biopsies with a prior PSMA-PET/CT scan were also included in our previous publication [21]. Baseline patient characteristics are summarized in table 1. The overall success percentage for histological confirmation of prostate cancer in the biopsies was 76.4% (84 out of 110 biopsies). Successful molecular characterization was performed in 66.4% of all biopsies and in 86.9% of biopsies with histological confirmation of prostate cancer. There were no procedural complications.

Clinical parameters

The mean age at biopsy was 67 years (interquartile range [IQR]: 48-82). Seven men had hormone sensitive prostate cancer at the time of biopsy. No statistically significant differences were found between the groups in age, hormone status, GS and prior radiotherapy (table 1).

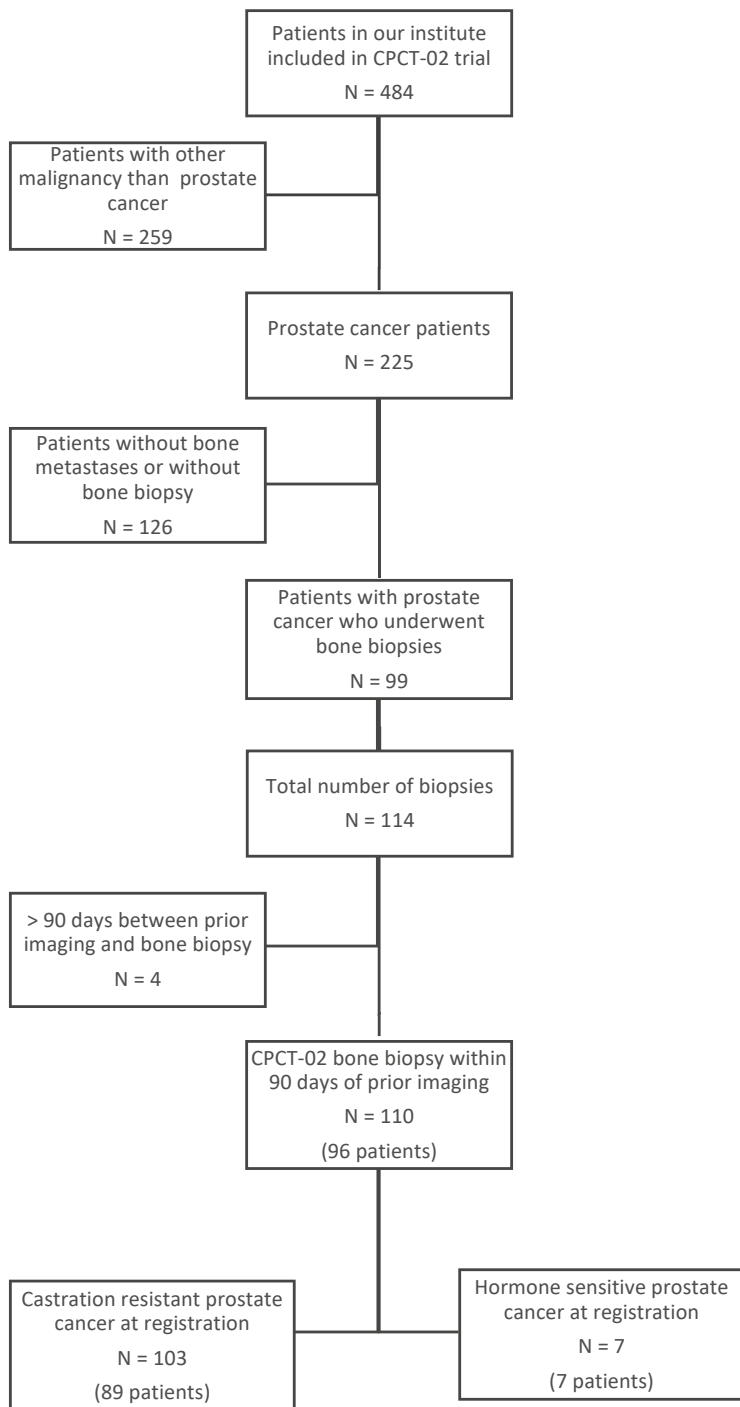


Figure 1. Flowchart.

Table 1. Clinical characteristics and denominators of total biopsies.

	No tumor cells detected	Tumor cells present	p-Value*	Insufficient tumor yield (<30%)	Sufficient tumor yield for molecular analysis (≥30%)	p-Value*
	Median (q1-q3) or percent				Median (q1-q3) or percent	
Total		76.4% (84/110)			66.4% (73/110) 86.9% (73/84)	
Age at the time of biopsy (years)	65.0 (58.0-72.3)	68.0 (62.0-73.0)	p=0.281	65.0 (59.5-71.0)	69.0 (62.0-74.0)	p=0.137
Hormone status at the time of biopsy			p=0.751			p=0.769
HSPC [†]	28.6% (N=2)	71.4% (N=5)		28.6% (N=2)	71.4% (N=5)	
CRPC [‡]	23.3% (N=24)	76.7% (N=79)		34.0% (N=35)	66.0% (N=68)	
Prior radiotherapy on biopsied metastasis			p=0.751			p=0.769
Yes	28.6% (N=2)	71.4% (N=5)		28.6% (N=2)	71.4% (N=5)	
No	23.3% (N=24)	76.7% (N=79)		34.0% (N=35)	66.0% (N=68)	
Gleason score at primary diagnosis			p=0.948			p=0.437
< 8		22/28 (78.6%)			18/28 (64.3%)	
≥ 8		57/72 (79.2%)			52/72 (72.2%)	
Laboratory values						
PSA (ug/L)	38.0 (9.4-110.0)	98.0 (20.5-245.0)	p=0.029	54.0 (12.0-147.5)	95.5 (21.3-315.0)	p=0.126
Alkaline phosphatase (U/L)	109.0 (78.5-140.3)	117.0 (87.0-224.5)	p=0.376	105.0 (78.0-138.0)	128.0 (87.5-232.8)	p=0.100
Albumin (g/L)	34.0 (33.0-36.0)	36.0 (34.0-38.3)	p=0.040	34.0 (33.0-39.0)	36.0 (34.0-38.0)	p=0.567
LDH (U/L)	221.0 (197.8-264.3)	220.0 (180.0-249.0)	p=0.636	220.5 (201.5-264.8)	220.0 (179.0-247.0)	p=0.768
Hemoglobin (mmol/L0	7.9 (7.4-8.3)	7.7 (6.8-8.3)	p=0.376	7.9 (7.1-8.4)	7.7 (6.9-8.3)	p=0.795
Leukocytes (x109/L	6.6 (5.5-7.9)	6.1 (4.8-7.9)	p=0.340	6.0 (5.2-7.4)	6.1 (4.8-8.2)	p=0.910
Thrombocytes (x109/L)	236.0 (202.5-287.5)	234.0 (171.3-284.0)	p=0.550	228.5 (180.5-286.3)	238.0 (184.0-286.0)	p=0.448

*Chi-Squared Test for nominal variables and Mann-Whitney-U Test for continuous variable; †Hormone sensitive prostate cancer; ‡Castration-resistant prostate cancer

PSA and albumin levels differed significantly between patients with histologically successful and negative biopsies ($p=0.029$ and $p=0.040$, respectively, table 1). A non-significantly higher PSA was seen for those patients with a successful molecular biopsy outcome (95.5 vs 54.0; $p=0.126$). Other laboratory values were comparable between groups (table 1).

Imaging and procedural characteristics

Prior imaging with PSMA-PET/CT appeared useful to select site of bone biopsied, as this resulted in a higher proportion of success (85.5% and 72.6% for histological confirmation and successful molecular characterization, respectively) compared to other imaging (63.9% and 58.3% for CT, and 66.7% and 58.3% for MRI, respectively) (table 2). Biopsies from the spine resulted in significant higher proportion of successful biopsies (histological and molecular) compared to other locations: 95.8% and 91.7% for spine vs 72.2% and 59.5% for pelvis and 57.1% and 57.1% for other locations. With regard to features derived from the CT-scan performed at the biopsy procedure, both lower HU and deviation (Dev) resulted in more successful biopsies (histological and molecular; $p=0.025$ and $p=0.010$, resp. for HU; $p=0.023$ and $p=0.006$, resp. for Dev; table 2). Other imaging and procedural characteristics were not significantly different (table 2). Due to high proportion of missing data of needle gauge used (54% missing) and the number of cores taken during biopsy (17% missing) no robust analyses could be performed with these variables.

Uni- and multivariable analyses

Table 3 summarizes the results of the univariate analysis. Patients with prior PSMA-PET/CT were more than three times more likely to have a histological successful biopsy compared to patients with prior CT scan (OR 3.33). Biopsies from the spine were also more likely to have a histological successful and a molecular successful biopsy compared to biopsies from the pelvis (OR 8.88 and OR 7.49, respectively). Both lower HU and Dev were associated with a successful biopsy (histological and molecular) (table 3). On multivariate analysis Dev alone was significantly associated with biopsy result (OR 0.990, $p=0.017$ and OR 0.989, $p=0.008$ for histological and molecular positivity, respectively).

Table 2. Imaging and procedural characteristics.

Imaging and procedural characteristics		Tumor cells present (N=84)	p-Value*	Sufficient tumor yield for molecular analysis (≥30%) (N=73)		p-Value*	
		Median (q1-q3) or number (percent)		Median (q1-q3) or number (percent)			
Imaging characteristics							
Imaging type			p=0.037			p=0.292	
	CT	23/36 (63.9%)			21/36 (58.3%)		
	MRI	8/12 (66.7%)			7/12 (58.3%)		
	PSMA-PET/CT†	53/62 (85.5%)			45/62 (72.6%)		
⁶⁸ Ga-PSMA N = 52; F18-PSMA N = 10)							
Biopsy location			p=0.027			p=0.012	
	Pelvis	57/79 (72.2%)			47/79 (59.5%)		
	Spine	23/24 (95.8%)			22/24 (91.7%)		
	Other (3 rib, 3 extremity, 1 scapula)	4/7 (57.1%)			4/7 (57.1%)		
Procedural characteristics							
Radiologist/fellow Radiologist		56/73 (76.7%)	p=0.942		51/73 (69.9%)	p=0.268	
	Fellow	17/23 (73.9%)			12/23 (52.2%)		
	Internist	11/14 (78.6%)			10/14 (71.4%)		
Quantitative attenuation		No tumor cells	Tumor cells present	p-Value	Insufficient tumor yield	Sufficient tumor yield	p-Value
	HU ‡	597.6 (327.4-824.9)	447.4 (206.4-579.1)	p=0.025	581.9 (333.0-807.2)	445.8 (182.7-553.1)	p=0.010
	Dev ‡	174.4 (102.3-223.8)	119.3 (72.0-154.7)	p=0.023	174.6 (104.4-220.7)	111.3 (71.6-147.1)	p=0.006
	ROI ‡	39.6 (33.6-45.0)	34.0 (26.5-41.6)	p=0.108	38.6 (32.3-44.7)	34.0 (26.0-41.8)	p=0.193

* Chi-Squared Test for nominal variables and Mann-Whitney-U Test for continuous variables; † Prostate-specific membrane antigen; ‡ Deviation of lesion; § Region of interest

Table 3. Univariate logistic regression.

Variable	Successful histology OR [†] (95% CI)	P=Value	Successful genetic analysis OR [†] (95% CI)	P=Value
Imaging Type				
CT	A		A	
MRI	1.13 (0.29-4.49)	p=0.862	1.00 (0.27-3.76)	p=1.000
PSMA-PET/CT	3.33 (1.25-8.88)	p=0.016	1.89 (0.795-4.496)	p=0.150
Biopsy location				
Pelvis	B		B	
Spine	8.88 (1.13-69.77)	p=0.038	7.49 (1.65-34.09)	p=0.009
Other	0.52 (0.11-2.49)	p=0.409	0.91 (0.19-4.33)	p=0.903
HU	0.998 (0.996-1.000)	p=0.034	0.998 (0.996-1.000)	p=0.016
Dev	0.990 (0.983-0.998)	p=0.017	0.989 (0.981-0.997)	p=0.008
ROI	0.986 (0.953-1.020)	p=0.420	0.992 (0.960-1.025)	p=0.639
ROI log 10	0.110 (0.003-3.797)	p=0.222	0.186 (0.006-5.365)	p=0.327

[†] odds ratio, A: The CT was used as a reference to compare the other variables (MRI and PSMA PET-CT) to, as also stated in the text above the table; B: The pelvis was used as a reference to compare the other variables (Spine and other) to, as also stated in the text above the table.

Imaging prediction model

Low HU represents osteoblastic and high HU represents a more osteosclerotic, commonly non- tumor containing lesion, while low Dev represents a more homogeneous lesion and high Dev a more heterogeneous lesion with regard to HU. In figure 2, an illustration shows two these different types of bone biopsy lesions, per HU and dev, as imaged on a pre-biopsy CT scan. When we categorized HU and Dev into quartiles, the fourth quartile of both HU and Dev was associated with most negative biopsies. Three groups were defined in an exploratory model: (1) patients with HU and Dev both lower than the 75th percentile, (2) patients with HU or Dev greater than the 75th percentile, and (3) patients with both HU and Dev greater than the 75th percentile. The lowest success rate, as described in table 4 was seen in lesions with both higher HU and Dev, resembling sclerotic lesions (figure 2a). There was a statistically significant higher success rate in lesions with both lower HU and Dev, resembling (figure 2b). Biopsies from the first group resulted in significant more histological confirmed biopsies compared to those in group 2 and 3: 81.8% vs 55.6% and 44.4%, respectively (p=0.023). Low HU and Dev (group 1) also resulted in more successful molecular analysis: 77.3% vs 44.4% and 33.3% (p=0.007) (table 4).

When the cut-off was set at median for HU and Dev (492.30 and 127.20, respectively), groups with both HU and Dev above median also had significantly fewer successful biopsies.

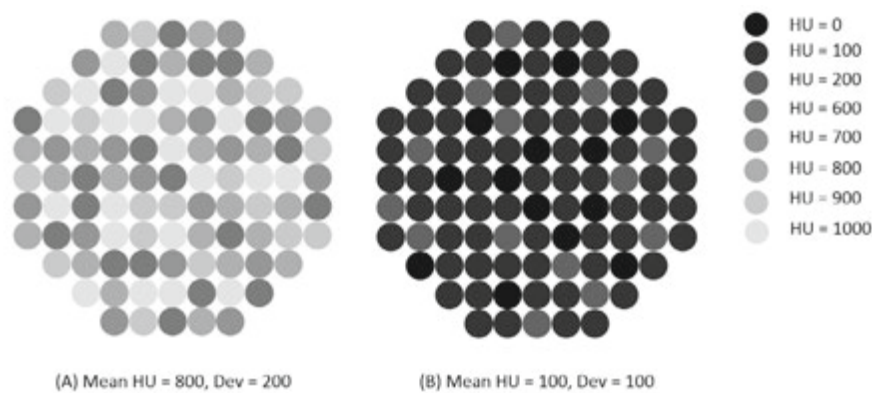


Figure 2. Schematic pictures showing the mean Hounsfield units (HUs) and deviation (Dev) of a lesion on CT-scan. **(A)** demonstrates a lesion with a high HU and high Dev. **(B)** demonstrates a lesion with low HU and low Dev.

Table 4. Prediction based on HU and deviation.

Groups categorized by HU and Dev	Tumor cells present	Odds ratio	Successful molecular analysis ($\geq 30\%$)	Odds ratio
Group 1 HU < 713.50 and Dev < 178.90	36/44 (81.8%)	A	34/44 (77.3%)	A
Group 2 HU ≥ 713.50 or Dev ≥ 178.90	10/18 (55.6%)	0.278 ($p=0.037$)	8/18 (44.4%)	0.235 ($p=0.235$)
Group 3 HU ≥ 713.50 and Dev ≥ 178.90	4/9 (44.4%)	0.178 ($p=0.026$)	3/9 (33.3%)	0.147 ($p=0.016$)

A: Group 1 was used as a reference to compare the other variables (group 2 and 3) to.

Druggable pathogenic mutations within a bone-predominant cohort

Figure 3 illustrates a summary of the targetable genetic mutations within our cohort. In 14% of our patients, a mutation in the HR-related pathway was found, which are druggable by PARP-inhibitors and/or platinum chemotherapy [22,23]. In 3%, we identified mutations in the MMRd-pathway resulting in mismatch repair deficiency, druggable with by anti-PD1 checkpoint inhibitors [24]. Finally, 44% of our patients had an activated PI3K-pathway which could be treated by PIK3CA or PIK3CB inhibitors, or with AKT-inhibitors [25].

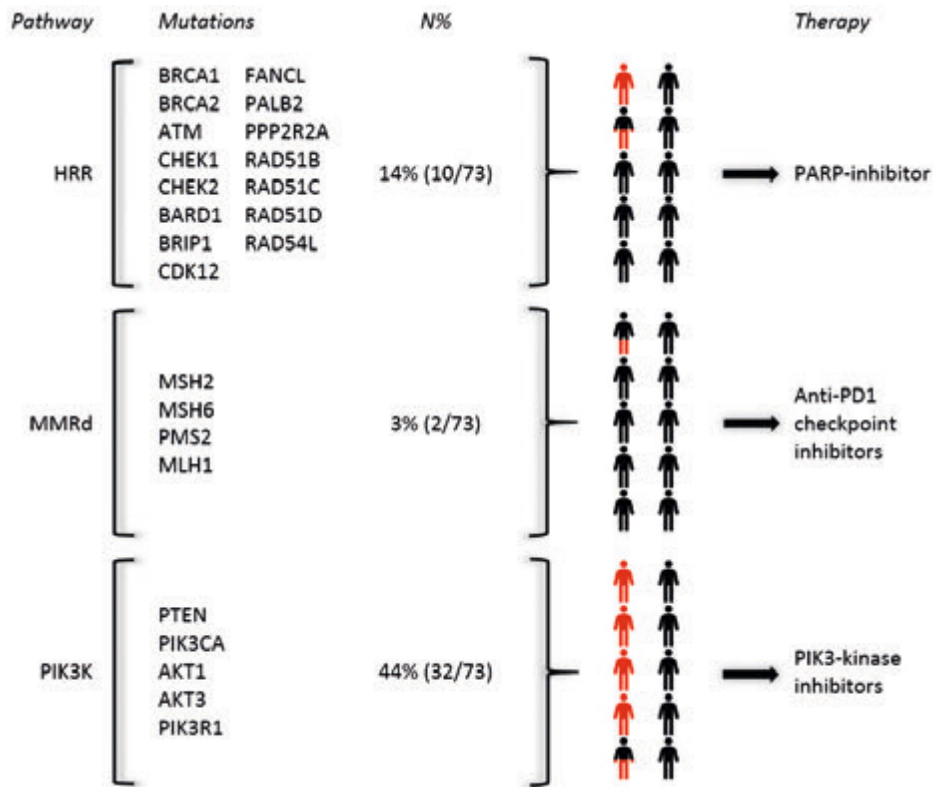


Figure 3. Targetable mutations in our cohort.

DISCUSSION

Previous studies have shown histological successful results in 25.5-85.7% of biopsies [9,15-20]. Tissue with a sufficient amount of tumor cells containing high quality nucleic acids is necessary for further molecular testing. In only a few studies molecular analyses were also performed on bone biopsies with a success rate of 39-81.7% by whole-exome sequencing or targeted NGS [15,19,20]. In comparison, this study had a diagnostic yield of 76.4% and a sufficient tumor cell percentage to allow for molecular analysis in 86.9% of those biopsies. Table 5 provides a literature overview of previous published studies.

Table 5. Results of previous studies compared to the current study.

<i>Reference</i>	<i>N</i>	<i>Imaging</i>	<i>Diagnostic yield</i>	<i>Sufficiency for molecular analysis</i>	<i>Type of molecular analysis</i>
[15]	80	CT-guided	69%	64%	RNA NGS [‡]
[16]	115	Unguided	62,5%	Not performed	
[9]	39	CT-guided	77%	Not performed	
[17]	43	MRI	72,1%	Not performed	
[18]	184	Unguided	25,5%	Not performed	
[19]	70	CT-guided	85,7%	WES [†] 81,7% → RNA-seq 33,3%	DNA WES [†]
[20]	54	CT-guided	67%	39%	RNA microarray analysis
[26]	10	CBCT-guided*	90%	80%	Single molecular inversion probe and WES [†]
Current study	110		76.4%	66,4% of total; 86,8% of biopsies with histological documentation of tumor cells	Whole-genome sequencing and/or targeted NGS [‡] (possible when ≥ 30% tumor cells are available)

*Cone-beam CT-guided; † Whole-exome sequencing; ‡ Next-generation sequencing

In our study we investigated the impact of different imaging modalities for biopsy site planning and outcome results. We show that the introduction and utilization of PSMA-PET imaging resulted in a higher diagnostic yield, as well as an improved success rates of successful molecular analyses by approximately 15% compared to CT and MRI (table 2). Previous published radiomic studies utilizing CT-imaging variables show that biopsy success is associated with lesions that are either predominantly radiolucent or have a low mean HU, resulting in higher tumor percentages [15,16,20]. In the current study we found that homogeneous lesions with low Hounsfield units on CT-imaging contained highest diagnostic yield and proportion of tumor- containing osseous lesions where molecular profiling by NGS could be performed. We developed a simple prediction model with HU and Dev, where the lowest three quartiles associate with highest diagnostic yield and rates of molecular test success. As shown in this study, a homogeneous (low Dev) hypodense lesion (low HU) is associated with better biopsy results. Implementation of HU and Dev measurements could be prospectively used during CT-guided biopsy to select for optimal lesions, preferably from a PSMA-avid lesion. Further utilization of PSMA-PET parameters, such as a minimum standardized uptake value (SUV) of PSMA in the region of interest, could further enhance proportion of successful biopsies. Another retrospective multicenter study indicated that both HU_{mean} and SUV_{max} variables from CT and ^{68}Ga -PSMA-PET imaging, associate with an outcome of at least 30% tumor content in bone biopsies [21]. In a previous published prospective study of ten mCRPC patients, advanced planning with ^{68}Ga -PSMA-PET and diffusion-weighted MRI increased diagnostic yield up

to 90% on cone-beam CT-guided biopsy [26]. Further prospective studies are needed to assess and validate radiomic signatures to predict bone biopsy outcome utilizing CT, MRI and PSMA-PET imaging modalities.

New treatment modalities of mCRPC are based on molecular characterization. The pivotal phase III trial of olaparib in molecular selected patients with aberrations in genes directly or indirectly associated with homologous recombination deficiency, indicated that patients with BRCA1, BRCA2 and ATM derive benefit from targeted therapy with olaparib [27]. In almost 30% of patients that develop mCRPC, aberrations in DNA damage repair (DDR) genes are identified [28]. In addition, screening for patients with immunogenic prostate cancer, associated with mutations in mismatch repair [14,29,30] and CDK12 [31], is advocated within routine care and for clinical trial participation. Other targets include aberrations that activate the PI3 kinase pathway (PI3K) [25]. We identified genetic aberrations in DDR pathways of DNA sensing, homologous recombination and MMR, as well as recurrent aberrations in PI3K in the bone biopsies in 14, 3 and 44%, respectively (figure 3). Particularly for ATM, CDK12 and aberrations in PI3K it is known that these accumulate following castrate-resistance [32,33].

Our study has limitations due to the unplanned retrospective nature, multiple bias could be introduced. First, a time bias could influence results, as oldest biopsies were performed with older imaging modalities, and may affect biopsy results. Biopsies were not performed by the same radiologist, with varying experience in interventional radiology, and differences in equipment. Further, the quantitative attenuations of the lesions were determined retrospectively, but in a blinded manner. We aimed to avoid an intra-observer bias by determining the attenuation by one radiologist in our institute. Biopsy sites were pre-selected in a multidisciplinary meeting, however at time of intervention the pre-selected or alternative lesion was biopsied according to the performing intervention radiologists' judgement of feasibility and safety. Further, although the needle location in the tumor could be assessed, the exact location of each core sample could not be assessed retrospectively. Also, missing data e.g. on needle gauge and number of cores limited analyses for these factors. We didn't include metastasize size as a variable since the Prostate Cancer Working Group has classified the size of osseous lesions as non-measurable by MRI, CT or bone scintigraphy [34]. However, for future studies, solely focusing on PSMA-PET-guided biopsies, tumor size should be included. Finally, prior or current use of bone protective agents may influenced biopsy outcome, but was not assessed in our study. Because the data were from patients only from one academic center, the external validity of our prediction model will have to be validated in other centers including community hospitals.

MATERIALS AND METHODS

Study population

For this retrospective study, patients with metastatic prostate cancer were considered that were included in the Center for Personalized Cancer Treatment (CPCT)-02 trial (NCT01855477). Eligibility criteria for this study were patients with metastatic prostate cancer that underwent a biopsy of a bone metastasis in our institute between September 2016 and June 2019. We excluded patients with more than 90 days between prior imaging and bone biopsy. In this study an informed consent was obtained within the CPCT-02 trial from all patients and an additional approval was provided by the ethical committee at the University of the Radboud Medical Center Nijmegen (2019-5362, 15th April 2019). All clinical and imaging data were collected retrospectively from the electronic patient records in an electronic case report form (Castor).

Variable definition

Clinical and imaging variables were pre-defined and collected retrospectively from the electronic patient records. Clinical variables included (1) age at time of biopsy, (2) Gleason score (GS) of primary diagnosis, (3) hormone status at the time of biopsy, (4) prior radiotherapy on biopsied metastases and (5) laboratory values collected up to three weeks before or one week after biopsy. Imaging and procedural variables included (1) prior imaging type (^{68}Ga -PSMA-PET/CT or ^{18}F -PSMA-PET/CT imaging, magnetic resonance imaging (MRI), technetium-99 bone scintigraphy and CT-scan), (2) biopsy location, (3) needle gauge, (4) imaging characteristics during biopsy (Hounsfield Units (HU), Deviation (Dev) defined as the variation of the HU, Region of Interest (ROI)) and (5) type of image guidance. One experienced radiologist, blinded to the results, retrospectively determined quantitative attenuations (HU, Dev, ROI) of CT-guided biopsied metastases. When more types of imaging were performed prior to biopsy, the leading imaging was determined from the biopsy report.

Sample collection, DNA extraction and molecular analysis

Histological and molecular analyses of the bone biopsy were performed within the CPCT-02 trial. When more cores were available from the same biopsy additional targeted NGS results analyzed in our institute were also used for further analyses. As described by Priestley et al [35] biopsy cores analyzed within the CPCT-02 trial were first examined by an experienced pathologist for estimation of tumor cellularity on a 6 μm haematoxylin and eosin (H&E) stained section. When the tumor cellularity was estimated $>30\%$, 25 sections of 20 μm were collected in a tube for DNA isolation. Frozen tissues were pulverized in RNase free MQ (110 μl) using the Qiagen TissueLyzer II (2 min and 25 hrz) and a steel bead containing Sarstedt epp. Genomic DNA was isolated from 50 μl pulverized biopsy with the QIAasympyony DSP DNA Mini kit standard protocol for tissue (50 μl eluate). A total of 50-200 μg of DNA was used for whole-genome sequencing.

If available, cores from the same biopsy were analyzed in our institute. Tissue is fixed in formaldehyde 4% and go through a decalcification process with EDTA. Genomic DNA was isolated from tissue sections (generally 6 x 10um) using 5% Chelex-100 and 400mg proteinase K followed by purification using NaAc and EtOH precipitation. DNA concentrations were measured using the Qubit Broad Range kit (Thermo Fisher Scientific, Waltham, MA, USA). 60 ng DNA was used as input for the library preparation using the TruSight Oncology (TSO500) library preparation kit, as described previously [36]. Libraries were sequenced on a NextSeq 500 (Illumina, San Diego, CA, USA).

Outcomes

The objective of our study was to associate biopsy result to the type of imaging used to select for the site of the bone metastatic biopsy, and pre-defined laboratory, clinical and imaging variables. First, a biopsy was considered successful if presence of prostate cancer cells could be histologically confirmed. More stringently, we assessed the rate of biopsies with sufficient tumor yield allowing molecular characterization on bone metastatic lesions ($\geq 30\%$ tumor cells on $\geq 5 \text{ mm}^2$).

Statistical analysis

Descriptive statistics were performed for baseline clinical and imaging data. The median and interquartile ranges (IQR) are reported. Clinical and imaging differences between the groups (successful or negative biopsy) were analyzed using a Chi-Squared-Test for nominal and categorical variables and Mann-Whitney-U Test for continuous variables. Optimal dichotomization per quartile of continuous variables from imaging (HU, Dev, ROI) was established from visual inspection of generated histogram for patients with successful and negative biopsy results. All variables were analyzed using univariable logistic regression analysis with biopsy positivity (histological and molecular) as the dependent variables. Statistically significant variables were tested in a multivariable logistic regression model. A p-value < 0.05 was considered statistically significant. All statistical analyses were performed using IBM SPSS statistics version 25.

CONCLUSIONS

With our study we were able to identify clinical and imaging factors influencing tumor yield in bone biopsies in patients with metastatic prostate cancer. First, a prior PSMA-PET/CT improves biopsy outcome with regard to commonly used imaging methods. Second, a prediction tool of quantitative imaging attenuation improved the success rate of bone biopsies by selection of lesions with low HU and deviation. To validate these findings further prospective validation is needed.

REFERENCES

1. Bray, F.; Ferlay, J.; Soerjomataram, I.; Siegel, R.L.; Torre, L.A.; Jemal, A. Global cancer statistics 2018: GLOBOCAN estimates of incidence and mortality worldwide for 36 cancers in 185 countries. *CA Cancer J Clin* 2018, 68, 394-424, doi:10.3322/caac.21492.
2. Pienta, K.J.; Bradley, D. Mechanisms underlying the development of androgen-independent prostate cancer. *Clin Cancer Res* 2006, 12, 1665-1671, doi:10.1158/1078-0432.CCR-06-0067.
3. Huggins, C. Endocrine-induced regression of cancers. *Cancer Res* 1967, 27, 1925-1930.
4. Shah, R.B.; Mehra, R.; Chinnaiyan, A.M.; Shen, R.; Ghosh, D.; Zhou, M.; Macvicar, G.R.; Varambally, S.; Harwood, J.; Bismar, T.A., et al. Androgen-independent prostate cancer is a heterogeneous group of diseases: lessons from a rapid autopsy program. *Cancer Res* 2004, 64, 9209-9216, doi:10.1158/0008-5472.Can-04-2442.
5. Kumar, A.; Coleman, I.; Morrissey, C.; Zhang, X.; True, L.D.; Gulati, R.; Etzioni, R.; Bolouri, H.; Montgomery, B.; White, T., et al. Substantial interindividual and limited intraindividual genomic diversity among tumors from men with metastatic prostate cancer. *Nat Med* 2016, 22, 369-378, doi:10.1038/nm.4053.
6. Gillessen, S.; Attard, G.; Beer, T.M.; Beltran, H.; Bossi, A.; Bristow, R.; Carver, B.; Castellano, D.; Chung, B.H.; Clarke, N., et al. Management of Patients with Advanced Prostate Cancer: The Report of the Advanced Prostate Cancer Consensus Conference APCCC 2017. *Eur Urol* 2018, 73, 178-211, doi:10.1016/j.eururo.2017.06.002.
7. Bubendorf, L.; Schopfer, A.; Wagner, U.; Sauter, G.; Moch, H.; Willi, N.; Gasser, T.C.; Mihatsch, M.J. Metastatic patterns of prostate cancer: an autopsy study of 1,589 patients. *Hum Pathol* 2000, 31, 578-583.
8. Halabi, S.; Kelly, W.K.; Ma, H.; Zhou, H.; Solomon, N.C.; Fizazi, K.; Tangen, C.M.; Rosenthal, M.; Petrylak, D.P.; Hussain, M., et al. Meta-Analysis Evaluating the Impact of Site of Metastasis on Overall Survival in Men With Castration-Resistant Prostate Cancer. *J Clin Oncol* 2016, 34, 1652-1659, doi:10.1200/JCO.2015.65.7270.
9. McKay, R.R.; Zukotynski, K.A.; Werner, L.; Voznesensky, O.; Wu, J.S.; Smith, S.E.; Jiang, Z.; Melnick, K.; Yuan, X.; Kantoff, P.W., et al. Imaging, procedural and clinical variables associated with tumor yield on bone biopsy in metastatic castration-resistant prostate cancer. *Prostate Cancer Prostatic Dis* 2014, 17, 325-331, doi:10.1038/pcan.2014.28.
10. Mehra, R.; Kumar-Sinha, C.; Shankar, S.; Lonigro, R.J.; Jing, X.; Philips, N.E.; Siddiqui, J.; Han, B.; Cao, X.; Smith, D.C., et al. Characterization of bone metastases from rapid autopsies of prostate cancer patients. *Clin Cancer Res* 2011, 17, 3924-3932, doi:10.1158/1078-0432.CCR-10-3120.
11. Suprun, H.; Rywlin, A.M. Metastatic carcinoma in histologic sections of aspirated bone marrow: a comparative autopsy study. *South Med J* 1976, 69, 438-439, doi:10.1097/00007611-197604000-00018.
12. Viswanathan, S.R.; Ha, G.; Hoff, A.M.; Wala, J.A.; Carrot-Zhang, J.; Whelan, C.W.; Haradhvala, N.J.; Freeman, S.S.; Reed, S.C.; Rhoades, J., et al. Structural Alterations Driving Castration-Resistant Prostate Cancer Revealed by Linked-Read Genome Sequencing. *Cell* 2018, 174, 433-447 e419, doi:10.1016/j.cell.2018.05.036.

13. Quigley, D.A.; Dang, H.X.; Zhao, S.G.; Lloyd, P.; Aggarwal, R.; Alumkal, J.J.; Foye, A.; Kothari, V.; Perry, M.D.; Bailey, A.M., et al. Genomic Hallmarks and Structural Variation in Metastatic Prostate Cancer. *Cell* 2018, 174, 758-769.e759, doi:10.1016/j.cell.2018.06.039.
14. Robinson, D.; Van Allen, E.M.; Wu, Y.M.; Schultz, N.; Lonigro, R.J.; Mosquera, J.M.; Montgomery, B.; Taplin, M.E.; Pritchard, C.C.; Attard, G., et al. Integrative clinical genomics of advanced prostate cancer. *Cell* 2015, 161, 1215-1228, doi:10.1016/j.cell.2015.05.001.
15. Holmes, M.G.; Foss, E.; Joseph, G.; Foye, A.; Beckett, B.; Motamedi, D.; Youngren, J.; Thomas, G.V.; Huang, J.; Aggarwal, R., et al. CT-Guided Bone Biopsies in Metastatic Castration-Resistant Prostate Cancer: Factors Predictive of Maximum Tumor Yield. *J Vasc Interv Radiol* 2017, 28, 1073-1081 e1071, doi:10.1016/j.jvir.2017.04.019.
16. Lorente, D.; Omlin, A.; Zafeiriou, Z.; Nava-Rodrigues, D.; Perez-Lopez, R.; Pezaro, C.; Mehra, N.; Sheridan, E.; Figueiredo, I.; Riisnaes, R., et al. Castration-Resistant Prostate Cancer Tissue Acquisition From Bone Metastases for Molecular Analyses. *Clin Genitourin Cancer* 2016, 14, 485-493, doi:10.1016/j.clgc.2016.04.016.
17. Perez-Lopez, R.; Nava Rodrigues, D.; Figueiredo, I.; Mateo, J.; Collins, D.J.; Koh, D.M.; de Bono, J.S.; Tunariu, N. Multiparametric Magnetic Resonance Imaging of Prostate Cancer Bone Disease: Correlation With Bone Biopsy Histological and Molecular Features. *Invest Radiol* 2018, 53, 96-102, doi:10.1097/RLI.0000000000000415.
18. Ross, R.W.; Halabi, S.; Ou, S.S.; Rajeshkumar, B.R.; Woda, B.A.; Vogelzang, N.J.; Small, E.J.; Taplin, M.E.; Kantoff, P.W.; Cancer, et al. Predictors of prostate cancer tissue acquisition by an undirected core bone marrow biopsy in metastatic castration-resistant prostate cancer--a Cancer and Leukemia Group B study. *Clin Cancer Res* 2005, 11, 8109-8113, doi:10.1158/1078-0432.CCR-05-1250.
19. Sailer, V.; Schiffman, M.H.; Kossai, M.; Cyrta, J.; Beg, S.; Sullivan, B.; Pua, B.B.; Lee, K.S.; Talenfeld, A.D.; Nanus, D.M., et al. Bone biopsy protocol for advanced prostate cancer in the era of precision medicine. *Cancer* 2018, 124, 1008-1015, doi:10.1002/cncr.31173.
20. Spritzer, C.E.; Afonso, P.D.; Vinson, E.N.; Turnbull, J.D.; Morris, K.K.; Foye, A.; Madden, J.F.; Roy Choudhury, K.; Febbo, P.G.; George, D.J. Bone marrow biopsy: RNA isolation with expression profiling in men with metastatic castration-resistant prostate cancer--factors affecting diagnostic success. *Radiology* 2013, 269, 816-823, doi:10.1148/radiol.13121782.
21. de Jong, A.C.; Smits, M.; van Riet, J.; Futterer, J.J.; Brabander, T.; Hamberg, P.; van Oort, I.M.; de Wit, R.; Lolkema, M.P.; Mehra, N., et al. (68)Ga-PSMA guided bone biopsies for molecular diagnostics in metastatic prostate cancer patients. *J Nucl Med* 2020, 10.2967/jnumed.119.241109, doi:10.2967/jnumed.119.241109.
22. Mateo, J.; Carreira, S.; Sandhu, S.; Miranda, S.; Mossop, H.; Perez-Lopez, R.; Nava Rodrigues, D.; Robinson, D.; Omlin, A.; Tunariu, N., et al. DNA-Repair Defects and Olaparib in Metastatic Prostate Cancer. *N Engl J Med* 2015, 373, 1697-1708, doi:10.1056/NEJMoa1506859.
23. Cheng, H.H.; Pritchard, C.C.; Boyd, T.; Nelson, P.S.; Montgomery, B. Biallelic Inactivation of BRCA2 in Platinum-sensitive Metastatic Castration-resistant Prostate Cancer. *Eur Urol* 2016, 69, 992-995, doi:10.1016/j.eururo.2015.11.022.
24. Abida, W.; Cheng, M.L.; Armenia, J.; Middha, S.; Autio, K.A.; Vargas, H.A.; Rathkopf, D.; Morris, M.J.; Danila, D.C.; Slovin, S.F., et al. Analysis of the Prevalence of Microsatellite Instability in Prostate Cancer and Response to Immune Checkpoint Blockade. *JAMA Oncol* 2019, 5, 471-478, doi:10.1001/jamaoncol.2018.5801.

25. de Bono, J.S.; De Giorgi, U.; Rodrigues, D.N.; Massard, C.; Bracarda, S.; Font, A.; Arranz Arijia, J.A.; Shih, K.C.; Radavoi, G.D.; Xu, N., et al. Randomized Phase II Study Evaluating Akt Blockade with Ipatasertib, in Combination with Abiraterone, in Patients with Metastatic Prostate Cancer with and without PTEN Loss. *Clin Cancer Res* 2019, 25, 928-936, doi:10.1158/1078-0432.Ccr-18-0981.
26. van Steenberghe, T.R.F.; Smits, M.; Scheenen, T.W.J.; van Oort, I.M.; Nagarajah, J.; Rovers, M.M.; Mehra, N.; Futterer, J.J. (68)Ga-PSMA-PET/CT and Diffusion MRI Targeting for Cone-Beam CT-Guided Bone Biopsies of Castration-Resistant Prostate Cancer Patients. *Cardiovasc Intervent Radiol* 2019, 10.1007/s00270-019-02312-8, doi:10.1007/s00270-019-02312-8.
27. Hussain, M.; Mateo, J.; Fizazi, K.; Saad, F.; Shore, N.; Sandhu, S.; Chi, K.; Sartor, O.; Agarwal, N.; Olmos, D., et al. LBA12_PRPROfound: Phase III study of olaparib versus enzalutamide or abiraterone for metastatic castration-resistant prostate cancer (mCRPC) with homologous recombination repair (HRR) gene alterations. *Annals of Oncology* 2019, 30, doi:10.1093/annonc/mdz394.039.
28. Bono, J.; Fizazi, K.; Saad, F.; Shore, N.; Sandhu, S.; Mehra, N.; Kolinsky, M.; Roubaud, G.; Özgüroğlu, M.; Matsubara, N., et al. 847PDCentral, prospective detection of homologous recombination repair gene mutations (HRRm) in tumour tissue from >4000 men with metastatic castration-resistant prostate cancer (mCRPC) screened for the PROfound study. *Annals of Oncology* 2019, 30, doi:10.1093/annonc/mdz248.004.
29. Pritchard, C.C.; Morrissey, C.; Kumar, A.; Zhang, X.; Smith, C.; Coleman, I.; Salipante, S.J.; Milbank, J.; Yu, M.; Grady, W.M., et al. Complex MSH2 and MSH6 mutations in hypermutated microsatellite unstable advanced prostate cancer. *Nat Commun* 2014, 5, 4988, doi:10.1038/ncomms5988.
30. Nghiem, B.; Zhang, X.; Lam, H.M.; True, L.D.; Coleman, I.; Higano, C.S.; Nelson, P.S.; Pritchard, C.C.; Morrissey, C. Mismatch repair enzyme expression in primary and castrate resistant prostate cancer. *Asian J Urol* 2016, 3, 223-228, doi:10.1016/j.ajur.2016.09.002.
31. Wu, Y.M.; Cieslik, M.; Lonigro, R.J.; Vats, P.; Reimers, M.A.; Cao, X.; Ning, Y.; Wang, L.; Kunju, L.P.; de Sarkar, N., et al. Inactivation of CDK12 Delineates a Distinct Immunogenic Class of Advanced Prostate Cancer. *Cell* 2018, 173, 1770-1782.e1714, doi:10.1016/j.cell.2018.04.034.
32. Abida, W.; Armenia, J.; Gopalan, A.; Brennan, R.; Walsh, M.; Barron, D.; Danila, D.; Rathkopf, D.; Morris, M.; Slovin, S., et al. Prospective Genomic Profiling of Prostate Cancer Across Disease States Reveals Germline and Somatic Alterations That May Affect Clinical Decision Making. *JCO Precis Oncol* 2017, 2017, doi:10.1200/po.17.00029.
33. van Dessel, L.F.; van Riet, J.; Smits, M.; Zhu, Y.; Hamberg, P.; van der Heijden, M.S.; Bergman, A.M.; van Oort, I.M.; de Wit, R.; Voest, E.E., et al. The genomic landscape of metastatic castration-resistant prostate cancers reveals multiple distinct genotypes with potential clinical impact. *Nat Commun* 2019, 10, 5251, doi:10.1038/s41467-019-13084-7.
34. Scher, H.I.; Morris, M.J.; Stadler, W.M.; Higano, C.; Basch, E.; Fizazi, K. Trial Design and Objectives for Castration-Resistant Prostate Cancer: Updated Recommendations From the Prostate Cancer Clinical Trials Working Group 3. *J. Clin. Oncol.* 2016, 34, 1402-1418.
35. Priestley, P.; Baber, J.; Lolkema, M.P.; Steeghs, N.; de Bruijn, E.; Shale, C. Pan-cancer whole-genome analyses of metastatic solid tumours. *Nature* 2019, 575, 210-216.

36. Kroeze, L.I.; de Voer, R.M.; Kamping, E.J.; von Rhein, D.; Jansen, E.A.M.; Hermesen, M.J.W. Evaluation of a Hybrid Capture-Based Pan-Cancer Panel for Analysis of Treatment Stratifying Oncogenic Aberrations and Processes. *J. Mol. Diagn.* 2020, 22, 757–769.



PART II

**IMPROVING THE SUCCESS RATE OF MOLECULAR
ANALYSES IN BONE METASTATIC PROSTATE
CANCER**



CHAPTER 4

⁶⁸GA-PSMA-PET/CT AND DIFFUSION MRI TARGETING FOR CONE-BEAM CT-GUIDED BONE BIOPSIES OF CASTRATION-RESISTANT PROSTATE CANCER PATIENTS

T. R. F. van Steenbergen*

T. W. J. Scheenen

J. Nagarajah

N. Mehra

M. Smits*

I. M. van Oort

M. M. Rovers

J. J. Fütterer

* These authors contributed equally to this work.

Cardiovascular and Interventional Radiology. 2020;43(1):147-54

ABSTRACT

Introduction Precision medicine expands the treatment options in patients with metastatic castration resistant prostate cancer (mCRPC) by targeting druggable genetic aberrations. Aberrations can be identified following molecular analysis of metastatic tissue. Bone metastases, commonly present in mCRPC, hinder precision medicine due to a high proportion of biopsies with insufficient tumor cells for next-generation DNA sequencing. We aimed to investigate the feasibility of incorporating advanced target planning and needle guidance in bone biopsies and whether this procedure increases biopsy tumor yield and success rate of molecular analysis as compared to current standards in literature, utilizing only CT-guidance.

Materials and Methods

In a prospective pilot study, ten mCRPC patients received ^{68}Ga -prostate specific membrane antigen(PSMA)-PET/CT and diffusion-weighted MRI to plan the biopsy target on functional tumor information. Planning datasets were fused for targeting metastatic lesions with high tumor densities. Biopsies were performed under cone-beam CT (CBCT) guidance. Feasibility of target planning and needle guidance was assessed, and success of molecular analysis and tumor yield was reported.

Results

Fusion target planning and CBCT needle guidance was feasible. Nine out of ten biopsies contained prostate cancer cells, with a median of 39 and 40% tumor cells by two different sequencing techniques. Molecular analysis was successful in eight of ten patients (80%). This exceeds previous reports on CT-guided biopsies that ranged from 33 to 44%. In two patients important druggable genetic aberrations were found.

Discussion

A biopsy procedure using advanced target planning and needle guidance is feasible and can increase the success rate of molecular analysis in bone metastases, thereby having the potential of improving treatment outcome for patients with mCRPC.

INTRODUCTION

Metastatic castration-resistant prostate cancer (mCRPC) is a molecular heterogeneous disease with a high frequency of potentially actionable genetic alterations, supporting use of routine molecular profiling to expand on standard treatment options for these patients [1–3]. Whereas a low tumor yield from tumor biopsies is sufficient for classical pathological diagnostic assessments, a higher tumor content is required for tumor profiling using next-generation sequencing techniques. For targeted or whole genome sequencing (WGS), a minimum input of 50 nanogram of high quality DNA is necessary, corresponding to at least 10.000 cells. The preferred location for biopsy is soft tissue, because the tumor yield tends to be higher than in bone [4] and as a consequence molecular analyses are commonly unsuccessful from bone metastatic sites. In patients with mCRPC, bone is the predominant or sole site of metastases in 80.6% and 42.9% of all cases, respectively [5], leaving these patients underrepresented in molecular studies. Therefore the medical need exists to collect tissue from bone lesions, to increase success rate of molecular analyses, particularly from small osteoblastic sites. High tumor yield occurs in sites with high tumor density, which in case of prostate cancer (PCa) can be detected by ^{68}Ga -prostate-specific membrane antigen (PSMA)-PET/CT and diffusion-weighted MRI (DWI) [6,7]. We hypothesized that incorporating this functional information in biopsy planning using image fusion and displaying the planned path during cone-beam CT (CBCT)-guidance can improve the amount of tissue obtained by bone biopsies for molecular characterization.

The aim of this prospective pilot study is first to investigate whether target planning on fused ^{68}Ga -PSMA-PET/CT, DWI and CBCT image datasets and CBCT guidance for bone biopsies is feasible and second whether this procedure increases the success rate of molecular analyses on bone metastases in mCRPC patients.

MATERIALS AND METHODS

From December 2017 to February 2019, 10 mCRPC patients with at least one bone metastasis on diagnostic imaging and planned molecular analysis were enrolled in this pilot study. Patients with a soft tissue lesion accessible for biopsy were excluded. This study was approved by the local ethical committee. An informed consent was obtained from all participants.

Metastasis selection

Patients received both ^{68}Ga -PSMA-PET/CT and MRI for diagnostic workup. The nuclear medicine physician identified metastases with the highest uptake, indicating high tumor density. DWI sequences were focused on these metastases. The interventional radiologist

then selected an accessible metastasis with low ADC value and high b800 signal intensity as target lesion, because this suggests structural changes by tumor cells.

Target planning

The needle path, a straight line between target and entry point, was planned on a Syngo workstation (Syngo, Siemens Healthineers, Forchheim, Germany). For target planning the ^{68}Ga -PSMA-PET/CT and MRI were fused. Fusion was based on anatomical scans, T1-weighted MRI and low-dose CT (PET/CT), and target point planning was performed on functional scans, DWI with b-value 800 s/mm² and ^{68}Ga -PSMA-PET. The target point was planned on the area with the highest b800 pixel intensity (figure 1a), and then verified on PET (figure 1b). The skin entry point determined the needle path, balancing between: (1) avoiding vital structures; (2) approaching the bone surface perpendicularly; (3) avoiding a double oblique angle.

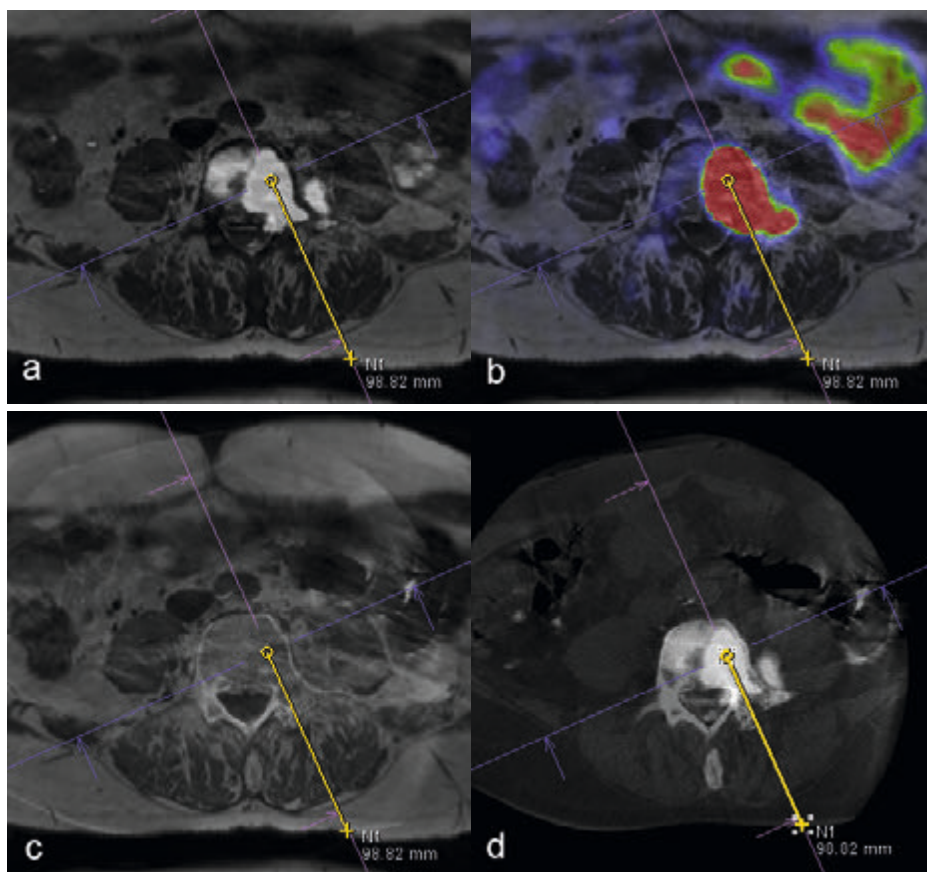


Fig. 1 A-D This example shows the target planning of patient 1 on fused datasets. **(A)** The target was initially planned on a fusion of T1 and b800 images. **(B)** This target was then verified on a fusion of T1 and ^{68}Ga -PSMA-PET images. **(C)** The CBCT scan showing the current anatomy was fused with the T1 to optimize the needle path. **(D)** The CBCT/b800 fusion with needle path was displayed on screens in the room during needle guidance.

Biopsy procedure

Patients were prone-positioned on a full carbon table, lying on thin gel mattresses and low pillows as to enable C-arm rotation around the pelvis. Instructions were given to the patient to minimize movement during the procedure, because movement decreases the accuracy of CBCT image fusion. A CBCT was obtained (Artis Zeego, Siemens Healthineers, Forchheim, Germany). The high dose protocol (6s DynaCT Body, visualization of lower contrast tissue) was used for initial fusion and assessment of vital structures along the needle path (figure 1c). Fluoroscopic needle guidance had the needle path overlay in three projection views: one perpendicular to the needle path showing entry point and angle through a laser beam, and two views along the needle path to determine needle progression and deflection in two planes (figure 2a,b). After advancing the biopsy needle (Arrow OnControl, Teleflex, Morrisville, NC) to the bone surface we took a low dose CBCT (5s DR Body Care, visualization of higher contrast tissue) to verify the needle position in 3D and to correct inaccuracies due to patient movement. If the needle position did not correspond to the planned path either the needle or planned entry point could be altered. The final needle position was again verified with a low dose CBCT before taking the biopsy. The window width and level were set to wide and high, respectively, to deal with the needle metal artifacts.

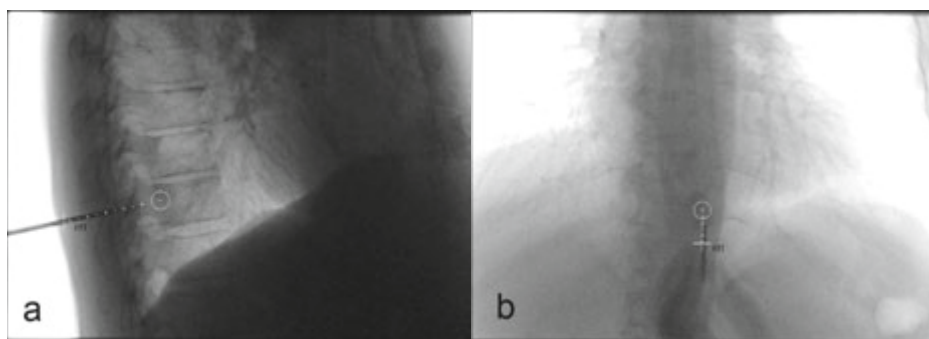


Fig. 2 A, B The planned needle path was overlaid on fluoroscopy images during needle guidance. This example shows the biopsy of the Th11 vertebra in patient 10. Two progression views can be used: **(A)** a lateral view and **(B)** a 30° angled frontal view.

Outcome measures

The primary outcome measure was feasibility of the target planning and needle guidance procedures. Target planning was feasible if fusing the scans resulted in precise matching of the target bone and lesion, allowing for target and entry point planning by the operator. Needle guidance was feasible if the needle could be advanced to the target lesion using the fluoroscopy overlay and control CBCT scans, and the interventional radiologist was

confident in the final needle position based on a fusion of the final control CBCT and the planning images.

Molecular analysis

If the procedure allowed it, a maximum of three 13G biopsy cores was taken. Two molecular analysis techniques were used, each on one core: single molecule Molecular Inversion Probe (smMIP) [8,9] and whole genome sequencing (WGS) [10]. The second outcome measure was success of analysis and tumor yield, defined as percentage neoplastic cells per biopsy core, reported for both analyzed cores.

RESULTS

Fusion target planning and CBCT needle guidance was feasible in all patients. Automatic image fusion did not work in two patients due to a MRI artifact (patients 3) and larger difference in spinal curvature (patient 10), necessitating full manual fusion. Minor manual adjustments after automatic fusion were done in six patients, all due to a difference in patient positioning between scans. Image fusion showed the difference in heterogeneity between PSMA uptake and diffusion restriction within some metastases, with regions of high uptake and high restriction not coinciding in three patients. Lesions could appear larger on DWI (figure 3) or on ^{68}Ga -PSMA-PET/CT (figure 4). The target points for these cases was planned on the regional overlap. For some patients we took more control CBCT scans (table 1) because following the planned needle path was challenging. This mostly occurred for double oblique needle paths. Ultimately, we preferred the initial CBCT rather than T1-weighted MRI as a base scan for fusion as this greatly sped up fusion with control CBCT scans.

Histopathological examination showed PCa cells in nine of the ten patients (90%) (Table 1). The biopsy cores of one patient did not contain tumor cells because the cortical bone was too compact to take a good biopsy. The nine CRPC positive biopsies were further analyzed. Tumor yield was >15% in eight of the smMIP cores (89%). Two cores were eventually not analyzed due to no clinical need, but their tumor yields (15% and 40%) would have sufficed for molecular analysis in case of good DNA quality. WGS was successful in seven cores (78%). In 8 out of 10 patients (80%) molecular analysis could be performed by either smMIP or WGSs. The median tumor yield in the WGS cores was 39%, compared to 40% in the smMIP cores. The most identified genetic alterations were loss of PTEN, aberrations in AR, TMRSS2-ERG fusion and mutation in TP53, as expected since these are most commonly identified in CRPC (Table 2). In two patients we found druggable genetic defects; one patient showed microsatellite instable prostate cancer and could be treated with checkpoint immunotherapy, and one patient had a pathogenic DNA damage repair defect and was eligible for treatment with a Poly (ADP-

ribose) polymerase inhibitor. In other patients we identified prognostic aberrations and hotspot mutations in the ligand binding domain of AR, which may lead to promiscuous activation by non-canonical steroid ligands such as prednisolone.

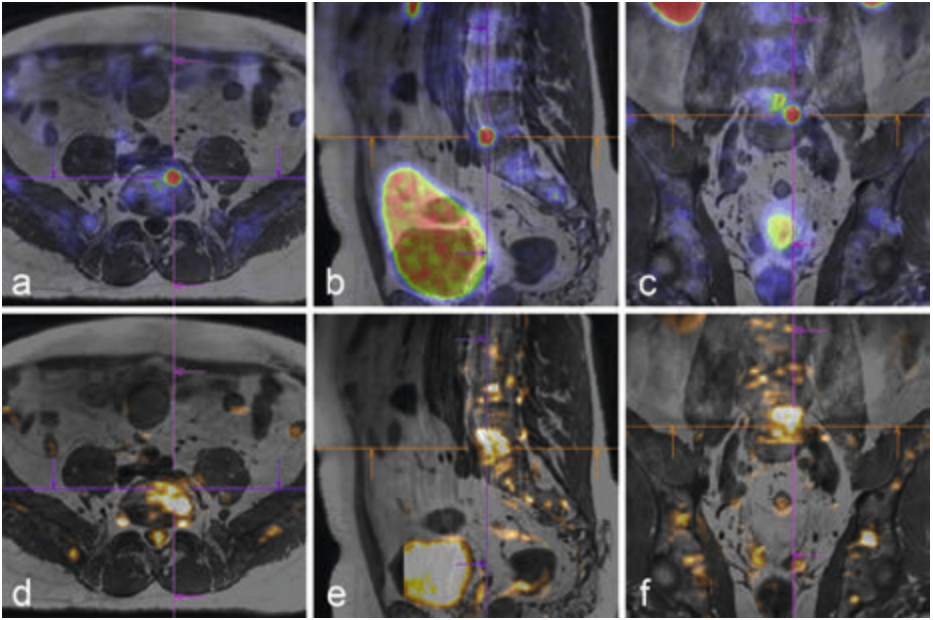


Fig. 3 A-F Image fusion showed the difference in heterogeneity between PSMA uptake and diffusion restriction within some metastases. In this example of patient 2, the lesion in L5 appears larger on DWI than on ^{68}Ga -PSMA-PET. The **(A-C)** ^{68}Ga -PSMA-PET and **(D-F)** DWI images are both fused with the T1 MRI and the lesion is visualized in **(A+D)** transversal, **(B+E)** sagittal and **(C+F)** coronal planes respectively. The cross is centered at the same position in the T1 MRI for all images and can be used as a reference location. The target point was planned in the regional overlap between high PSMA uptake and high diffusion restriction.

Table 1. Patient and procedure characteristics.

Patient no.	Age	Location	Number of control CBCT scans	Biopsy contains PCa cells
1	61	L4	3	Yes
2	58	L5	4	Yes
3	71	Os ilium left	2	Yes
4	57	Os ilium right	1	Yes
5	62	L1	6	Yes
6	63	Sacrum	3	Yes
7	68	Sacrum	2	Yes
8	64	Sacrum	2	Yes
9	69	Acetabulum right	1	No
10	64	Th11	4	Yes

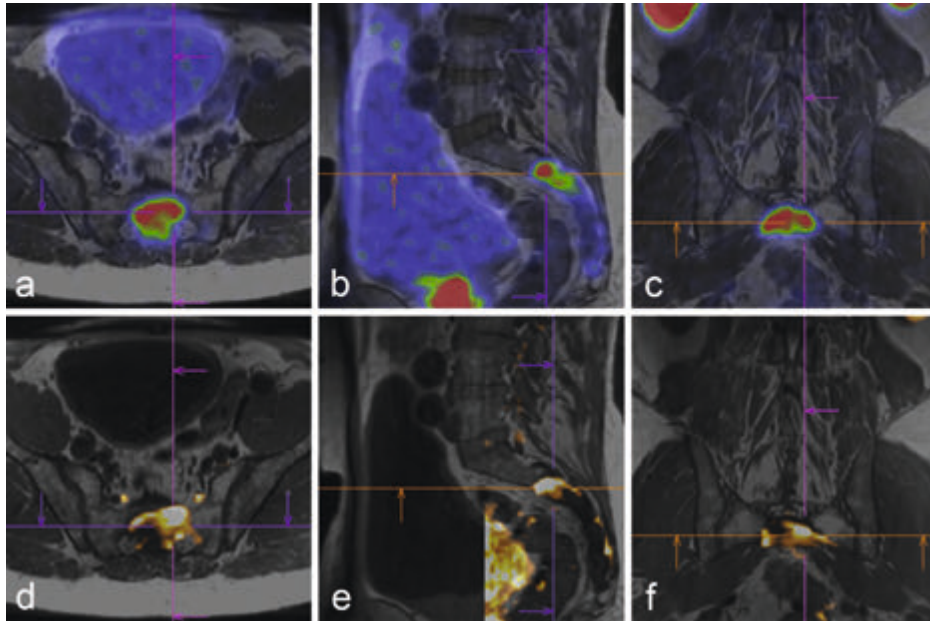


Fig. 4 A-F Image fusion showed the difference in heterogeneity between PSMA uptake and diffusion restriction within some metastases. In this example of patient 8, the lesion in the sacrum appears larger on ^{68}Ga -PSMA-PET than on DWI. The (A-C) ^{68}Ga -PSMA-PET and (D-F) DWI images are both fused with the T1 MRI and the lesion is visualized in (A+D) transversal, (B+E) sagittal and (C+F) coronal planes respectively. The cross is centered at the same position in the T1 MRI for all images and can be used as a reference location. The target point was planned in the regional overlap between high PSMA uptake and high diffusion restriction.

Table 2. The tumor yield and mutations found for the single molecule molecular inversion probe (smMIP) analysis and whole genome sequencing (WGS).

smMIP		WGS		
Patient no.	Pathology Tumor yield (%)	Mutations	Molecular Tumor yield (%)	Mutations
1	70-80	No druggable mutations, no MSI	60	AR gain*
2	40	No druggable mutations. Probably loss of MSH2 and MSH6 by immunohistochemistry, indicating MSI†	11	Mutation in the ligand binding domain of AR§ Tumor mutational load 127
3	5	Insufficient tumor yield	8	Insufficient tumor yield
4	20-30	Mutation in TP53*, no MSI	0	Insufficient tumor yield
5	40	Analysis not performed	40	Gain of AR*, Fusion of TMPRSS2-ETV4
6	15	Analysis not performed	65	Mutation in TP53 Gain of AR§ Loss of PTEN* and RAD51B† Fusion of TMPRSS2-ERG
7	30	No druggable mutations, no MSI	22	No alterations
8	60	No druggable mutations, no MSI	41	Mutation in the ligand binding domain of AR§ Fusion of TMPRSS2-ERG
9	No tumor	No tumor	No tumor	No tumor
10	40	Mutation in TP53*, no MSI	39	Mutation in TP53* Loss of PTEN*

Italics indicates molecular analysis could not be performed. † druggable aberration; * aberration with prognostic significance; § aberration with consequences for clinical management

DISCUSSION

Biopsy of bone metastatic lesions for molecular profiling is challenging due to a high proportion of biopsies with insufficient tumor yield. Unguided iliac crest bone marrow biopsies of metastases seen on CT were positive for PCa in 62.5% of the cases and in only 45% sufficient tumor cells were obtained for molecular analysis [11]. Molecular analysis success rates after CT guided biopsies from bone tissue were similar ranging from 33 to 44% of all biopsies [12–14]. This can be compared to the previous performance of our own institute, by looking at the success rate of 103 patients with prostate cancer were included in the CPCT-02 study, a nationwide study investigating the genomic landscape in relation to response to systemic anticancer therapy using WGS [10]. In these patients, bone biopsies were taken under CT guidance without image fusion, aided by a previously obtained CT scan (n=36), MRI scan (n=11) or ^{68}Ga PSMA-PET/CT scan (n=56). In retrospect, a prior ^{68}Ga PSMA-PET/CT scan led to the highest success rate of biopsies with sufficient tumor yield for molecular analysis (66.1%), compared to a prior CT or MRI scan (52.8% and 54.5% respectively).

Our results indicate that fusion target planning and CBCT guidance are feasible alternatives to CT guidance for taking bone biopsies. Fusion imaging and CBCT are promising techniques to improve biopsy and ablation guidance [15,16]. In this pilot study, in nine of ten (90%) biopsy cores PCa cells were found, and in eight patients (80%) molecular analysis using smMIP or WGS was successful. This suggests that high diffusion restriction and PSMA uptake are indicative for high tumor yield, and that the planned needle path overlay assists in accurate needle placement. Due to the simultaneous introduction of the combination of ^{68}Ga PSMA-PET/CT and MRI as prior imaging modalities and a new innovative method with CBCT-guidance to acquire tumor tissue, we were not able to differentiate which factor contributed most to the outcome of our pilot study. Further investigation is necessary to assess which planning image parameters best characterize the tumor through correlation with histology [17]. When the correlation between image parameters and tumor yield is better understood, a larger prospective study is required to reproduce the results and to compare CBCT-guidance with CT-guided biopsies.

In conclusion, target planning on fused ^{68}Ga PSMA-PET/CT, MRI and CBCT image datasets and CBCT needle guidance was feasible and increased the success rate of molecular analysis on bone biopsies of mCRPC patients compared to CT-guided biopsies in literature as well as in our own historical cohort. The implementation of the biopsy procedure described in this study could improve precision medicine in patients with solely bone metastatic sites and for those with small bone metastatic lesions. In addition, the procedure can be introduced earlier in the disease state with the potential of enhancing personalized treatment options and improving outcome for patients with metastatic prostate cancer.

REFERENCES

1. Robinson D, Van Allen EM, Wu YM, Schultz N, Lonigro RJ, Mosquera JM, et al. Integrative Clinical Genomics of Advanced Prostate Cancer. *Cell*. 2015;162:454.
2. Kumar A, Coleman I, Morrissey C, Zhang X, True LD, Gulati R, et al. Substantial interindividual and limited intraindividual genomic diversity among tumors from men with metastatic prostate cancer. *Nat Med*. 2016;22:369–78.
3. Smits M, Mehra N, Sedelaar M, Gerritsen W, Schalken JA. Molecular biomarkers to guide precision medicine in localized prostate cancer. *Expert Rev Mol Diagn*. 2017;17:791–804.
4. McKay RR, Zukotynski KA, Werner L, Voznesensky O, Wu JS, Smith SE, et al. Imaging, procedural and clinical variables associated with tumor yield on bone biopsy in metastatic castration-resistant prostate cancer. *Prostate Cancer Prostatic Dis*. 2014;17:325–31.
5. Halabi S, Kelly WK, Ma H, Zhou H, Solomon NC, Fizazi K, et al. Meta-analysis evaluating the impact of site of metastasis on overall survival in men with castration-resistant prostate cancer. *J Clin Oncol*. 2016;34:1652–9.
6. Padhani AR, Makris A, Gall P, Collins DJ, Tunariu N, De Bono JS. Therapy monitoring of skeletal metastases with whole-body diffusion MRI. *J Magn Reson Imaging*. 2014;39:1049–78.
7. Mannweiler S, Amersdorfer P, Trajanoski S, Terrett JA, King D, Mehes G. Heterogeneity of Prostate-Specific Membrane Antigen (PSMA) Expression in Prostate Carcinoma with Distant Metastasis. *Pathol Oncol Res*. 2009;15:167–72.
8. Eijkelenboom A, Kamping EJ, Kastner-van Raaij AW, Hendriks-Cornelissen SJ, Neveling K, Kuiper RP, et al. Reliable Next-Generation Sequencing of Formalin-Fixed, Paraffin-Embedded Tissue Using Single Molecule Tags. *J Mol Diagnostics*. 2016;18:851–63.
9. Radboudumc Nijmegen. Project PATH [Internet]. [cited 2019 Apr 12]. Available from: <https://www.netwerk-path.nl/index.php/path/path-test>
10. Center for Personalized Cancer Treatment (CPCT) -02 study (NCT01855477) [cited 2019 Apr 12]. Available from: <https://www.cpct.nl/cpct-02/>
11. Lorente D, Omlin A, Zafeiriou Z, Nava-Rodrigues D, Pérez-López R, Pezaro C, et al. Castration-Resistant Prostate Cancer Tissue Acquisition From Bone Metastases for Molecular Analyses. *Clin Genitourin Cancer*. 2016;14:485–93.
12. Spritzer CE, Afonso PD, Vinson EN, Turnbull JD, Morris KK, Foye A, et al. Bone Marrow Biopsy: RNA Isolation with Expression Profiling in Men with Metastatic Castration-resistant Prostate Cancer—Factors Affecting Diagnostic Success. *Radiology*. 2013;269:816–23.
13. Holmes MG, Foss E, Joseph G, Foye A, Beckett B, Motamedi D, et al. CT-Guided Bone Biopsies in Metastatic Castration-Resistant Prostate Cancer: Factors Predictive of Maximum Tumor Yield. *J Vasc Interv Radiol*. 2017;28:1073–1081.e1.
14. Sailer V, Schiffman MH, Kossai M, Cyrta J, Beg S, Sullivan B, et al. Bone biopsy protocol for advanced prostate cancer in the era of precision medicine. *Cancer*. 2018;124:1008–15.
15. Monfardini L, Orsi F, Caserta R, Sallemi C, Della Vigna P, Bonomo G, et al. Ultrasound and cone beam CT fusion for liver ablation: technical note. *Int J Hyperth*. 2018;35:500–4.
16. Mauri G, Gennaro N, De Beni S, Ierace T, Goldberg SN, Rodari M, et al. Real-time US-18FDG-PET/CT image fusion for guidance of thermal ablation of 18FDG-PET-positive liver metastases: the added value of contrast enhancement. *Cardiovasc Intervent Radiol*. 2019;42:60–8.
17. Perez-Lopez R, Rodrigues DN, Figueiredo I, Mateo J, Collins DJ, Koh DM, et al. Multiparametric magnetic resonance imaging of prostate cancer bone disease correlation with bone biopsy histological and molecular features. *Invest Radiol*. 2018;53:96–102.



PART III

**IMPROVING THE SUCCESS RATE OF MOLECULAR
ANALYSES IN BONE METASTATIC PROSTATE
CANCER**



CHAPTER 5

THE GENOMIC LANDSCAPE OF METASTATIC CASTRATION-RESISTANT PROSTATE CANCERS REVEALS MULTIPLE DISTINCT GENOTYPES WITH POTENTIAL CLINICAL IMPACT

Lisanne F. van Dessel*	Job van Riet*
Minke Smits	Yanyun Zhu
Paul Hamberg	Michiel S. van der Heijden
Andries M. Bergman	Inge M. van Oort
Ronald de Wit	Emile E. Voest
Neeltje Steeghs	Takafumi N. Yamaguchi
Julie Livingstone	Paul C. Boutros
John W.M. Martens	Stefan Sleijfer
Edwin Cuppen	Wilbert Zwart
Harmen J.G. van de Werken	Niven Mehra
Martijn P. Lolkema	

* These authors contributed equally to this work.

Nature Communications. 2019;10(1):5251

ABSTRACT

Metastatic castration-resistant prostate cancer (mCRPC) has a highly complex genomic landscape. With the recent development of novel treatments accurate stratification strategies are needed. Here we present the whole-genome sequencing (WGS) analysis of fresh-frozen metastatic biopsies from 197 mCRPC patients. Using unsupervised clustering based on genomic features, we define eight distinct genomic clusters. We observe potentially clinically relevant genotypes, including microsatellite instability (MSI), homologous recombination deficiency (HRD) enriched with genomic deletions and *BRCA2* aberrations, a tandem duplication genotype associated with *CDK12*^{-/-} and a chromothripsis-enriched subgroup. Our data suggests that stratification on WGS characteristics may improve detection of MSI, *CDK12*^{-/-} and HRD patients. From WGS and ChIP-seq data, we show the potential clinical relevance of recurrent alterations in non-coding regions identified with WGS and highlight the central role of *AR* signaling in tumor progression. These data underline the potential value of using WGS to accurately stratify mCRPC patients into clinically actionable subgroups.

INTRODUCTION

Prostate cancer is known to be a notoriously heterogeneous disease and the genetic basis for this interpatient heterogeneity is poorly understood [1,2]. The ongoing development of new therapies for metastatic prostate cancer that target molecularly defined subgroups further increases the need for accurate patient classification and stratification[3-5]. Analysis of whole-exome sequencing data of metastatic prostate cancer tumors revealed that 65% of patients had actionable targets in non-androgen receptor related pathways, including PI3K, WNT and DNA repair [6]. Several targeted agents involved in these pathways, including mTOR/AKT pathway inhibitors [7] and PARP inhibitors [8], are currently in various phases of development and the first clinical trials show promising results. Therefore, patients with metastatic prostate could benefit from better stratification to select the proper therapeutic options. More extensive analysis using whole-genome sequencing (WGS) based classification of tumors may be useful to improve selection of patients for different targeted therapies. The advantage of WGS may be its comprehensive nature allowing it to detect patterns of mutations as has been suggested by the successful treatment of patients with high tumor mutational burden with immune checkpoint blockade therapy [9-12]. Moreover, WGS detects structural variation and aberrations in non-coding regions, both important features of prostate cancer.

The stratification of prostate cancer patients, based on differences in the mutational landscape, have mainly focused on mutually-exclusive mutations, copy number alterations or distinct patterns in RNA-sequencing caused by the abundant TMPRSS2-ERG fusion, which is recurrent in 50% of primary prostate tumors [6,13-18]. More recently, WGS of metastatic prostate cancer tumors demonstrated that structural variations (SVs) arise from specific alterations such as *CDK12*^{-/-} and *BRCA2*^{-/-} genotypes and are strongly associated with genome-wide events such as large tandem duplications or small genomic deletions, respectively [19-23]. Advances in WGS and interpretation have revealed rearrangement signatures in breast cancer relating to disease stage, homologous recombination deficiency (HRD) and *BRCA1/BRCA2* defects based on size and type of structural variant [22-24]. Thus, WGS enables the identification of patterns of DNA aberrations (i.e. genomic scars) that may profoundly improve classification of tumors that share a common etiology if performed in a sufficiently powered sample size.

In this study, we analyzed the WGS data obtained from 197 metastatic castration-resistant prostate cancer (mCRPC) patients. We describe the complete genomic landscape of mCRPC, including tumor specific single and multi-nucleotide variants (SNVs and MNVs), small insertions and deletions (InDels), copy number alterations (CNAs), mutational signatures, kataegis, chromothripsis and structural rearrangements (SVs). Next, we compared the

mutational frequency of the detected driver genes and genomic subgroups with an unmatched WGS cohort of primary prostate cancer ($n = 210$), consisting of exclusively of Gleason score 6-7 tumors [15,25]. We investigated the presence of possible driver genes by analyzing genes with enriched (non-synonymous) mutational burdens and recurrent or high-level copy number alterations [26,27]. By utilizing various basic genomic features reflecting genomic instability and employing unsupervised clustering, we were able to define eight distinct genomic subgroups of mCRPC patients. We combine our genomic findings with AR, FOXA1 and H3K27me ChIP-seq data and confirmed that important regulators of MYC and AR-mediated signaling are located in non-coding regions with open chromatin and highlight the central role of AR signaling in tumor progression.

RESULTS

Characteristics of the mCRPC cohort and sequencing approach

We analyzed fresh-frozen metastatic tumor samples and matched blood samples from 197 castration-resistant prostate cancer (CRPC) patients using WGS generating to date the largest WGS dataset for mCRPC (Fig. 1a). Clinical details on biopsy site, age and previous treatments of the included patients are described in Fig. 1 and supplementary Table 2. WGS data was sequenced to a mean coverage of 104X in tumor tissues and 38X in peripheral blood (Supplementary Fig. 1a). The median estimated tumor cell purity using *in silico* analysis of our WGS data was 62% (range: 16-96%; Supplementary Fig. 1b). Tumor cell purity correlated weakly with the frequency of called SNVs (Spearman correlation; $\rho = 0.2$; $p = 0.005$), InDels (Spearman correlation; $\rho = 0.35$; $p < 0.001$), MNVs (Spearman correlation; $\rho = 0.25$; $p < 0.001$) and structural variants (Spearman correlation; $\rho = 0.22$; $p = 0.002$; Supplementary Fig. 1c).

Landscape of mutational and structural variants in mCRPC

The median tumor mutational burden (TMB) on genomic level (SNVs and InDels per Mbp) was 2.7 in our mCRPC cohort, including 14 patients with high TMB (> 10). We found a median of 6621 single-nucleotide variants (SNVs; IQR: 5048-9109), 1008 small insertions and deletions (InDels; IQR: 739-1364), 55 multi-nucleotide variants (MNVs; IQR: 34-86) and 224 SVs (IQR: 149-370) per patient (Supplementary Fig. 2a-c). We observed a highly complex genomic landscape consisting of multiple driver mutations and structural variants in our cohort.

We confirmed that known driver genes of prostate cancer were enriched for non-synonymous mutations (Fig. 2 and supplementary Fig. 2e) [13, 15, 28]. In total, we detected 11 genes enriched with nonsynonymous mutations: *TP53*, *AR*, *FOXA1*, *SPOP*, *PTEN*, *ZMYM3*, *CDK12*, *ZFP36L2*, *PIK3CA* and *APC*. *ATM* was mutated in 11 samples, but after multiple-testing correction appeared not to be enriched.

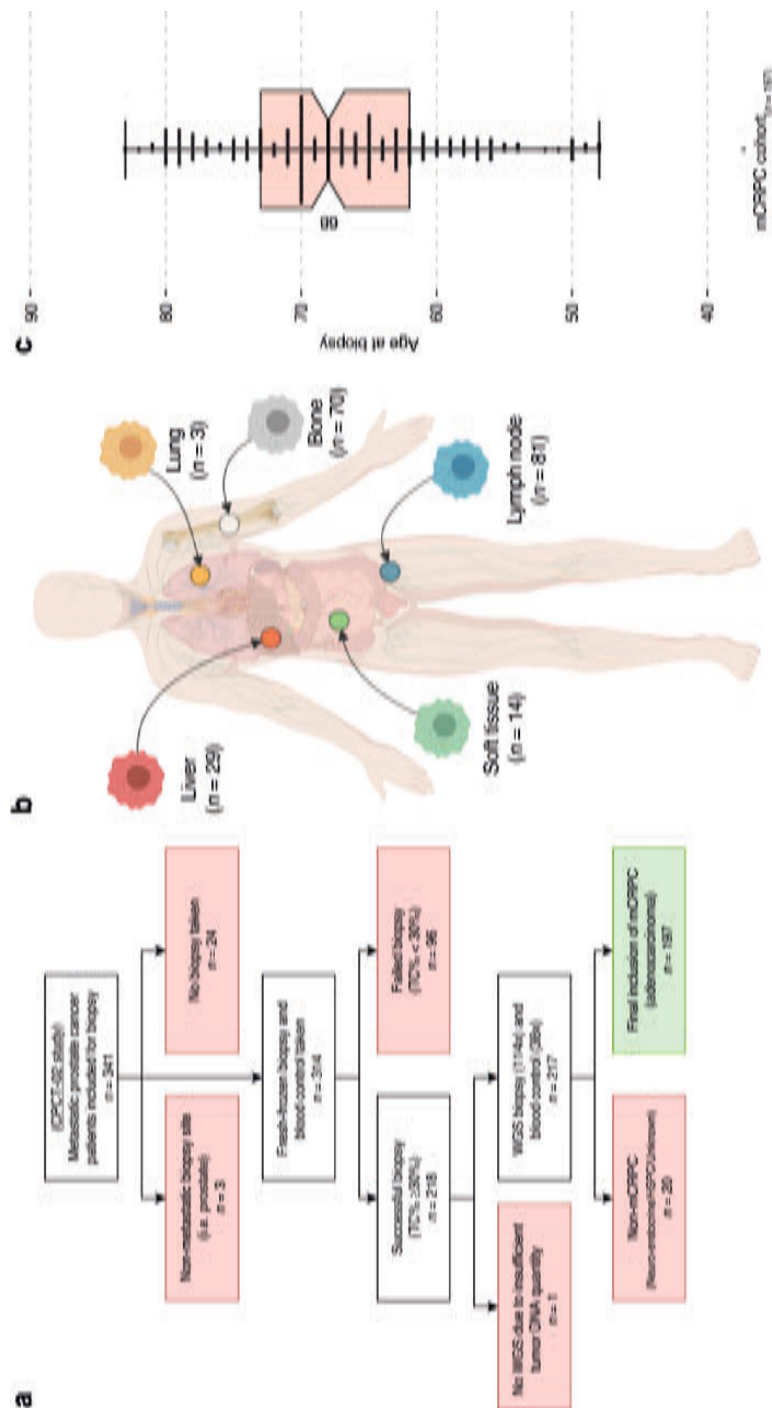


Fig. 1. Overview of study design and patient cohort (n = 197). **a** Flowchart of patient inclusion. From the CPTC-02 cohort, patients with metastatic prostate cancer were selected. Patients were excluded if data from metastatic samples were not available and if clinical data indicated that patients had hormone sensitive or neuro-endocrine prostate cancer or unknown disease status at the time of analysis. **b** Overview of the biopsy sites. Number of biopsies per metastatic site analyzed with WGS. **c** Age of patients at biopsy. Bee-swarm boxplot with notch of the patient age distribution. Boxplot depicts the upper and lower quartiles, with the median shown as a solid line; whiskers indicate 1.5 times the interquartile range (IQR). Data points outside the IQR are shown.

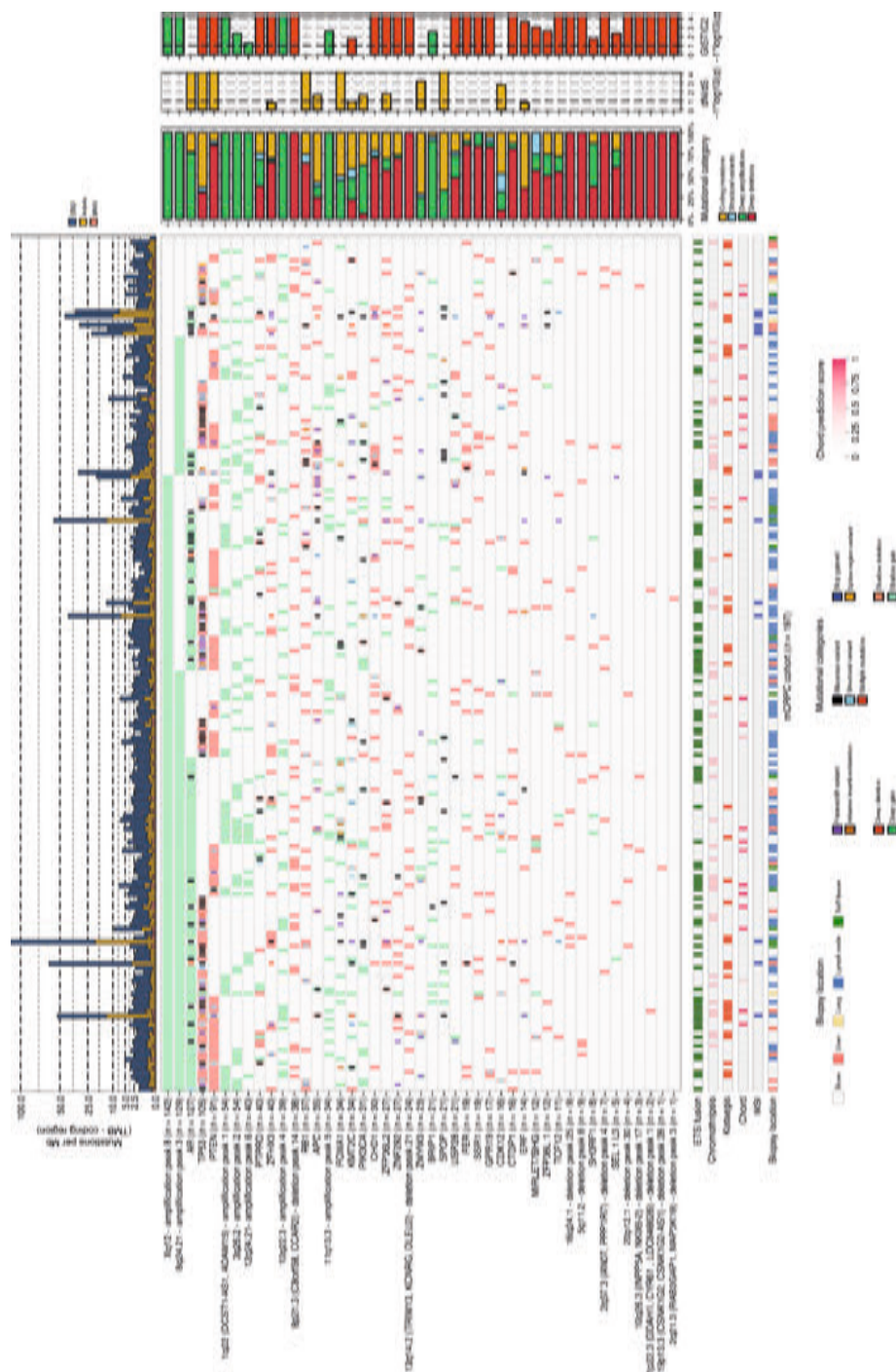


Fig 2. (caption on page 92)

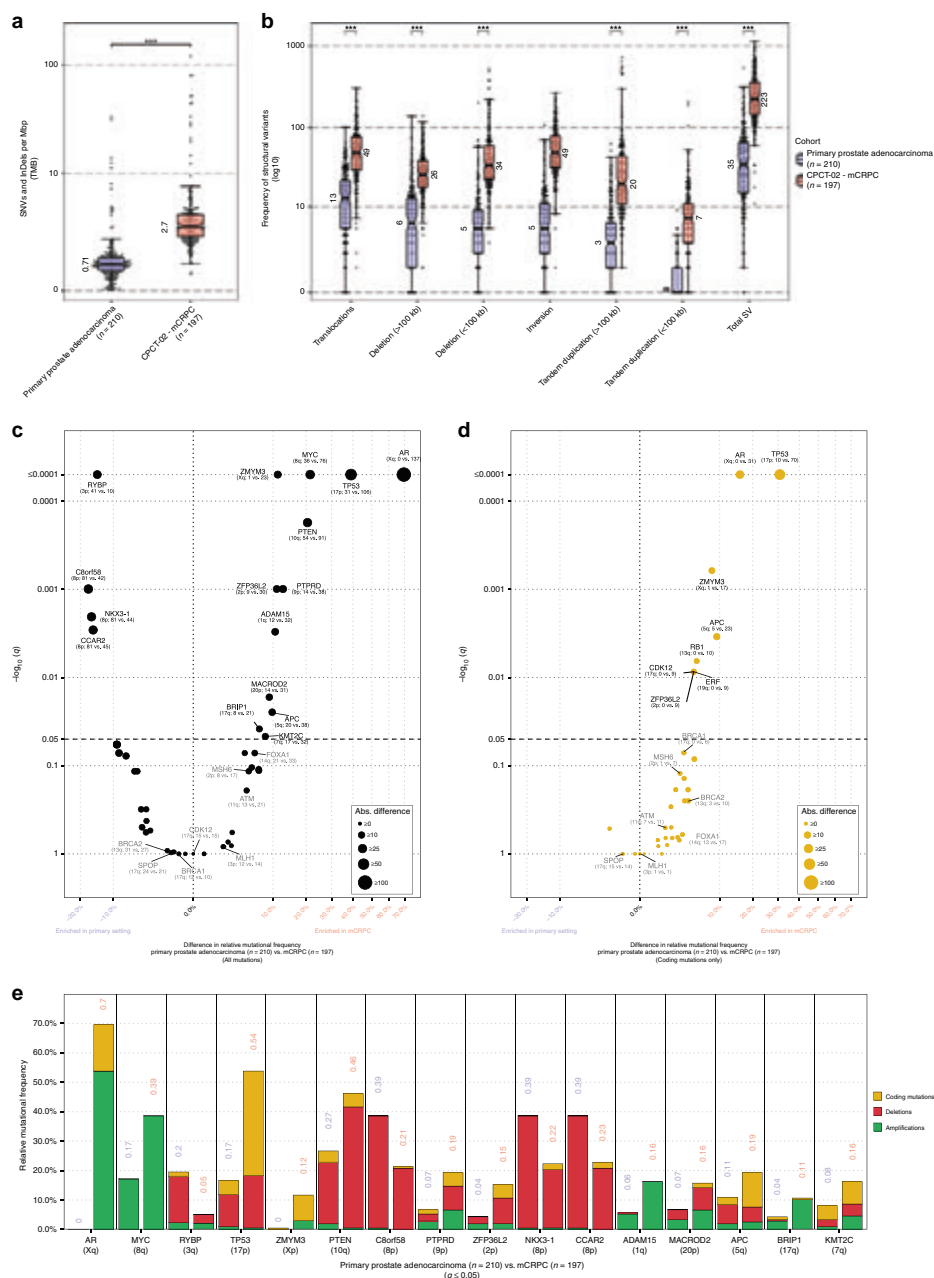


Fig 3. (caption on page 92)

Fig. 2. mCRPC shows multiple recurrent somatic alterations affecting several oncogenic pathways. Based on dN/dS ($q \leq 0.1$) and GISTIC2 focal peak ($q \leq 0.1$) criteria, we show the genes and focal genomic foci that are recurrently mutated, amplified, or deleted in our mCRPC cohort of 197 patients. The upper track (top bar plot) displays the number of genomic mutations per Mbp (TMB) per SNV (blue), InDel (yellow), and MNV (orange) category in coding regions (square-root scale). Samples are sorted based on mutual-exclusivity of the depicted genes and foci. The heatmap displays the type of mutation(s) per sample; (light-)green or (light-)red backgrounds depict copy-number aberrations while the inner square depicts the type of (coding) mutation(s). Relative proportions of mutational categories (coding mutations [SNV, InDels, and MNV] (yellow), SV (blue), deep amplifications [high-level amplifications resulting in many additional copies] (green), and deep deletions [high-level losses resulting in (near) homozygous losses] (red)) per gene and foci are shown in the bar plot next to the heatmap. Narrow GISTIC2 peaks covering ≤ 3 genes were reduced to gene-level rows if one of these genes is present in the dN/dS ($q \leq 0.1$) analysis or is a known oncogene or tumor-suppressor. For GISTIC2 peaks covering multiple genes, only deep amplifications and deep deletions are shown. Recurrent aberrant focal genomic foci in gene deserts are annotated with their nearest gene. Significance scores ($-1 \times \log_{10}(q)$) of the dN/dS and GISTIC2 analysis are shown on the outer-right bar plots; bars in the GISTIC2 significance plot are colored red if these foci were detected as a recurrent focal deletion and green if detected as a recurrent focal gain. Per sample, the presence of (predicted) ETS fusions (green), chromothripsis (light pink), kataegis (red), CHORD prediction score (HR-deficiency) (pink gradient), MSI status (dark blue), and biopsy location are shown as bottom tracks.

Fig. 3. Comparison of the mutational landscape between primary prostate cancer and mCRPC. **a** Tumor mutational burden (SNVs and InDels per Mbp) from a primary prostate cancer ($n = 210$) and the CPTC-02 mCRPC cohort ($n = 197$). Bee-swarm boxplot with notch of the tumor mutational burden. Boxplot depicts the upper and lower quartiles, with the median shown as a solid line; whiskers indicate 1.5 times the interquartile range (IQR). Data points outside the IQR are shown. Statistical significance was tested with Wilcoxon rank-sum test and $p \leq 0.001$ is indicated as ***. **b** Frequency of structural variant events from an unmatched cohort of primary prostate cancer ($n = 210$) and the CPTC-02 mCRPC cohort ($n = 197$). Boxplot depicts the upper and lower quartiles, with the median shown as a solid line; whiskers indicate 1.5 times the interquartile range (IQR). Data points outside the IQR are shown. Statistical significance was tested with Wilcoxon rank-sum test and $p \leq 0.001$ is indicated as ***. **c** Comparison of the mutational frequencies for driver genes detected by dN/dS and/or GISTIC2, or subtype-specific genes, enriched in mCRPC relative to primary prostate cancer or vice-versa. The difference in relative mutational frequency is shown on the x-axis and the adjusted p-value (two-sided Fisher's Exact Test with BH correction) is shown on the y-axis. Size of the dot is proportional to the absolute difference in mutational frequency between both the cohorts. Symbols of genes with p-values below 0.05 are depicted in black and additional genes-of-interests are highlighted in gray. The general genomic foci of the gene and absolute number of samples with an aberration per cohort in primary prostate cancer and mCRPC, respectively, is shown below the gene symbol. This analysis was performed on coding mutations, gains and deletions per gene. **d** Same as in c but using only coding mutations. **e** Overview of the mutational categories (coding mutations [yellow], deletions [red] and amplifications [green]) of the driver genes detected by dN/dS and/or GISTIC2, or subtype-specific genes, enriched in mCRPC relative to primary prostate cancer ($q \leq 0.05$). For each gene the frequency in primary prostate cancer is displayed followed by the frequency in mCRPC.

Our copy number analysis revealed distinct amplified genomic regions including 8q and Xq and deleted regions including 8p, 10q, 13q and 17p (Supplementary Fig. 2d). Well-known prostate cancer driver genes [8,16], such as *AR*, *PTEN*, *TP53* and *RB1*, are located in these regions. In addition to large-scale chromosomal copy number alterations, we could identify narrow genomic regions with recurrent copy number alterations across samples which could reveal important prostate cancer driver genes (Supplementary data file 1).

TMPRSS2-ERG gene fusions were the most common fusions in our cohort ($n = 84$ out of 197; 42.6%) and were the majority of the *ETS* family fusions ($n = 84$ out of 95; 88.4%; Fig.

2 and supplementary Fig. 3). This is comparable to primary prostate cancer, where *ETS* fusions are found in approximately 50% of tumors [13,15]. The predominant deletion site was located upstream of the second exon of *ERG*, which preserves its *ETS* domain in the resulting fusion gene.

In 42 patients (21.3%) we observed regional hypermutation (kataegis; Fig. 2 and supplementary Fig. 4). In addition, we did not observe novel mutational signatures specific for metastatic disease or possible pre-treatment histories (Supplementary Fig. 5) [29].

To further investigate whether our description of the genome-wide mutational burden and observed alterations in drivers and/or subtype-specific genes in mCRPC were metastatic specific, we compared our data against an unmatched WGS cohort of primary prostate cancer ($n = 210$) [15,25], consisting of Gleason score 6-7 disease. Comparison of the median genome-wide TMB (SNVs and InDels per Mbp) revealed that the TMB was roughly 3.8 times higher in mCRPC (Fig. 3a) and the frequency of structural variants also differed (Fig. 3b) between disease stages, increasing as disease progresses. Analysis on selected driver and subtype-specific genes showed that the mutational frequency of several genes (*AR*, *TP53*, *MYC*, *ZMYM3*, *PTEN*, *PTPRD*, *ZFP36L2*, *ADAM15*, *MARCOD2*, *BRIP1*, *APC*, *KMT2C*, *CCAR2*, *NKX3-1*, *C8orf58* and *RYBP*) was significantly altered ($q \leq 0.05$) between the primary and metastatic cohorts (Fig. 3c-e). All genes for which we observed significant differences in mutational frequency, based on coding mutations, were enriched in mCRPC (Fig. 3d). We did not identify genomic features that were specific for the metastatic setting. We cannot exclude from these data that matched sample analysis or larger scale analysis could reveal such aberrations.

We next determined whether previous treatments affected the mutational landscape. Using treatment history information, we grouped prior secondary anti-hormonal therapy, taxane-based chemotherapy and systemic radionucleotide therapy into different groups (Supplementary Fig. 6). This analysis did not reveal systematic biases due to pretreatment in aberrations, such as TMB, kataegis, chromothripsis, *ETS* fusions, or somatically altered genes (Supplementary data file 1).

The role of the AR-pathway in mCRPC

Focusing on the AR-pathway revealed that aberrant AR signaling occurred in 80% of our patients. In 57.3% of patients both *AR* and the *AR*-enhancer (~66.13 Mb on chromosome X; located about 629 upstream of the *AR* gene [20]) were affected (Fig. 4a). In an additional 6.6% and 14.7% of patients only *AR* alterations or *AR*-enhancer amplification occurred, respectively. The percentage of mCRPC patients with the exclusive *AR*-enhancer amplification is similar to previous observations (4 out of 20 mCRPC patients; 17%) [20].

Concurrent amplification of AR and AR-enhancer was not necessarily of equal magnitude, which resulted in differences in copy number enrichment of these loci (Fig. 4b).

To date no AR ChIP-seq data has been reported in human mCRPC samples and evidence of increased functional activity of the amplified enhancer is based on cell line models [30]. To resolve this, we performed AR ChIP-seq on two selected mCRPC patient samples with AR enhancer amplification based on WGS data. As controls we used two prostate cancer cell-lines (LNCaP and VCaP) and three independent primary prostate cancer samples that did not harbor copy number alterations at this locus (Supplementary Fig. 7) [31].

We observed active enhancer regions (H3K27ac) in the castration-resistant setting, co-occupied by AR and FOXA1, at the amplified AR-enhancer. This is substantially stronger when compared to the hormone-sensitive primary prostate cancer samples without somatic amplifications (Fig. 4c and Supplementary Fig. 7). Furthermore, a recurrent focal amplification in a non-coding region was observed at 8q24.21 near PCAT1. This locus bears similar epigenetic characteristics to the AR-enhancer with regard to H3K27ac and, to a lesser extent, binding of AR and/or FOXA1 in the mCRPC setting (Fig. 4d and Supplementary Fig. 7)

Fig. 4. WGS reveals novel insight into the various (non-coding) aberrations affecting AR regulation. **a** Mutational overview of top recurrently mutated genes affecting AR regulation and their putative enhancer foci (as detected by GISTIC2). The first track represents the number of genomic mutations per Mbp (TMB) per SNV (blue), InDels (yellow), and MNV (orange) category genome-wide (square-root scale). Samples are sorted based on mutual-exclusivity of the depicted genes and foci. The heatmap displays the type of mutation(s) per sample, (light-) green or (light-)red backgrounds depict copy-number aberrations while the inner square depicts the type of (coding) mutation(s). Relative proportions of mutational categories (coding mutations [SNV, InDels and MNV] (yellow), SV (blue), deep amplifications (green), and deep deletions (red)) per gene and foci are shown in the bar plot next to the heatmap. The presence of chromothripsis (light pink), kataegis (red), CHORD prediction score (HR-deficiency) (pink gradient), MSI status (dark blue), and biopsy location are shown as bottom tracks. **b** Overview of the copy-number deviations between putative enhancer and gene regions for AR and MYC. Samples were categorized as enhancer- (blue) or gene- (red) enriched if enhancer-to-gene ratio deviated >1 studentized residual (residual in standard deviation units) from a 1:1 ratio. **c** Copy number and ChIP-seq profiles surrounding the AR and PCAT1/MYC gene loci (with 1.25 additional Mbp up-/downstream). The upper panel displays the selected genomic window and the overlapping genes. The first and second track display the aggregated mean copy number (per 0.1 Mbp window) of the enhancer- and gene-enriched samples, respectively. These profiles identify distinct amplified regions (indicated by red asterisk) in proximity to the respective gene bodies. The 3th to 8th tracks represent AR ChIP-seq profiles (median read-coverage per 0.1 Mbp windows) in two mCRPC patients (# 3 and 4), LNCaP (# 5) and LNCaP with R1881 treatment (# 6), VCaP (# 7) and bicalutamide-resistant VCaP (# 8). The 9th to 11th tracks represent FOXA1 ChIP-seq profiles (median read-coverage per 0.1 Mbp windows) in two mCRPC patients (#9 and 10) and LNCaP with R1881 treatment (# 11). The 12th to 14th tracks represent H3K27ac ChIP-seq profiles (median read-coverage per 0.1 Mbp windows) in two mCRPC patients (# 12 and 13) and LNCaP with R1881 treatment (# 14) reflecting active enhancer regions. ChIP-seq peaks (MACS/MACS2; $q < 0.01$) are shown as black lines per respective sample. ----->

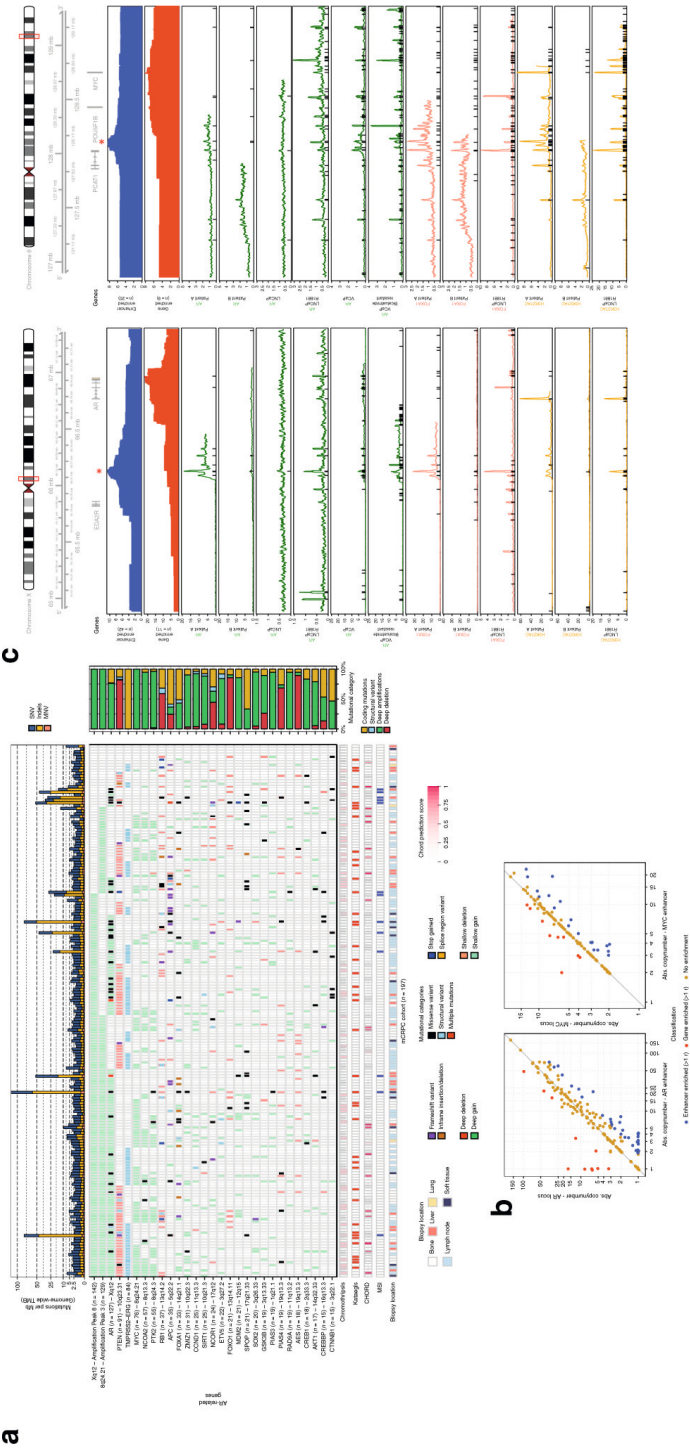


Fig 4.

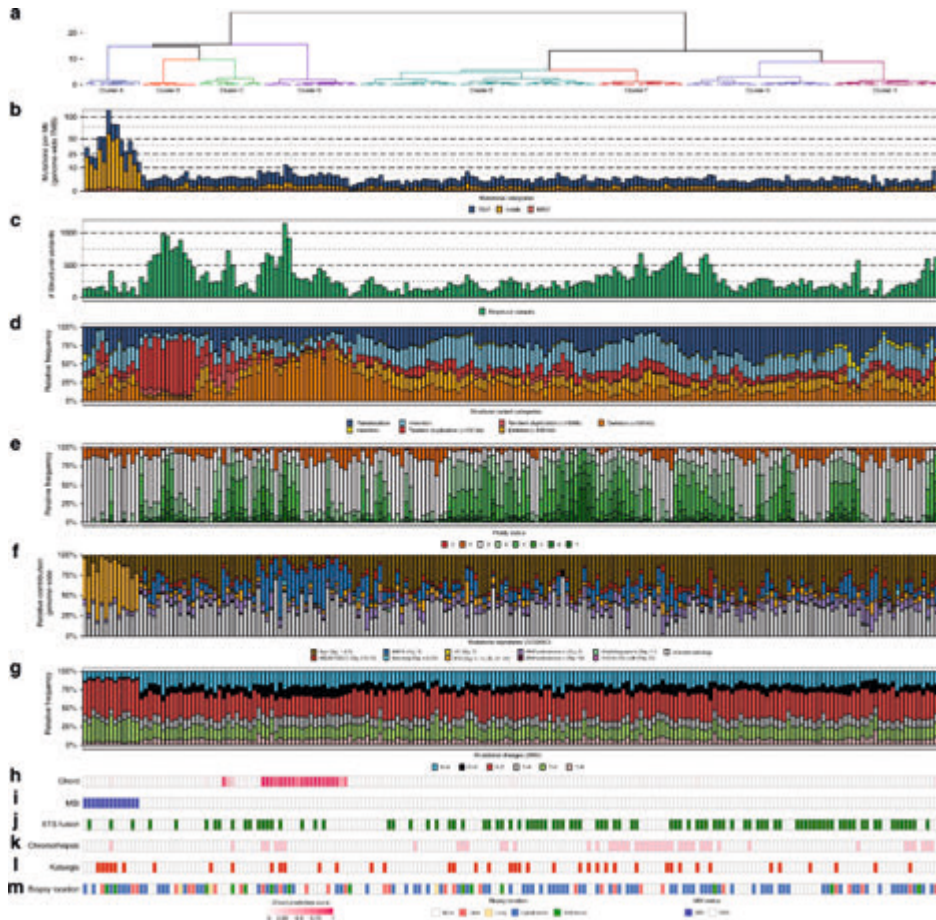


Fig. 5. Unsupervised clustering of mCRPC reveals distinct genomic phenotypes. **a** Dendrogram of unsupervised clustering with optimal leaf ordering. Top eight clusters are highlighted and denoted based on order of appearance (left to right): A to H. y-axis displays clustering distance (Pearson correlation; ward.D). **b** Number of genomic mutations per Mbp (TMB) per SNV (blue), InDels (yellow), and MNV (orange) category. All genome-wide somatic mutations were taken into consideration (square-root scale). **c** Absolute number of unique structural variants per sample. **d** Relative frequency per structural variant category (translocations, inversions, insertions, tandem duplications, and deletions). Tandem Duplications and Deletions are subdivided into >100 kbp and <100 kbp categories. This track shows if an enrichment for particular category of (somatic) structural variant can be detected, which in turn, can be indicative for a specific mutational aberration. **e** Relative genome-wide ploidy status, ranging from 0 to ≥ 7 copies. This track shows the relative percentage of the entire genome, which is (partially) deleted (ploidy <2 per diploid genome) or amplified (>2 per diploid genome). **f** Relative contribution to mutational signatures (COSMIC) summarized per proposed etiology. This track displays the proposed etiology of each SNV based on their mutational contexts. **g** Relative frequency of different SNV changes. **h** HR-deficient prediction score as assessed by CHORD. The binary prediction score of CHORD (ranging from 0 to 1) is shown, in which higher scores reflect more evidence for HR-deficiency in a given sample. **i** MSI status as determined using a stringent threshold of MSI characteristics [40]. **j** Presence of a fusion with a member of the ETS transcription factor family. Green color indicates a possible fusion. **k** Presence of chromothripsis. Pink color indicates presence of chromothripsis as estimated by ShatterSeek. **l** Presence of kataegis. Red color indicates presence of one or more regions showing kataegis. **m** General biopsy location.

Table 1. Overview of the distinctive characteristics for each cluster (A-H)

	Number of patients (n; % of cohort)	Tumor mutational burden (CDS)	SNV/InDel ratio	Number of structural variants	Main structural variant category	Ploidy status	Main mutational signature	Top 3 cluster-specific aberrations (% of cluster)	ETS-fusions (n)	Chromothripsis (n)	Kataegis (n)
Cluster A	13 (6.6)	36,88	0,99	149	None	1,92	MSI	MSH6 (69.2), JAK1 (69.2), CIC (58.3)	3	1	6
Cluster B	13 (6.6)	2,44	7,07	669	Tandem duplications (>100kb)	2,39	N/A	CDK12 (84.6), FGF3 (69.2), FGF4 (69.2)	2	0	1
Cluster C	15 (7.6)	3,00	6,73	237	Tandem duplications (<100kb)	3,19	N/A	None	7	1	2
Cluster D	22 (11.2)	4,39	7,28	323	Deletions (>100kb)	2,16	BRCA	BRCA2 (68.2)	7	5	5
Cluster E	55 (27.9)	2,12	7,13	178	None	3,24	N/A	None	25	8	13
Cluster F	20 (10.2)	2,51	6,15	400	None	3,35	N/A	Chromothripsis (80,0)	10	16	7
Cluster G	34 (17.3)	2,12	6,13	222	None	2,98	N/A	None	23	8	5
Cluster H	25 (12.7)	2,30	5,81	201	Insertions	1,97	N/A	None	16	7	3

All numbers are median of the cluster, unless otherwise indicated
CDS coding sequence

WGS-based stratification defines genomic subgroups in mCRPC

Our comprehensive WGS data and large sample size enabled us to perform unsupervised clustering on several WGS characteristics to identify genomic scars that can define subgroups of mCRPC patients. We clustered our genomic data using the total number of SVs, relative frequency of SV category (translocations, inversions, insertions, tandem duplications, and deletions), genomewide TMB encompassing SNV, InDels and MNV, and tumor ploidy. Prior to clustering, we subdivided tandem duplications and deletions into two major categories based on the respective genomic size of the aberration (smaller and larger than 100 kbp) since previous studies revealed distinctions based on similar thresholds for these structural variants in relation to specific mutated genes [19–21,32]. Similarly, we observed a difference in genomic size and number in our subgroups of mCRPC patients (Supplementary Fig. 8).

This analysis defined eight distinct subgroups (Figs. 5, 6 and Supplementary Figs. 8–11): (A) microsatellite instability (MSI) signature with high TMB and association with mismatch repair deficiency; (B) tandem duplication (>100 kbp) phenotype associated with biallelic CDK12 inactivation; (D) homologous recombination deficiency (HRD) features with many deletions (>100 kbp) and association with (somatic) mutations in BRCAness-associated genes; this was supported by high HR-deficiency scores (CHORD; Supplementary Figs. 8 and 9); (F) chromothripsis; (C, E, G, H); non-significant genomic signature without any currently known biological association. Table 1 summarizes the key features of each subgroup.

Clusters A and B represent previously identified genomic subgroups (MSI and *CDK12*^{-/-}) [6,19,21,33]. In cluster B, only two patients were allocated to this subgroup without a specific somatic mutation in the identifying gene. The well-known mismatch repair genes: *MLH1*, *MSH2*, and *MSH6* are among the cluster specific-mutated genes in cluster A (Fig. 6a). Twelve out of these thirteen patients had at least one inactivating alteration in one of these genes (Fig. 6b). Interestingly, cluster B (*CDK12*^{-/-}) harbors two patients without non-synonymous *CDK12* mutation or copy-number alteration; the cause of their tandem duplication phenotype is currently unknown (Fig. 6b). Cluster D shows significant features of HRD, specifically biallelic *BRCA2* inactivation (Supplementary Fig. 12), mainly mutational signature 3, enrichment of deletions (< 100 kbp) and is supported by high HR-deficiency scores (CHORD) (Supplementary Figs. 8 and 9) [22, 34]. Remarkably, seven out of twenty-two patients did not have a biallelic *BRCA2* inactivation. However, four of these patients showed at least one (deleterious) aberration in other BRCAness-related genes (Figure 6b) [35].

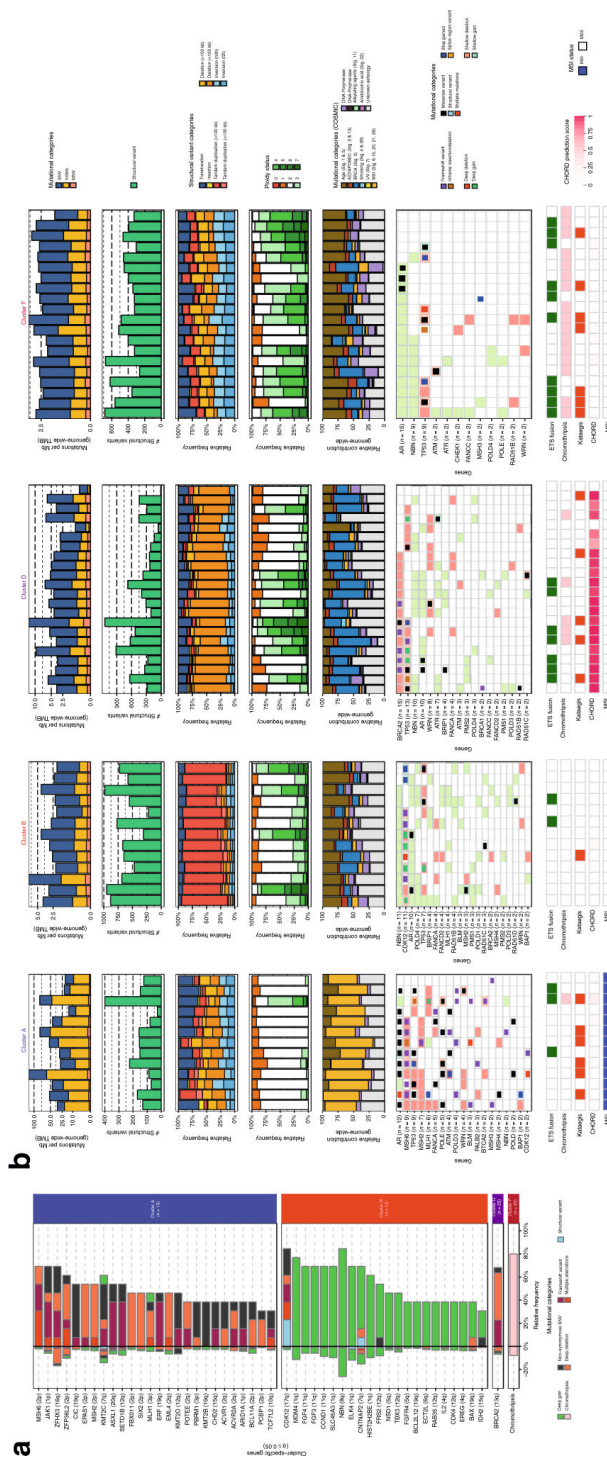


Fig. 6. Distinct genomic phenotypes in mCRPC are enriched by mutually exclusive aberrations in key pathways. **a** Cluster-specific enrichment of mutated genes (multiple colors), chromothripsis (light pink), and structural variants (light blue) (Fisher's Exact Test with BH correction; $q \leq 0.05$). Percentages to the left of the black line represent the relative mutational frequency in mCRPC samples, which are not present in the respective cluster, while the percentages to the right of the black line represent the relative mutational frequency present in the samples from the tested cluster. **b** Genomic overview with biologically relevant genes in the clusters A, B, D, and F with mutational enrichment of genes or large-scale events. The first track represents the number of genomic mutations per Mb (TMB) per SNV (blue), indels (yellow), and MNV (orange) category genome-wide (square-root scale). The second track represents the absolute number of unique structural variants (green) per sample. The third track represents the relative frequency per structural variant category. Tandem duplications and deletions are subdivided into >100 kbp and <100 kbp categories. The fourth track represents the relative genome-wide ploidy status, ranging from 0 to ≥ 7 copies. The fifth track represents the relative contribution to mutational signatures (COSMIC) summarized per proposed etiology. The sixth track displays somatic mutations in the relevant genes found in at least one cluster. The lower tracks represent presence of ETs fusions (green), chromothripsis (pink), kataegis (red), CHORD prediction scores (HR-deficiency) (pink gradient), and MSI status (blue) based on a threshold of MSI characteristics.

Cluster F was enriched for chromothripsis events, however we could not reproduce a previous finding suggesting chromothripsis was associated with inversions and p53 inactivation in prostate cancer [21]. Apart from the chromothripsis events, no clear gene aberration was associated with this cluster (Fig. 6b). In the remaining patients, there were no distinct genomic signatures or biologic rationale for patient clustering (cluster C, E, G, H). In cluster C, conjoint aberrations of *BRCA1* and *TP53* were observed in one patient with a high HR-deficiency prediction score (CHORD), which is known to lead to a small tandem duplication phenotype (< 100 kbp) [32]. Two other patients within cluster C displayed a weak CHORD scoring associated with HR-deficiency, however no additional definitive evidence was found for a *BRCA1* loss-of-function mutation within these patients.

In addition to our unsupervised clustering approach, we clustered our samples using the clustering scheme proposed by TCGA (Supplementary Fig. 13a), which defines seven clusters based on coding mutations and copy-number aberrations in *SPOP*, *FOXA1*, *IDH1*, and *ETS* family gene fusions (and overexpression) per promiscuous partner (*ERG*, *ETV1*, *ETV4*, and *FLI1*) [13]. Unfortunately, we currently lack matched mRNA-sequencing data in our cohort and therefore cannot observe overexpression of fused *ETS* family members, which restricted us to only characterize the genomic breaks of these promiscuous partners. Without incorporation of *ETS* family overexpression, this proposed clustering scheme categorizes 61% of mCRPC into these seven groups versus 68% of the original cohort containing primary prostate cancer described by TCGA (Supplementary Fig. 13b) [13]. There was no significant correlation between the TCGA clustering scheme and our defined genomic subtypes such as MSI, BRCAness or *CDK12*–/–. In addition, we did not detect statistical enrichment or depletion ($q \leq 0.05$) between these supervised clusters and additional-mutated genes, kataegis and chromothripsis, only the known enrichment of homozygous *CHD1* deletions in the *SPOP*-cluster was observed [13].

Performing unsupervised clustering and principal component analysis on the primary prostate cancer and metastatic cohorts revealed no striking primary-only genomic subgroup nor did we detect the presence of the mCRPC-derived genomic subgroups in the primary prostate cancer cohort (Supplementary Fig. 14). This could reflect the absence of *CDK12* mutations and the presence of only three sporadic *BRCA2*-mutated samples (1%) in the primary prostate cancer cohort. Furthermore, only one sample (1%) with MSI-like and high TMB (>10), respectively, was observed in the primary cancer cohort. Indeed, there is a striking difference in the mutational load between both disease settings.

DISCUSSION

We performed WGS of metastatic tumor biopsies and matched normal blood obtained from 197 patients with mCRPC to provide an overview of the genomic landscape of mCRPC. The size of our cohort enables classification of patients into distinct disease subgroups using unsupervised clustering. Our data suggest that classification of patients using genomic events, as detected by WGS, improves patient stratification, specifically for clinically actionable subgroups such as *BRCA*-deficient and MSI patients. Furthermore, we confirm the central role of AR signaling in mCRPC that mediates its effect through regulators located in non-coding regions and the apparent difference in primary versus metastatic prostate cancers.

The classification of patients using WGS has the advantage of being, in theory, more precise in determining genomically defined subgroups in prostate cancer compared to analyses using targeted panels consisting of a limited number of genes, or exome sequencing. The identification of subgroups based on predominant phenotypic characteristics encompassing genomic signatures may be clinically relevant and our clustering analysis refines patient classification. In cluster A, we observed a high TMB, which has been associated in other tumor types with a high sensitivity to immune check-point inhibitors [9,11,12]. Clinical trials using pembrolizumab in selected mCRPC patients are underway (KEYNOTE-028, KEYNOTE-199)[36,37]. Interestingly, in both cluster B and cluster D, we identified patients that did not have the defining biallelic *CDK12* or *BRCA2* (somatic) mutation. Such patients might be deemed false-negatives when using FDA-approved assays (BRCAAnalysis™ and FoundationFocus™), currently used in breast cancer diagnosis and based on the presence of *BRCA1/2* mutations, to predict response to poly(ADP-ribose) polymerase (PARP) inhibitors and/or platinum compounds. The first clinical trials combining PARP inhibitors with AR-targeted therapies in mCRPC show promising results [8]. Thus, WGS-based stratification may improve the patient classification of DNA repair-deficient tumors as it uses the genome-wide scars caused by defective DNA repair to identify tumors that have these deficiencies.

The use of WGS also allowed us to gain more insight into the role of non-coding regions of the genome in prostate cancer. We confirmed the amplification of a recently reported AR-enhancer [20,21,30]. In line with the cell line-based observations, we show AR binding at these mCRPC-specific enhancer regions, providing the first clinical indication that AR-enhancer amplification also increases AR signaling in mCRPC tumors. These findings are supported by previous studies demonstrating that this amplification ultimately resulted in significantly elevated expression of AR itself [20,21,30]. Furthermore, we confirm a recurrent focal amplification near *PCAT1*, which shows robust chromatin binding for AR

in mCRPC samples, providing clinical proof-of-concept of a functional enhancer that is also active and AR-bound in cell line models. Recent research elucidated the functional importance of this region in regulating *MYC* expression in prostate cancer, which could highlight a putative role of this somatically acquired amplification [31]. However, the WGS and ChIP-seq data presented here are not conclusive in elucidating the definitive role of this amplified region in regulating *MYC* expression and further mechanistic studies are needed to establish a potential link to *MYC* regulation.

In addition, *PCAT1* is a long non-coding RNA, which is known to be upregulated in prostate cancer and negatively regulates *BRCA2* expression while positively affecting *MYC* expression [38,39]. Combining our WGS approach with AR, *FOXA1*, and H3K27ac ChIP-seq data, we identify non-coding regions affecting both AR itself, and possibly *MYC*, through AR-enhancer amplification as a potential mechanism contributing to castration resistance.

A potential pitfall of our clustering analysis is the selection of features used; for this we made a number of assumptions based on the literature and distribution of the structural variants within our cohort [19–21,32]. As the input of features and weights for clustering analysis are inherent to the clustering outcome, we performed additional clustering analyses using various combinations of these features and applied alternative approaches but did not detect striking differences compared to the current approach. Another potential pitfall of the employed hierarchical clustering scheme is that patients are only attributed to a single cluster. An example of this can be seen in cluster A where a patient is grouped based on its predominant genotype (MSI) and associated mutations in MMR-related genes (*MLH1*, *POLE*, *POLD3*, and *BLM*), but this sample also displays an increased number of structural variants and increased ploidy status and harbors a pathogenic *BRCA2* mutation. However, it is missing the characteristic number of genomic deletions (< 100 kbp) and BRCA mutational signature associated with *BRCA2*–/– samples that define cluster D. Despite these pitfalls we conclude that unbiased clustering contributes towards improved classification of patients.

The CPCT-02 study was designed to examine the correlation of genomic data with treatment outcome after biopsy at varying stages of disease. Our cohort contains patients with highly variable pre-treatment history and since the treatments for mCRPC patients nowadays significantly impacts overall survival, the prognosis of patients differs greatly. Therefore, correlation between genomic data and clinical endpoints, such as survival is inherently flawed due to the very heterogeneous nature of the patient population. Moreover, our analysis comparing primary and metastatic samples shows a significant increase in the number of genomic aberrations with advancing disease, meaning that

the difference in timing of the biopsies may bias the prognostic value of the data. In future studies, we plan to gather all known clinically defined prognostic information and determine whether the genomic subtypes increase the ability to predict outcome. Unfortunately, some clinical parameters with prognostic importance such as ethnicity will not be available due to ethical regulations. Moreover, we will increase the sample size, in order to correlate genomic features to clinical parameters to better determine whether the subtypes we identified are stable over time. Therefore, we are currently unable to present meaningful correlations between clinical endpoints and the clusters we identified.

Overall, we show the added value of WGS-based unsupervised clustering in identifying patients with genomic scars who are eligible for specific therapies. Since our clustering method does not rely on one specific genetic mutation we are able to classify patients even when WGS (or our methodology) does not find conclusive evidence for (biallelic) mutations in the proposed gene-of-interest. Further research should validate clinical response and outcome on specific therapies in matched subgroups. This study also shows that a large population of mCRPC patients do not fall into an as-of-yet clinically relevant or biologically clear genotype and further research can help elucidate the oncogenic driver events and provide new therapeutic options.

METHODS

Patient cohort and study procedures

Patients with metastatic prostate cancer were recruited under the study protocol (NCT01855477) of the Center for Personalized Cancer Treatment (CPCT). This consortium consists of 41 hospitals in The Netherlands (Supplementary Table 1). This CPCT-02 protocol was approved by the medical ethical committee (METC) of the University Medical Center Utrecht and was conducted in accordance with the Declaration of Helsinki. Patients were eligible for inclusion if the following criteria were met: (1) age \geq 18 years; (2) locally advanced or metastatic solid tumor; (3) indication for new line of systemic treatment with registered anti-cancer agents; (4) safe biopsy according to the intervening physician. For the current study, patients were included for biopsy between 03 May 2016 and 28 May 2018. Data were excluded of patients with the following characteristics: (1) hormone-sensitive prostate cancer; (2) neuroendocrine prostate cancer (as assessed by routine diagnostics); (3) unknown disease status; (4) prostate biopsy (Fig. 1a). All patients provided written informed consent before any study procedure. The study procedures consisted of the collection of matched peripheral blood samples for reference DNA and image-guided percutaneous biopsy of a single metastatic lesion. Soft tissue lesions were

biopsied preferentially over bone lesions. The clinical data provided by CPCT have been locked at 1st of July 2018.

Collection and sequencing of samples

Blood samples were collected in CellSave preservative tubes (Menarini-Silicon Biosystems, Huntington Valley, PA, USA) and shipped by room temperature to the central sequencing facility at the Hartwig Medical Foundation [40]. Tumor samples were fresh-frozen in liquid nitrogen directly after the procedure and send to a central pathology tissue facility. Tumor cellularity was estimated by assessing a hematoxylin-eosin (HE) stained 6 micron thick section. Subsequently, 25 sections of 20 micron were collected for DNA isolation. DNA was isolated with an automated workflow (QiaSymphony) using the DSP DNA Midi kit for blood and QiaSymphony DSP DNA Mini kit for tumor samples according to the manufacturer's protocol (Qiagen). DNA concentration was measured by Qubit™ fluorometric quantitation (Invitrogen, Life Technologies, Carlsbad, CA, USA). DNA libraries for Illumina sequencing were generated from 50 to 100 ng of genomic DNA using standard protocols (Illumina, San Diego, CA, USA) and subsequently whole-genome sequenced in a HiSeq X Ten system using the paired-end sequencing protocol (2 × 150 bp). Whole-genome alignment (GRCh37), somatic variants (SNV, InDel (max. 50 bp), MNV), structural variant and copy number calling and in silico tumor cell percentage estimation were performed in a uniform manner as detailed by Priestley et al. [40]. Mean read coverages of reference and tumor BAM were calculated using Picard Tools (v1.141; CollectWgsMetrics) based on GRCh37 [41].

Additional annotation of somatic variants and heuristic filtering

In addition, heuristic filtering removed somatic SNV, InDel, and MNV variants based on the following criteria: (1) minimal alternative reads observations ≤ 3 ; (2) gnomAD exome (ALL) allele frequency ≥ 0.001 (corresponding to ~62 gnomAD individuals); and (3) gnomAD genome (ALL) ≥ 0.005 (~75 gnomAD individuals) [42]. gnomAD database v2.0.2 was used. Per gene overlapping a genomic variant, the most deleterious mutation was used to annotate the overlapping gene. Structural variants, with BAF ≥ 0.1 , were further annotated by retrieving overlapping and nearest up- and downstream annotations using custom R scripts based on GRCh37 canonical UCSC promoter and gene annotations with respect to their respective up- or downstream orientation (if known) [43]. Only potential fusions with only two different gene-partners were considered (e.g., TMPRSS2-ERG); structural variants with both breakpoints falling within the same gene were simply annotated as structural variant mutations. Fusion annotation from the COSMIC (v85), CGI and CIVIC databases were used to assess known fusions [44–46]. The COSMIC (v85), OncoKB (July 12, 2018), CIVIC (July 26, 2018), CGI (July 26, 2018) and the list

from Martincorena et al.²⁶ (dN/dS) were used to classify known oncogenic or cancer-associated genes [44–46].

Ploidy and copy-number analysis

Ploidy and copy-number (CN) analysis was performed by a custom pipeline as detailed by Priestley et al. [40]. Briefly, this pipeline combines B-allele frequency (BAF), read depth, and structural variants to estimate the purity and CN profile of a tumor sample. Recurrent focal and broad CN alterations were identified by GISTIC2.0 (v2.0.23) [27]. GISTIC2.0 was run with the following parameters: (a) genegistic 1; (b) gcm extreme; (c) maxseg 4000; (d) broad 1; (e) brlen 0.98; (f) conf 0.95; (g) rx 0; (h) cap 3; (i) saveseg 0; (j) armpeel 1; (k) smallmem 0; (l) res 0.01; (m) ta 0.1; (n) td 0.1; (o) savedata 0; (p) savegene 1; (q) gvt 0.1. Categorization of shallow and deep CN aberration per gene was based on thresholded GISTIC2 calls. Focal peaks detected by GISTIC2 were re-annotated, based on overlapping genomic coordinates, using custom R scripts and UCSC gene annotations. GISTIC2 peaks were annotated with all overlapping canonical UCSC genes within the wide peak limits. If a GISTIC2 peak overlapped with ≤ 3 genes, the most-likely targeted gene was selected based on oncogenic or tumor-suppressor annotation in the COSMIC (v85), OncoKB (July 12, 2018), CIVIC (July 26, 2018), and CGI (July 26, 2018) lists [26,44–46]. Peaks in gene deserts were annotated with their nearest gene.

Estimation of tumor mutational burden

The mutation rate per megabase (Mbp) of genomic DNA was calculated as the total genome-wide amount of SNV, MNV, and InDels divided over the total amount of callable nucleotides (ACTG) in the human reference genome (hg19) FASTA sequence file:

$$\text{TMB}_{\text{genomic}} = \frac{(\text{SNV}_g + \text{MNV}_g + \text{InDels}_g)}{\left(\frac{2858674662}{10^6}\right)} \quad (1)$$

The mutation rate per Mbp of coding mutations was calculated as the amount of coding SNV, MNV, and InDels divided over the summed lengths of distinct non-overlapping coding regions, as determined on the subset of protein-coding and fully supported (TSL = 21) transcripts in GenCode v28 (hg19) [47]:

$$\text{TMB}_{\text{coding}} = \frac{(\text{SNV}_c + \text{MNV}_c + \text{InDels}_c)}{\left(\frac{28711682}{10^6}\right)} \quad (2)$$

MSI and HR-deficiency prediction

HR-deficiency/BRCAness was estimated using the CHORD classifier (Nguyen, van Hoeck and Cuppen, manuscript in preparation). This classifier was based on the HRDetect [48] algorithm, however, redesigned to improve its performance beyond primary BC. The binary prediction score (ranging from 0 to 1) was used to indicate BRCAness level within a sample. To elucidate the potential target gene(s) in the HR-deficient samples (Fig. 4), we used the list of BRCAness genes from Lord et al. [35].

MSI status was determined based on the following criteria: if a sample contained >11,436 genomic InDels (max. 50 bp, with repeat-stretches of ≥ 4 bases, repeat length sequence between 2 and 4, or if these InDels consist of a single repeat sequence, which repeats ≥ 5 times), the sample was designated as MSI [40].

Detection of (onco-)genes under selective pressure

To detect (onco-)genes under tumor-evolutionary mutational selection, we employed a Poisson-based dN/ dS model (192 rate parameters; under the full trinucleotide model) by the R package *dndscv* (v0.0.0.9) [26]. Briefly, this model tests the normalized ratio of non-synonymous (missense, nonsense, and splicing) over background (synonymous) mutations while correcting for sequence composition and mutational signatures. A global q-value ≤ 0.1 (with and without taking InDels into consideration) was used to identify statistically significant (novel) driver genes.

Identification of hypermutated foci (kataegis)

Putative kataegis events were detected using a dynamic programming algorithm, which determines a globally optimal fit of a piecewise constant expression profile along genomic coordinates as described by Huber et al. [49] and implemented in the *tilingarray* R package (v1.56.0). Only SNVs were used in detecting kataegis. Each chromosome was assessed separately and the maximum number of segmental breakpoints was based on a maximum of five consecutive SNVs (max. 5000 segments per chromosome). Fitting was performed on log10-transformed intermutational distances. Per segment, it was assessed if the mean intermutational distance was ≤ 2000 bp and at least five SNVs were used in the generation of the segment. A single sample with >200 distinct observed events was set to zero observed events as this sample was found to be hypermutated throughout the entire genome rather than locally. Kataegis was visualized using the R package *karyoploteR* (v1.4.1) [50].

Mutational signatures analysis

Mutational signatures analysis was performed using the *MutationalPatterns* R package (v1.4.2) [51]. The 30 consensus mutational signatures, as established by Alexandrov

et. al, (matrix S_{ij} ; $i = 96$; number of trinucleotide motifs; $j = 30$; number of signatures) were downloaded from COSMIC (as visited on 23-05-2018) [29]. Mutations (SNVs) were categorized according to their respective trinucleotide context (hg19) into a mutational spectrum matrix M_{ij} ($i = 96$; number of trinucleotide contexts; $j = 196$; number of samples) and subsequently, per sample a constrained linear combination of the thirty consensus mutational signatures was constructed using non-negative least squares regression implemented in the R package *pracma* (v1.9.3).

Between two and 15 custom signatures were assessed using the NMF package (v0.21.0) with 1000 iterations [52]. By comparing the cophenetic correlation coefficient, residual sum of squares and silhouette, we opted to generate five custom signatures. Custom signatures were correlated to existing (COSMIC) signatures using cosine similarity.

Detection of chromothripsis-like events

Rounded absolute copy number (excluded Y chromosome) and structural variants (BAF ≥ 0.1) were used in the detection of chromothripsis-like events by the Shatterseek software (v0.4) using default parameters [53]. As a precise standardized definition of chromothripsis has not yet been fully established, and as per the author's instruction, we performed visual inspection of reported chromothripsis-like events after dynamically adapting criteria thresholds (taking the recommended thresholds into consideration). We opted to use the following criteria: (a) Total number of intrachromosomal structural variants involved in the event ≥ 25 ; (b) max. number of oscillating CN segments (two states) ≥ 7 or max. number of oscillating CN segments (three states) ≥ 14 ; (c) Total size of chromothripsis event ≥ 20 Mbp; (d) Satisfying the test of equal distribution of SV types ($p > 0.05$); and (e) Satisfying the test of non-random SV distribution within the cluster region or chromosome ($p \leq 0.05$).

Unsupervised clustering of mCRPC WGS characteristics

Samples were clustered using the Euclidian distance of the Pearson correlation coefficient ($1 - r$) and Ward. D hierarchical clustering based on five basic whole-genome characteristics; number of mutations per genomic Mbp (SNV, InDel, and MNV), mean genome-wide ploidy, number of structural variants and the relative frequencies of structural variant categories (inversions, tandem duplications (larger and smaller than 100 kbp), deletions (larger and smaller than 100 kbp), insertions and interchromosomal translocations). Data was scaled but not centered (root mean square) prior to calculating Pearson correlation coefficients. After clustering, optimal leaf ordering (OLO) was performed using the seriation package (v1.2.3) [54]. The elbow method was employed to determine optimal number of discriminating clusters (Supplementary Fig. 10) using

the factoextra package (v1.0.5). Bootstrapping was performed using the pvclust package (v2.0) with 5000 iterations.

Cluster-specific enrichment of aberrant genes (either through SV, deep copynumber alteration, or coding SNV/InDel/MNV), kataegis, chromothripsis, GISTIC2 peaks, and predicted fusions between clusters was tested using a two-sided Fisher's Exact Test and Benjamini–Hochberg correction.

A principal component analysis (with scaling and centering) using the prcomp R package [55] was performed on the chosen genomic features and cos2 values for each feature per principal component were retrieved to determine the importance of each feature per respective principal component.

To test the robustness of our clustering, we performed unsupervised clustering, and also other techniques, using various combinations of structural variants and clustering mechanisms as a surrogate for different genome-instability metrics but this analysis did not reveal any striking new clusters.

Supervised clustering based on mutually exclusive aberrations

Samples were sorted on mutual-exclusivity of *SPOP*, *FOXA1*, and *IDH1* coding mutations and copy-number aberrations and *ETS* family gene fusions (and overexpression) per promiscuous partner (*ERG*, *ETV1*, *ETV4*, and *FLI1*) as defined in primary prostate cancer [13]. Supplementary Table S1A of the article “The Molecular Taxonomy of Primary Prostate Cancer” [13] was used to determine the relative frequency and mutational types of each of the respective primary prostate cancer within the TCGA cohort. In addition, as the TCGA cohort did not denote high-level/deep amplifications, we did not incorporate these either in this analysis.

Correlation of the detection rate of genomic aberrations versus tumor cell percentages

Absolute counts of SNV, InDels, MNV and SV were correlated to the in silico estimated tumor cell percentage using Spearman's correlation coefficient.

Correlation of pre-treatment history with detected aberrations and WGS characteristics

Pre-treatment history of patients was summarized into ten groups:

1. Only chemo-treatment (with radio-nucleotides).
2. Only chemo-treatment (without radio-nucleotides).

3. Only radio-nucleotides.
4. Only secondary anti-hormonal therapy (with radio-nucleotides).
5. Only secondary anti-hormonal therapy (without radio-nucleotides).
6. Secondary anti-hormonal therapy + one chemo-treatment (with radio-nucleotides)
7. Secondary anti-hormonal therapy + two chemo-treatment (with radio-nucleotides)
8. Secondary anti-hormonal therapy + one chemo-treatment (without radio-nucleotides)
9. Secondary anti-hormonal therapy + two chemo-treatment (without radio-nucleotides)
10. No additional treatment after androgen deprivation therapy.

Association with mutated genes, presence of chromothripsis, presence of kataegis, MSI-status, and genomic subtypes was tested with a two-sided Fisher's exact test with Benjamini–Hochberg correction.

ChIP-seq experimental set-up and analysis

ChIP-seq cell culturing: VCaP cells were incubated in RPMI medium in addition with 10% fetal bovine serum (FBS). Bicalutamide-resistant VCaP cells (VCaP-Bic) were cultured in RPMI medium supplemented with 10% dextran charcoal-stripped bovine serum (DCC) and 10⁻⁶ M bicalutamide. VCaP cells were hormone deprived in RPMI medium with 10% DCC for 3 days before the ChIP-seq experiment.

ChIP-seq and peak calling analysis: For both cell and tissue ChIPs, 5 µg of antibody and 50 µg of magnetic protein A or G beads (10008D or 10009D, Thermo Fisher Scientific) were used per IP. The following antibodies were used: Foxa1/2 (M-20, sc-6554 Santa Cruz Biotechnology), AR (N-20, sc-816 Santa Cruz Biotechnology), and H3K27ac (39133, Active Motif). ChIP-seq was performed as described previously [56]. In brief, fresh-frozen tissue was cryosectioned into 30 micron thick slices and stored at –80 °C till processing. Samples were fixed using 2 mM DSG (20593; Thermo Fisher Scientific) in solution A (50 mM Hepes KOH, 100 mM NaCl, 1 mM EDTA, 0.5 mM EGTA) while rotating for 25 min at room temperature, followed by the addition of 1% formaldehyde and another 20 min incubation at room temperature. The reaction was quenched by adding a surplus of glycine. Subsequently, tissue sections were pelleted and washed with cold PBS. Tissue was disrupted using a motorized pellet pestle (Sigma-Aldrich) to disrupt the tissue in cold PBS and obtain a cell suspension, after which the nuclei were isolated and the chromatin was sheared. During immunoprecipitation, human control RNA (4307281; Thermo Fisher Scientific) and recombinant Histone 2B (M2505S; New England Biolabs) were added as carriers, as described previously [57].

Immunoprecipitated DNA was processed for sequencing using standard protocols and sequenced on an Illumina HiSeq 2500 with 65 bp single end reads. Sequenced samples

were aligned to the reference human genome (Ensembl release 55: Homo sapiens GRCh 37.55) using Burrows-Wheeler Aligner (BWA, v0.5.10) [58], reads with a mapping quality >20 were used for further downstream analysis.

For the tissues, peak calling was performed using MACS2 [59] with option `--nomodel`. In addition, peaks were called against matched input using DFilter [60] in the refine setting with a bandwidth of 50 and a kernel size of 30. Only peaks that were shared between the two algorithms were considered.

For the cell lines, peaks were obtained with MACS (v1.4; $p \leq 10^{-7}$).

The AR and FOXA1 ChIP-seq data for LNCAP with/-out R1881 was obtained from GSE94682 [61]. The H3K27ac ChIP-seq data for LNCAP was obtained from GSE114737 [56].

Determining enrichment of enhancer to gene ratios: Absolute copy-numbers segments overlapping the gene loci and putative enhancer region (as detected by GISTIC2; focal amplification peaks with a width 1 studentized residual from equal 1:1 gene-to-enhancer ratios (linear model: $\log_2(\text{copy number of enhancer}) - \log_2(\text{copy number of gene locus}) \sim 0$) were categorized as gene or enhancer enriched. Based on the direction of the ratio, samples were either denoted as enhancer (if positive ratio) or gene (if negative ratio) enriched.

Comparison of unmatched primary prostate cancer and mCRPC

Mutational frequencies of the drivers (dN/dS and or GISTIC2) and subtype-specific genes were compared to a separate (unmatched) cohort of primary prostate cancer (n = 210) focusing on Gleason score (GS) of 3 + 3, 3 + 4, or 4 + 3, as described by Fraser et al. [15] and Espiritu et al. [25]. Briefly, whole-genome sequencing reads were mapped to the human reference genome (GRCh37) using BWA [58] (v0.5.7) and downstream analysis was performed using Strelka [62] (v1.0.12) for mutational calling using a matched-normal design (SNVs and InDels), copy-number alterations were estimated with TITAN [63] (v1.11.0), and SNP array data as described in Espiritu et al. [25] with Delly [64] (v0.5.5 and v0.7.8) was used for detecting structural variants (translocations, inversions, tandem duplications, and deletions). Large insertion calls and overall ploidy was not available for the primary prostate cancer cohort.

Tumor mutational burden (TMB) was calculated by dividing the number of SNVs and InDels by the total amount of callable bases in the human reference genome (GRCh37), identical to Eq. 1. MNV calls were not available for the primary prostate cancer cohort.

Multiple aberrations per gene within a sample were summarized as a single mutational event, e.g., a deletion and mutation in PTEN would only count for a single mutation in the sample. Only non-synonymous mutations and gains/ deletions overlapping with coding regions were used. Statistically significant differences in mutational frequencies were calculated using a two-sided Fisher's Exact test with Benjamini–Hochberg correction.

The primary prostate cancer dataset was clustered together with the mCRPC cohort using the Euclidian distance of the Pearson correlation coefficient ($1 - r$) and Ward.D hierarchical clustering based on three basic whole-genome characteristics, which were available for all samples; number of mutations per genomic Mbp (SNVs and InDels), number of structural variants and the relative frequencies of structural variant categories (inversions, tandem duplications (larger and smaller than 100 kbp), deletions (larger and smaller than 100 kbp), and interchromosomal translocations).

SUPPLEMENTARY INFORMATION

Supplementary information is available at <https://doi.org/10.1038/s41467-019-13084-7>.

REFERENCES

1. Boyd, L. K., Mao, X. & Lu, Y. J. The complexity of prostate cancer: Genomic alterations and heterogeneity. *Nature Reviews Urology* (2012). doi:10.1038/nrrol.2012.185
2. Wei, L. et al. Intratumoral and Intertumoral Genomic Heterogeneity of Multifocal Localized Prostate Cancer Impacts Molecular Classifications and Genomic Prognosticators. *Eur. Urol.* (2017). doi:10.1016/j.eururo.2016.07.008
3. Mullane, S. A. & Van Allen, E. M. Precision medicine for advanced prostate cancer. *Current Opinion in Urology* (2016). doi:10.1097/MOU.0000000000000278
4. Ciccicarese, C. et al. Prostate cancer heterogeneity: Discovering novel molecular targets for therapy. *Cancer Treatment Reviews* (2017). doi:10.1016/j.ctrv.2017.02.001
5. Shtivelman, E., Beer, T. M. & Evans, C. P. Molecular pathways and targets in prostate cancer. *Oncotarget* (2014). doi:10.18632/oncotarget.2406
6. Robinson, D. et al. Integrative clinical genomics of advanced prostate cancer. *Cell* 161, 1215–1228 (2015).
7. Chow, H. et al. A phase 2 clinical trial of everolimus plus bicalutamide for castration-resistant prostate cancer. *Cancer* (2016). doi:10.1002/cncr.29927
8. Clarke, N. et al. Olaparib combined with abiraterone in patients with metastatic castration-resistant prostate cancer: a randomised, double-blind, placebo-controlled, phase 2 trial. *Lancet Oncol.* (2018). doi:10.1016/S1470-2045(18)30365-6
9. Yarchoan, M., Hopkins, A. & Jaffee, E. M. Tumor Mutational Burden and Response Rate to PD-1 Inhibition. *N. Engl. J. Med.* (2017). doi:10.1056/NEJMc1713444
10. Chan, T. A. et al. Development of tumor mutation burden as an immunotherapy biomarker: Utility for the oncology clinic. *Annals of Oncology* (2019). doi:10.1093/annonc/mdy495
11. Rizvi, N. A. et al. Mutational landscape determines sensitivity to PD-1 blockade in non-small cell lung cancer. *Science* (80-.). (2015). doi:10.1126/science.aaa1348
12. Samstein, R. M. et al. Tumor mutational load predicts survival after immunotherapy across multiple cancer types. *Nature Genetics* (2019). doi:10.1038/s41588-018-0312-8
13. Cancer Genome Atlas Research Network et al. The Molecular Taxonomy of Primary Prostate Cancer. *Cell* 163, 1011–25 (2015).
14. Angeles, A. K., Bauer, S., Ratz, L., Klauck, S. M. & Söltmann, H. Genome-Based Classification and Therapy of Prostate Cancer. *Diagnostics* 8, (2018).
15. Fraser, M. et al. Genomic hallmarks of localized, non-indolent prostate cancer. *Nature* 541, 359–364 (2017).
16. Schoenborn, J. R., Nelson, P. & Fang, M. Genomic profiling defines subtypes of prostate cancer with the potential for therapeutic stratification. *Clin. Cancer Res.* (2013). doi:10.1158/1078-0432.CCR-12-3606
17. Nam, R. K. et al. Expression of TMPRSS2 ERG gene fusion in prostate cancer cells is an important prognostic factor for cancer progression. *Cancer Biol. Ther.* (2007). doi:10.4161/cbt.6.1.3489

18. Tomlins, S. A. et al. Role of the TMPRSS2-ERG gene fusion in prostate cancer. *Neoplasia* (2008).
19. Wu, Y.-M. et al. Inactivation of CDK12 Delineates a Distinct Immunogenic Class of Advanced Prostate Cancer Article Inactivation of CDK12 Delineates a Distinct Immunogenic Class of Advanced Prostate Cancer. *Cell* 173, 1770-1782.e14 (2018).
20. Viswanathan, S. R. et al. Structural Alterations Driving Castration-Resistant Prostate Cancer Revealed by Linked-Read Genome Sequencing. *Cell* 174, 433-447.e19 (2018).
21. Quigley, D. A. et al. Genomic Hallmarks and Structural Variation in Metastatic Prostate Cancer. *Cell* 174, 758-769.e9 (2018).
22. Nik-Zainal, S. et al. Landscape of somatic mutations in 560 breast cancer whole-genome sequences. *Nature* 534, 47–54 (2016).
23. Taylor, R. A. et al. Germline BRCA2 mutations drive prostate cancers with distinct evolutionary trajectories. *Nat. Commun.* (2017). doi:10.1038/ncomms13671
24. Davies, H. et al. Whole-genome sequencing reveals breast cancers with mismatch repair deficiency. *Cancer Res.* (2017). doi:10.1158/0008-5472.CAN-17-1083
25. Espiritu, S. M. G. et al. The Evolutionary Landscape of Localized Prostate Cancers Drives Clinical Aggression. *Cell* (2018). doi:10.1016/j.cell.2018.03.029
26. Martincorena, I. et al. Universal Patterns of Selection in Cancer and Somatic Tissues. *Cell* 171, 1029-1041.e21 (2017).
27. Mermel, C. H. et al. GISTIC2.0 facilitates sensitive and confident localization of the targets of focal somatic copy-number alteration in human cancers. *Genome Biol.* 12, R41 (2011).
28. Armenia, J. et al. The long tail of oncogenic drivers in prostate cancer. *Nat. Genet.* (2018). doi:10.1038/s41588-018-0078-z
29. Alexandrov, L. B. et al. Signatures of mutational processes in human cancer. *Nature* 500, 415–421 (2013).
30. Takeda, D. Y. et al. A somatically acquired enhancer of the androgen receptor is a noncoding driver in advanced prostate cancer. *Cell* (2018). <https://doi.org/10.1016/j.cell.2018.05.037>
31. Mazrooei, P. et al. Somatic Mutations and Risk-Variants Converge on Cis-Regulatory Elements to Reveal the Cancer Driver Transcription Regulators in Primary Prostate Tumors. *SSRN Electron. J.* (2018). doi:10.2139/ssrn.3245213
32. Menghi, F. et al. The Tandem Duplicator Phenotype Is a Prevalent Genome-Wide Cancer Configuration Driven by Distinct Gene Mutations. *Cancer Cell* 34, 197-210.e5 (2018).
33. Pritchard, C. C. et al. Complex MSH2 and MSH6 mutations in hypermutated microsatellite unstable advanced prostate cancer. *Nat. Commun.* 5, (2014).
34. Polak, P. et al. A mutational signature reveals alterations underlying deficient homologous recombination repair in breast cancer. *Nat. Genet.* (2017). doi:10.1038/ng.3934
35. Lord, C. J. & Ashworth, A. BRCAness revisited. *Nat. Rev. Cancer* 16, 110–120 (2016).
36. Hansen, A. R. et al. Pembrolizumab for advanced prostate adenocarcinoma: Findings of the KEYNOTE-028 study. *Ann. Oncol.* (2018). doi:10.1093/annonc/mdy232
37. De Bono, J. S. et al. KEYNOTE-199: Pembrolizumab (pembro) for docetaxel-refractory metastatic castration-resistant prostate cancer (mCRPC). *J. Clin. Oncol.* (2018). doi:10.1200/JCO.2018.36.15_suppl.5007

38. Prensner, J. R. et al. The Long Non-Coding RNA PCAT-1 Promotes Prostate Cancer Cell Proliferation through cMyc. *Neoplasia* 16, 900–908 (2014).
39. Prensner, J. R. et al. PCAT-1, a long noncoding RNA, regulates BRCA2 and controls homologous recombination in cancer. *Cancer Res.* 74, 1651–1660 (2014).
40. Priestley, P. et al. Pan-cancer whole genome analyses of metastatic solid tumors. *bioRxiv* 415133 (2018). doi:10.1101/415133
41. Broad Institute. Picard tools. <https://broadinstitute.github.io/picard/> (2016). Available at: <https://broadinstitute.github.io/picard/%5Cnhttp://broadinstitute.github.io/picard/>.
42. Lek, M. et al. Analysis of protein-coding genetic variation in 60,706 humans. *Nature* 536, 285–291 (2016).
43. Casper, J. et al. The UCSC Genome Browser database: 2018 update. *Nucleic Acids Res.* 46, D762–D769 (2018).
44. Forbes, S. A. et al. COSMIC: Somatic cancer genetics at high-resolution. *Nucleic Acids Res.* 45, D777–D783 (2017).
45. Tamborero, D. et al. Cancer Genome Interpreter annotates the biological and clinical relevance of tumor alterations. *Genome Med.* 10, 25 (2018).
46. Griffith, M. et al. CIViC is a community knowledgebase for expert crowdsourcing the clinical interpretation of variants in cancer. *Nat. Genet.* 49, 170–174 (2017).
47. Harrow, J. et al. GENCODE: The reference human genome annotation for the ENCODE project. *Genome Res.* 22, 1760–1774 (2012).
48. Davies, H. et al. HRDetect is a predictor of BRCA1 and BRCA2 deficiency based on mutational signatures. *Nat. Med.* 23, 517–525 (2017).
49. Huber, W., Toedling, J. & Steinmetz, L. M. Transcript mapping with high-density oligonucleotide tiling arrays. *Bioinformatics* 22, 1963–1970 (2006).
50. Gel, B. & Serra, E. karyoploteR: an R/Bioconductor package to plot customizable genomes displaying arbitrary data. *Bioinformatics* 33, 3088–3090 (2017).
51. Blokzijl, F., Janssen, R., van Boxtel, R. & Cuppen, E. MutationalPatterns: Comprehensive genome-wide analysis of mutational processes. *Genome Med.* (2018). doi:10.1186/s13073-018-0539-0
52. Gaujoux, R. & Seoighe, C. A flexible R package for nonnegative matrix factorization. *BMC Bioinformatics* 11, (2010).
53. Cortés-ciriano, I., Lee, J., Xi, R., Jain, D. & Jung, Y. L. Comprehensive analysis of chromothripsis in 2, 658 human cancers using whole-genome sequencing. (2018).
54. Hahsler, M., Hornik, K. & Buchta, C. Getting Things in Order : An Introduction to the R Package seriation. *J. Stat. Softw.* 25, 1–27 (2008).
55. Venables, W. N. & Ripley, B. D. *Modern Applied Statistics with S.* (2002). doi:10.1007/978-0-387-21706-2
56. Abhishek A. Singh, Karianne Schuurman, Ekaterina Nevedomskaya, Suzan Stelloo, Simon Linder, Marjolein Droog, Yongsoo Kim, Joyce Sanders, Henk van der Poel, Andries M Bergman, Lodewyk FA Wessels, W. Z. Optimized ChIP-seq method facilitates transcription factor profiling in human tumors. *Life Sci. Alliance* In Press,

57. Zwart, W. et al. A carrier-assisted ChIP-seq method for estrogen receptor-chromatin interactions from breast cancer core needle biopsy samples. *BMC Genomics* (2013). doi:10.1186/1471-2164-14-232
58. Li, H. & Durbin, R. Fast and accurate short read alignment with Burrows-Wheeler transform. *Bioinformatics* 25, 1754–1760 (2009).
59. Zhang, Y. et al. Model-based analysis of ChIP-Seq (MACS). *Genome Biol.* 9, (2008).
60. Kumar, V. et al. Uniform, optimal signal processing of mapped deep-sequencing data. *Nat. Biotechnol.* 31, 615–622 (2013).
61. Stelloo, S. et al. Endogenous androgen receptor proteomic profiling reveals genomic sub-complex involved in prostate tumorigenesis. *Oncogene* 37, 313–322 (2018).
62. Kim, S. et al. Strelka2: Fast and accurate variant calling for clinical sequencing applications. doi.org 192872 (2017). doi:10.1101/192872
63. Ha, G. et al. TITAN: inference of copy number architectures in clonal cell populations from tumor whole-genome sequence data. *Genome Res.* (2014). doi:10.1101/gr.180281.114
64. Rausch, T. et al. DELLY: Structural variant discovery by integrated paired-end and split-read analysis. *Bioinformatics* (2012). doi:10.1093/bioinformatics/bts378



CHAPTER 6

RESPONSIVENESS TO IMMUNE CHECKPOINT INHIBITORS IS ASSOCIATED WITH A PERIPHERAL BLOOD T-CELL SIGNATURE IN METASTATIC CASTRATION-RESISTANT PROSTATE CANCER

Donjete Simnica*
Edith Willscher
Iris S.H. Kloots
Winald Gerritsen
Mascha Binder

Minke Smits*
Lorenzo F. Fanchi
Inge van Oort
Niven Mehra

* These authors contributed equally to this work.

JCO Precision Oncology. 2020;4:1374-85

ABSTRACT

Purpose

Although most patients with microsatellite instable (MSI) metastatic castration-resistant prostate cancer (mCRPC) respond to immune checkpoint blockade (ICB), only a small subset of patients with microsatellite stable (MSS) tumors have similar benefit. Biomarkers defining ICB-susceptible subsets of patients with MSS mCRPC are urgently needed.

Methods

Using next-generation T cell repertoire sequencing, we explored immune signatures in 54 patients with MSS and MSI mCRPC who were treated with or without ICB. We defined subset-specific immune metrics as well as T cell clusters and correlated the signatures with treatment benefit.

Results

Consistent overlaps between tumor and peripheral T cell repertoires suggested that blood was an informative material to identify relevant T cell signatures. We found considerably higher blood T cell richness and diversity and more shared T cell clusters with low generation probability (pGen) in MSI versus MSS mCRPC potentially reflecting more complex T cell responses due to greater neoepitope load in the MSI subset. Interestingly, patients with MSS mCRPC with shared low pGen T cell clusters showed significantly better outcomes with ICB, but not with other treatments, compared to patients without such clusters. Blood clearance of T cell clusters upon ICB treatment initiation seemed to be compatible with T cell migration to the primary tumor or metastatic sites during the process of clonal replacement as described for other tumors receiving ICB.

Conclusion

The MSI mCRPC subset shows a distinct T cell signature that can be detected in blood. This signature points to immune parameters that could help to identify a subset of patients with MSS mCRPC who may have an increased likelihood to respond to ICB or to combination approaches including ICB.

INTRODUCTION

Cancer immunotherapy has revolutionized the treatment of many cancers in recent years. Prostate cancer as the most common cancer in men has recently become recognized as amenable to immunotherapy: Sipuleucel-T, an autologous active cellular immunotherapy, demonstrated a survival benefit in a phase III trial leading to Food and Drug Administration (FDA) approval [1]. However, other approaches such as treatment with ProstateVax VF, a virus-based prostate-specific antigen (PSA) vaccine, showed no effect [2].

Immune checkpoint blockade (ICB) is probably the treatment principle that most profoundly changed our treatment algorithms across the spectrum of solid tumors. ICB has been licensed for many indications, even agnostic of tumor type for all microsatellite instable (MSI) advanced solid tumors [3,4]. In contrast to its use in other urological tumors, the use of ICB in prostate cancer has thus far been limited because approximately 90% of patients have microsatellite stable (MSS) tumors [5] for which clinical trials (in molecularly unselected cohorts) did not show consistent activity signals. While the CTLA-4 inhibitor ipilimumab did not increase overall survival in patients with chemotherapy-naïve or chemotherapy-pretreated metastatic castration-resistant prostate cancer (mCRPC), increases in progression-free survival or PSA response suggested signs of activity at least in subsets of patients [6,7]. The phase Ib KEYNOTE-028 trial showed objective responses in 17% of patients, with a median duration of response of 14 months in a small cohort of patients with programmed cell death ligand 1 (PD-L1)-positive mCRPC treated with anti-programmed cell death protein 1 (PD1) inhibitor pembrolizumab [8]. Data from the phase II KEYNOTE-199 trial of single-agent pembrolizumab, which included 198 patients with measurable disease per RECIST1.1 criteria and 60 patients with bone-only disease revealed that only 9% of patients had a biochemical response and that 5% of evaluable patients showed an objective radiographic response [9]. Responsiveness was not associated with PD-L1 positivity. In the subset of patients who responded to ICB, the responses seemed durable.

Enrichment of patients by genomic signature seems promising; in addition to MSI disease, a recently identified subset of prostate cancer with a tandem duplicator phenotype associated with CDK12 biallelic inactivation and high neoantigen burden may also identify patients who benefit from ICB [10-13]. Multiple trials are testing combinations of ICB with other agents such as radium-223, enzalutamide, docetaxel and olaparib to increase antigenicity for unselected patients with mCRPC. Given the high overall response rates and the durability of responses observed in patients with MSI mCRPC, identification of immunogenic subtypes within the MSS subset is highly sought after [10,11,13].

We reasoned that insight into immunological signatures of MSI mCRPC could help identify subsets of patients with MSS tumors with functionally similar immune metrics and higher responses to single-agent ICB. To derive such signatures, we performed next-generation T-cell repertoire sequencing of peripheral blood and tumor-infiltrating lymphocytes in two cohorts: 15 patients with MSS and MSI mCRPC treated with ICB (cohort 1) and 39 patients with MSS mCRPC not treated with ICB (cohort 2).

METHODS

Study approval

Informed consent was obtained for the use of biomaterials as approved by the Ethics commission of the Radboudumc, Nijmegen (NL60249.091.16) and Ethikkommission der Ärztekammer Hamburg (PV4767). The study was performed in accordance with the declaration of Helsinki of 1975.

Patients

Between March 2017 and April 2019, biomaterial was collected from a cohort of 15 patients with mCRPC (cohort 1) before and during treatment with anti-PD-1 and anti-PD-L1 ICB, and from 13 healthy donors (HDs). In addition, blood of 39 patients with MSS tumors who did not receive ICB treatment (cohort 2) was collected at mCRPC. In cohort 1, PBMCs were collected at baseline and before the second or third cycle of ICB. Whenever possible, a fresh tissue core biopsy was obtained before initiation of ICB per institutional protocol. Patients with MSI disease and the CDK12 phenotype were included independent of PD-L1 status, and patients with MSS disease were PD-L1 positive. MSI was identified by loss of mismatch repair proteins MSH2, MSH6, MLH1 or PMS2 or by assessment of instable microsatellites by next-generation sequencing (NGS); PD-L1 positivity was assessed by clone E1L3N; CDK12 mutation or loss was assessed by targeted or whole-genome sequencing. Treatment was given in the context of a clinical trial that selected a cohort of patients with tumor-agnostic MSI disease for nivolumab [14], a patient-access program of pembrolizumab for PD-L1 positive cancers (Merck), and atezolizumab on a compassionate use basis (Roche). Clinical and treatment data are summarized in Table 1 and Appendix Table A1. Tumor mutational burden (TMB) was assessed by dividing the number of SNVs and InDels by the total amount of callable bases in the human reference genome (GRCh37).

Table 1. Clinical characteristics and response to checkpoint inhibitors

Characteristic/Response	Total group (N=15)	MSI (N=6)	MSS (N=9)
Age at diagnosis, years, mean (range)	61.4 (50-74)	59.5 (53-64)	62.7 (50-74)
Total Gleason score at diagnosis			
< 8	3 (18.7)	2 (33.3)	1 (11.1)
≥ 8	11(68.8)	4 (66.7)	7 (77.%)
Unknown	1 (6.3)	0 (0)	1 (11.1)
Metastasis status at diagnosis			
M0	7 (46.7)	2 (33.3)	5 (55.6)
M1	8 (53.3)	4 (66.7)	4 (44.4)
Previous therapies for CRPC			
Chemotherapy			
Docetaxel	12 (75)	6 (100)	6 (66.7)
Cabazitaxel	6 (37.5)	3 (50)	3 (33.3)
Carboplatin	1 (6.3)		1 (11.1)
Second-generation ADT			
Abiraterone	7 (43.8)	4 (66.7)	3 (33.3)
Enzalutamide	11 (68.8)	4 (66.7)	7 (77.8)
Nuclear therapy			
Radium-223	2 (12.5)	1 (16.7)	1 (11.1)
PSMA-Lu-177	1 (6.3)	0 (0)	1 (11.1)
Experimental therapy			
Dendritic cell vaccination	1 (6.3)	0 (0)	1 (11.1)
Olaparib (PARP inhibitor)	5 (31.3)	1 (16.7)	4 (44.4)
Nivolumab (checkpoint inhibitor)	1 (6.3)	1 (16.7)	0 (0)
CDK12 loss or mutation	3 (20)	1 (16.7)	2 (22.2)
ICB received as			
First-line CRPC treatment	0 (0)	0 (0)	0 (0)
Second-line CRPC treatment	3 (20)	1 (16.7)	2 (22.2)
Third-line CRPC treatment	4 (26.7)	2 (33.3)	2 (22.2)
≥ Fourth-line CRPC treatment	8 (53.3)	3 (50)	5 (55.6)
Checkpoint inhibitors received ¹			
Nivolumab	6 (40)	6 (100)	0 (0)
Pembrolizumab	7 (41.2)	0 (0)	7 (77.8)
Atezolizumab	3 (20)	1 (16.7)	2 (22.2)
Response to checkpoint inhibitors			
Duration until PSA progression, months, median (range) ²	2.8 (1.7-17.1)	3.7 (2.6-17.1)	2.5 (1.7-3.5)
Duration of ICB, months, median (range)	3.2 (1.4-27.6)	5.5 (2.3-27.6)	2.8 (1.4-3.7)

Table 1. (Continued)

Characteristic/Response	Total group (N=15)	MSI (N=6)	MSS (N=9)
PSA decline >50% ³	7 (41.2)	5 (71.4)	2 (22.2)
Response in patients with CDK12 loss ⁴			
PSA decline >50%	2 (66.7)	1 (100)	1 (50)
Duration until PSA progression, months, median (range) ²	2.6 (1.7-3.5)		2.6 (1.7-3.5)
Duration of ICB, months, median (range)	3.7 (2.6-3.7)	3.7	3.2 (2.6-3.7)

NOTE. Data are presented as No. (%) unless indicated otherwise.

Abbreviations: ADT, androgen-deprivation therapy; CRPC, castration-resistant prostate cancer; ICB, immune checkpoint blockade; MSI, microsatellite instable; MSS, microsatellite stable; PARP, poly (ADP-ribose) polymerase; PSA, prostate-specific antigen; PSMA, prostate-specific membrane antigen.

¹One patient with MSI disease received both nivolumab (stop due to grade 2 colitis), followed one year later by atezolizumab

²One patient with MSI disease has not reached PSA progression

³One patient with MSI disease receiving nivolumab and atezolizumab achieved a PSA decline >50% during both ICB

⁴Total group (N=3), MSI (n=1), MSS (n=2)

NGS and data analysis

Amplification of the T cell receptor β (*TRB*) repertoire was performed on up to 250ng DNA as described elsewhere [15]. Sequencing was performed on the Illumina MiSeq platform (San Diego, CA) with 2x301 cycles (single indexed, paired-end) at a coverage of 80,000x. Analysis of the *TRB* locus was computed using the MiXCR analysis tool V3.0.5 [16]. Productive sequences with a read count ≥ 2 were included. To account for differences in sequencing depth, all *TRB* repertoires were normalized. Analyses were carried out using R (version 3.4.4), tcr [17] and GraphPad Prism 7 (San Diego, CA).

TRB repertoire metrics

Descriptive repertoire metrics (diversity, richness, clonality) were calculated as published elsewhere [15]. The similarity of two repertoires was evaluated by shared clonotypes analysis using tcr [17].

GLIPH analysis

We applied the GLIPH version 1.0 [18] (grouping of lymphocyte interaction by paratope hotspots) on baseline blood *TRB* repertoires from patients with mCRPC (cohort 1) and HDs. Briefly, this algorithm clusters T cell clones on the basis of similar antigen recognition inferred from the global and local similarity of the CDR3 amino acid sequences. The mean frequency of a cluster is calculated from the mean of the frequencies of the T-cell clones of which it consists. For the MSI and MSS cluster plots, the mean frequency of each MSS exclusive cluster was transformed to a negative value for plotting purposes. Moreover,

the absolute difference of shared clusters was calculated using the mean frequency for each cluster and subgroup, respectively, and by deducting the MSS mean frequency values from MSI mean frequency values for plotting purposes. The generation probability (pGen) of each TRB cluster amino acid consensus sequence was calculated using OLGA with default parameters and is plotted as Log₂ value [19].

RESULTS

Clinical characteristics of prostate cancer cohorts

Fifteen patients with mCRPC (cohort 1) were selected for this study, comprising six patients with MSI and nine patients with MSS tumors. In the MSS cohort, two patients had CDK12 alterations. In nine of 15 patients, data on TMB were available showing high levels in patients with MSI disease (median 38.8 mutations/Mb), whereas patients with MSS disease exhibited much lower TMB levels with a median 2.1 mutations/Mb ($p = .0065$; Table 2). Patients received nivolumab, pembrolizumab or atezolizumab until complete response, progressive disease or unacceptable toxicity. As of March 30, 2020, time to progression (TTP) was 9.3 in the MSI group and 2.6 months in the MSS group ($p = 0.0026$, Figure 1A). A PSA decline of >50% was seen in 71.4% and 22.2% of patients in the MSI and the MSS group, respectively (Figure 1B). Although patients were treated with ICB from early onset of castration-resistance to end-stage mCRPC, there were no differences between the groups in hormonal status and the number of prior therapies, as listed in Table 1.

Table 2. Tumor mutational burden

Patient ID	Mutations/ Mb	Group
2.1	74.4	MSI
2.2	48.0	MSI
3	39.6	MSI
4	38.8	MSI
5	24.6	MSI
6	18.1	MSI
8	1.9	MSS
10	7.7	MSS
12	1.9	MSS
16	2.3	MSS

Abbreviations: MSI, microsatellite instable; MSS, microsatellite stable

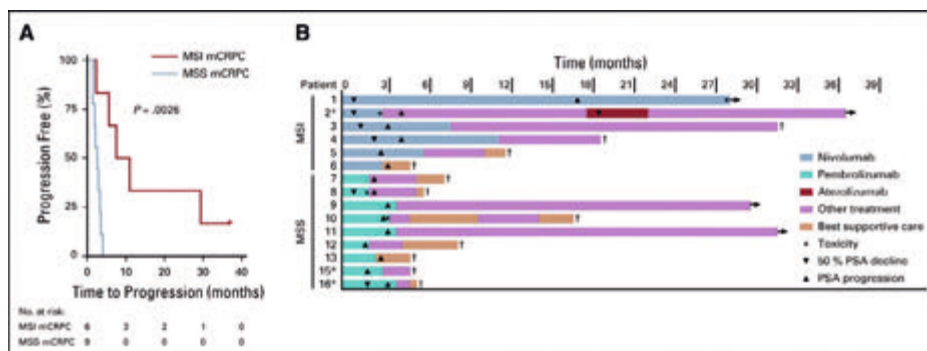


Figure 1. Treatment benefit from immune checkpoint blockade (ICB) in patients with microsatellite instable (MSI) and microsatellite stable (MSS) metastatic castration-resistant prostate cancer (mCRPC).

(A) Kaplan-Meier curves of time to progression from start of ICB treatment. (B) Swimmer plots of patient subsets with MSI and MSS mCRPC receiving ICB treatment. The statistical analysis was performed using a log-rank test. PSA, prostate-specific antigen. (*) patients with CDK12 aberration(s); (f) death.

Global blood and tumor immune metrics of patients with MSS and MSI mCRPC

We searched for subset-specific immune signatures by next-generation T-cell repertoire sequencing of blood and tumor tissue (cohort 1). Six pre-treatment tumor biopsies, 16 pre-treatment and 15 on-treatment blood samples, and 13 blood samples of age- and sex-matched HD controls were studied.

First, we assessed if blood-circulating T cells reflected, to some extent, the T cells found in tumors of the same patient. We performed a repertoire overlap analysis of all analyzed samples (Figure 2A). As expected, this analysis showed the most pronounced clonal overlap between blood and tumor samples from the same patient. This illustrates the potential of peripheral blood findings to (partially) mirror the tumor-infiltrating T-cell composition suggesting that subsequent analyses could be restricted to blood.

We analyzed T-cell repertoire richness, diversity and clonality as parameters commonly used to compare immune architectures. This analysis showed higher blood T-cell richness and diversity in the MSI subset compared with patients with MSS mCRPC and HDs (Figure 2B).

In the patient subset with MSS disease, which generally showed less favorable outcomes with ICB than did patients with MSI mCRPC (Figure 1A and B), the individual patients showed different levels of T-cell richness and diversity. Despite the rather limited size of the cohort, we found a positive trend for T-cell repertoire diversity (similar to the MSI cohort) and clinical outcomes with ICB ($R^2 = 0.39$; $p = 0.068$, Figure 2C).

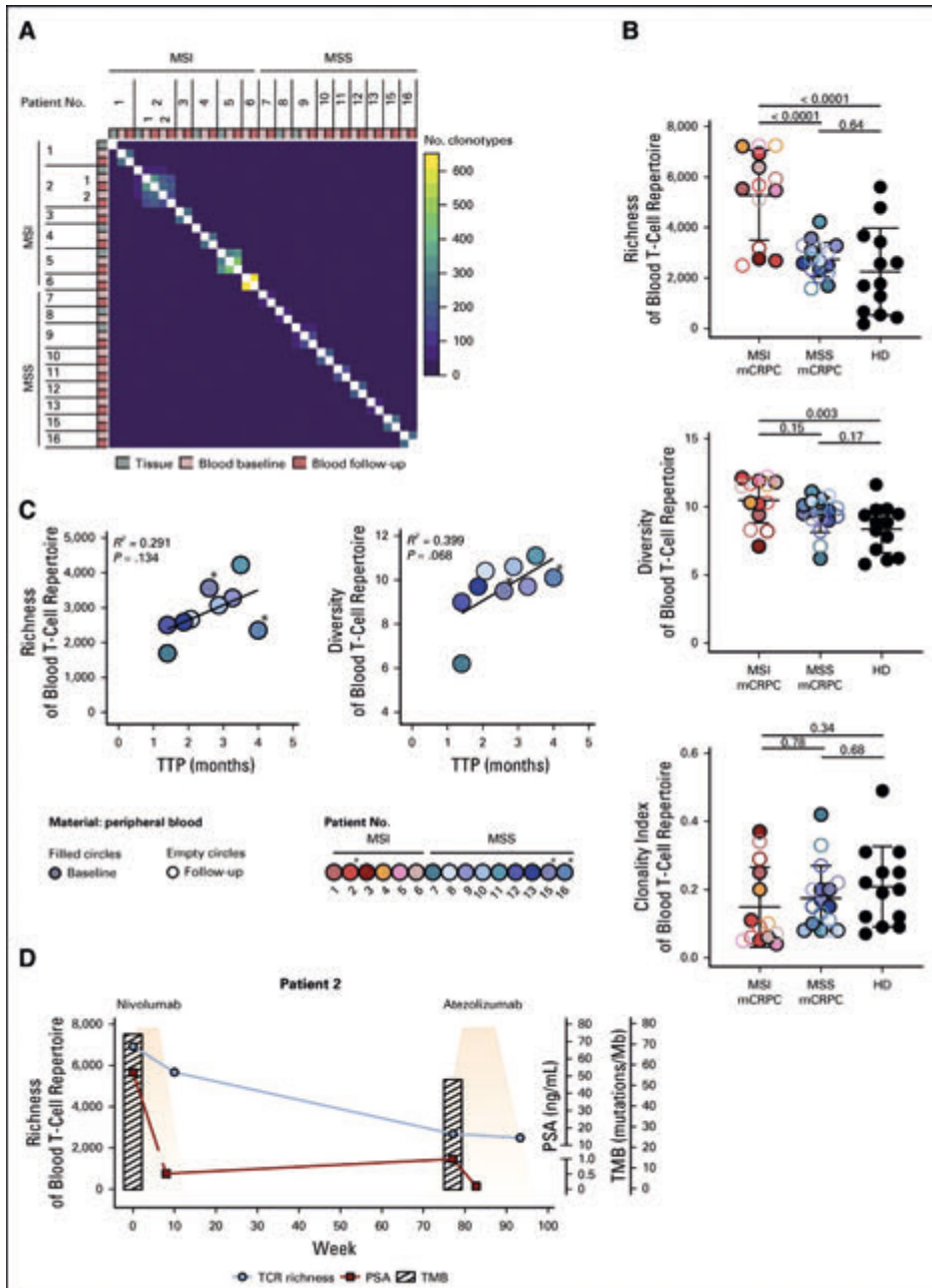


Figure 2. (*Continued*) (B) Richness, diversity (Shannon index) and clonality as peripheral blood T-cell repertoire metrics are shown for cohort 1 as well as healthy donor (HD) controls. One-way analysis of variance was used to study differences between cohorts. (C) Pearson correlation between baseline peripheral blood T-cell repertoire richness and diversity with time to progression (TTP) in patients with MSS mCRPC (cohort 1). Black line indicates regression model. (*) Patients with CDK12 aberration(s). (D) Peripheral blood - cell receptor richness, tumor mutational burden (TMB) and prostate-specific (PSA) levels of patient 2 over the course of treatment with nivolumab and atezolizumab. TCR, T-cell receptor.

We studied T-cell metrics over time in one informative case that was treated sequentially on two ICB regimens with four sequential blood samples available (Figure 2D). This patient received nivolumab with a partial response per RECIST1.1 criteria and deep PSA response (99% reduction). Because of toxicity, treatment was interrupted and was later switched to atezolizumab. While receiving atezolizumab, the patient responded again with a PSA decline of 99% and a complete remission on imaging. TMB was high at the start of nivolumab treatment (74 mutations/Mb) and was reduced significantly when the patient started receiving atezolizumab (48 mutations/Mb). This suggested that the first-line ICB treatment leading to a dramatic response had already cleared some of the tumor subclones contributing to high TMB in this patient. Intriguingly, we found that T-cell richness decreased, accompanying the drop in TMB. This case not only showed dynamic evolution of T-cell richness over time, but also suggested that this parameter may correlate with TMB/neoepitope burden, in line with the association between T-cell richness and MSI status.

T-cell cluster analysis in patients with MSS and MSI mCRPC

Our data showed that basic blood immune metrics differed between the MSI and MSS subcohorts and that there may be a subset of patients with MSS mCRPC who show immune parameters similar to those of patients with MSI mCRPC. We explored in more detail whether specific T-cell receptors or clusters could be identified that may more accurately predict treatment benefit in the MSS subcohort.

Our repertoire overlap analysis (Figure 2A) showed that no individual T-cell receptor sequences were shared among patients with mCRPC. We performed GLIPH analysis from the MSI, and MSS groups (cohort 1) and HDs to group T-cell clones on the basis of presumed antigen specificity, thereby reducing the complexity of the dataset [18]. We found 246 T-cell clusters that were shared only in the HD group, whereas a much higher number of 1307 clusters were shared exclusively among patients with mCRPC (Figure 3A). To understand whether the mCRPC T-cell clusters were present in either of the mCRPC subsets or enriched in one of them, we plotted the mean cluster frequencies in patients with MSS versus MSI disease (Figure 3A lower panel). Most of the 1307 mCRPC clusters were found to be enriched in the MSI subgroup.

Clusters with low pGen ($<1/10^9$) are only expected to be shared between individuals if selected for functionality [20]. We found 232 low pGen mCRPC clusters shared between at least two patients with mCRPC, potentially presenting T-cell receptors directed either against common prostate cancer antigens or against neoepitopes in patients with overlapping genetic loci. If we chose a more stringent threshold (to exclude contamination bias, which might have occurred during sequencing and/or sample preparation), and considered only clusters shared among at least three individuals, we were left with five mCRPC T-cell clusters with a low pGen (Figure 3A, marked with numbers 1-5, Appendix Table A2). Of note, these clusters were found only in the pre-ICB blood of these patients, not in blood drawn during ICB therapy. Overall, five out of six patients with MSI mCRPC showed CDR3 sequences belonging to at least one of the five shared low pGen clusters (Appendix Table A2). However, five patients from our MSS mCRPC cohort, including two patients with CDK12 loss, also showed these clusters. In the MSS subcohort, individuals with shared low pGen clusters showed significantly longer TTP with ICB compared with patients without these clusters (mean TTP 3.9 vs. 2.1 months, $p = .0025$, Figure 3B).

Because the patients in the MSS subset of cohort 1 were selected for PD-L1 positivity or loss of CDK12, we investigated how many patients from our unselected MSS mCRPC cohort 2 showed the previously identified shared low pGen T-cell clusters. Using a search algorithm for the respective cluster sequences, we found that three out of 39 patients showed the identified clusters, suggesting that the proportion of unselected patients with MSS mCRPC with this special cluster signature may have been approximately 10%. These three patients did not have more favorable outcomes with their first line non-ICB treatment as compared with their peers (mean TTP 6.9 versus 11.2 months, $p=0.88$). However, this finding needs to be interpreted with caution because of the limited cohort size.

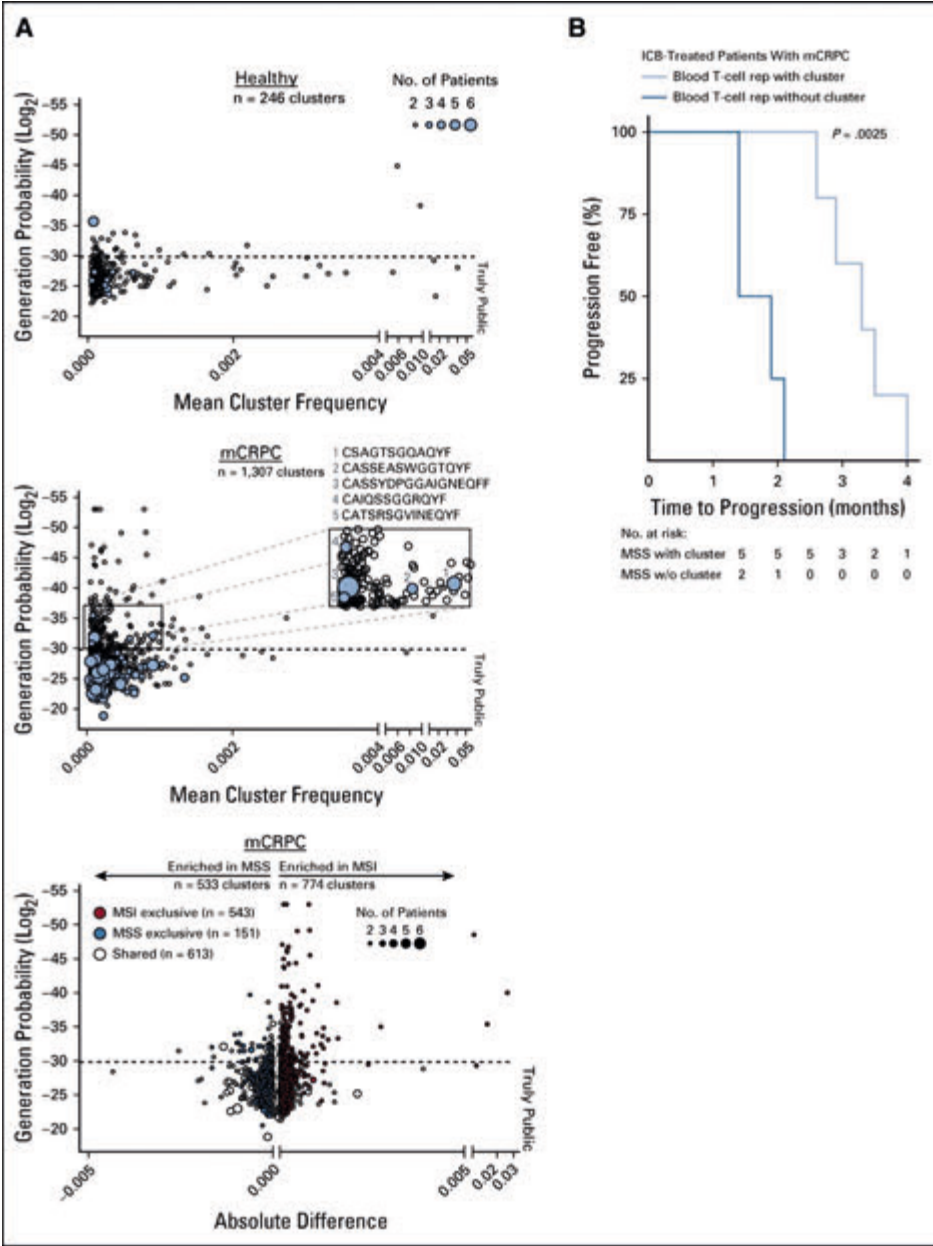


Figure 3. Peripheral blood T-cell cluster analysis in patients with microsatellite stable (MSS) and microsatellite instable (MSI) metastatic castration-resistant prostate cancer (mCRPC).

(A) Generation probability (pGen) and mean frequency of T-cell clusters found in healthy donors and patients with MSI or MSS mCRPC. The size of the dots represents the number of individuals in whom the cluster was found. Clusters shared in three or more individuals are shown as blue-filled dots in both upper panels. -----> (Continued on following page)

Figure 3. (Continued) The lower panel presents the 1307 mCRPC clusters according to the subgroups in which they were found. Filled dots represent clusters found exclusively in one subgroup and empty dots represent clusters shared between both MSI and MSS subgroups. (B) Time to progression Kaplan-Meier analysis of immune checkpoint blockade (ICB) treatment for patients with MSS mCRPC (cohort 1) with one or more versus no shared low generation probability T-cell clusters at baseline testing. The statistical analysis was performed using log-rank test. rep, repertoire.

DISCUSSION

Prostate cancer is the most commonly diagnosed cancer in males. Recent years have brought a great deal of therapeutic progress for patients with metastatic castration-resistant disease, notably through advances in novel hormone therapies. Recently, the immune checkpoint inhibitor pembrolizumab showed high response rates in tumors with mismatch-repair deficiency regardless of primary tumor site leading to a tumor-agnostic FDA approval. With up to 12% of prostate cancers harboring a hypermutated state because of MSI disease [21], immune checkpoint inhibitors represent new therapeutic options for a subset of patients with mCRPC. Yet for the majority of mCRPC patients with MSS tumors, efficient immunotherapeutics are currently lacking.

To our knowledge, our immunologic analyses provide the first evidence that patients with MSI mCRPC show an immunologic fingerprint characterized by high peripheral blood T-cell repertoire richness and diversity. Moreover, we show that the majority of patients with MSI mCRPC harbor shared T-cell clusters with low pGen, suggesting their functional importance and relevance for immune control in this disease. Additional analyses suggested that the cluster signature could also identify patients with MSS tumors that may derive benefit from immune checkpoint inhibition.

Although they were acquired on the basis of informative but small patient cohorts with, admittedly, heterogeneous ICB treatment, we believe that our data are hypothesis generating and valuable for the translational design of future immunoncology trials in this entity. There were several aspects that we found surprising and that need interpretation. First, we found important differences between T-cell repertoire richness and diversity in patients with MSI mCRPC when compared with patients with MSS tumors. In our view, this most likely reflects a greater neoepitope load triggering highly diverse T-cell responses in this subset. Interestingly, this also supported a finding of a recent study by Li et al. [22] showing that high TMB may increase tumor-infiltrating lymphocytes diversity. Still, the strong association evidenced by our work seemed surprising at first glance. It indicates that the numbers of T-cell clonotypes able to recognize a specific MHC-displayed neoepitope have to be high enough and the expansion of the respective clone important enough to produce an effect on blood T-cell metrics. In fact, some previous studies have

in estimated that up to one million different T-cell clonotypes may be able to recognize a given epitope [23]. This supports the concept of an effect on blood T-cell metrics, given a TMB of 18-74 mutations/Mb in MSI tumors. At the same time, T-cell clusters with presumably identical antigen recognition were found to be shared among patients with MSI tumors (as well as between some of the patients with MSS tumors). This indicated that, although the T-cell response against neoantigens might be diverse and unique in each patient, there seems to be a common, patient-overlapping T-cell response to several antigens, even in MSI mCRPC. The shared characteristics among patients may indicate that part of these clusters may be directed against broadly expressed tumor antigens such as PSMA. However, because of the enrichment of this signature in MSI disease, at least part of this response might be directed against individual neoepitopes, despite the fact that these are generally considered exclusive to the patient. In fact, a whole-genome sequencing analysis of tumor biopsies from 148 patients with metastatic prostate cancer suggested recurrent frameshift mutations in gene loci also shared in patients with other MSI cancer types [24,25]. An updated analysis of >350 patients with metastatic prostate cancer confirms recurrent mutations such as hotspot missense mutations in CLOCK, TGF β 2, ASXL1 or POLD3 across the high TMB/MSI subset. This finding may corroborate our interpretation, but additional study of more T cell repertoires in larger genetically characterized cohorts is needed to infer potential antigen recognition from the cluster patterns by association analyses.

Interestingly, baseline T-cell clusters were not found in repeated samplings with ICB treatment. The loss of these clusters in the periphery after initiation of ICB could indicate migration to the primary tumor or metastatic sites during the process of clonal replacement, as described recently after PD-1 blockade in skin cancer as well as after Sipuleucel T treatment in prostate cancer [26,27]. Despite the small size of our cohorts, we found noteworthy that, although patients with mCRPC with the cluster signature seemed to show benefit from ICB, there was no evidence that such patients did better when receiving non-ICB treatments, as evidenced by the analysis of an unrelated mCRPC cohort with, however, the limitation of the sample size of this second cohort. This suggested that the T-cell cluster signature may be associated with specific treatment benefit from ICB rather than generally reflecting immune fitness potentially associated with longer survival.

A prospective validation of the data presented here would be of high clinical relevance because it might open up avenues for using blood T-cell profiles as predictive biomarker for checkpoint inhibition in MSS mCRPC. This will be possible in multiple phase III studies with ICB and combination approaches that ICB, in which patients are currently enrolling.

DATA AVAILABILITY

The datasets generated for this study can be found in the European Nucleotide Archive (ENA). Accession number: PRJEB34378.

SUPPLEMENTARY INFORMATION

Table A1. Clinical characteristics of cohort 2.

Characteristic	Total group (N=39)
Age at diagnosis, years, mean (range)	64.8 (48-77)
Total Gleason score at diagnosis	
< 8	14 (35.9)
≥ 8	21 (53.8)
unknown	4 (10.3)
Metastasis status at diagnosis	
M0	17 (43.6)
M1	17 (43.6)
Unknown	5 (12.8)
First therapy for CRPC	
Chemotherapy	
Docetaxel	6 (15.4)
Cabazitaxel	1 (2.6)
Cisplatin	1 (2.6)
Second-generation ADT	
Abiraterone	20 (76.9)
Enzalutamide	10 (25.6)
Checkpoint inhibitor	
Atezolizumab	1 (2.6)
Response to therapy	
Median duration to progression, months, median (range)	5.8 (0.3-27)
Median duration of therapy, months, median (range)	8.9 (0.3-35)

NOTE. Data are presented as No. (%) unless indicated otherwise. Abbreviations: ADT, androgen-deprivation therapy; CRPC, castration-resistant prostate cancer.

Table A2. Sequences of T cell clusters and clones found in patients with mCRPC.

#	Cluster Sequence	TRB CDR3 AA Sequence	V gene	J gene	Frequency	Patient	Subgroup
1	CSAGTSGGAQYF	CASGTSGGSRYF	TRBV27	TRBJ2-5	1.15E-04	05	MSI
		CSAGTSGGAWYF	TRBV29-1	TRBJ2-3	2.80E-04	03	MSI
		CSAGTSGGAQYF	TRBV29-1	TRBJ2-3	0.0014/0.0013	09, 10	MSS
		CSVSSGGAQYF	TRBV29-1	TRBJ2-3	5.14E-05	09	MSS
2	CASSEASWGGTQYF	CAISEASGGGTQYF	TRBV10-3	TRBJ2-3	9.24E-04	10	MSS
		CASSEASWGGTQYF	TRBV6-1	TRBJ2-5	5.65E-04	09	MSS
		CSAREASGGGTQYF	TRBV20-1	TRBJ2-5	5.14E-05	11	MSS
		CAISEASGGGTQYF	TRBV10-3	TRBJ2-5	1.00E-04	63481	MSS, cohort 2
		CAISESGGTQYF	TRBV10-3	TRBJ2-3	1.61E-04	77565	MSS, cohort 2
		CSAREASGLGTQYF	TRBV20-1	TRBJ2-5	1.01E-04	58478	MSS, cohort 2
		CASRYDPGQGRNEQYF	TRBV6-2, TRBV6-3	TRBJ2-7	2.60E-04	16	MSS
		CASSYDPGDPNNSPLHF	TRBV6-2, TRBV6-3	TRBJ1-6	1.18E-04	10	MSS
		CASSYDPGGAIGNEQFF	TRBV6-5, TRBV6-1, TRBV12-3, TRBV12-4	TRBJ2-1	4.71E-05	01	MSI
		CASSYDPGGVMNTEAFF	TRBV6-5	TRBJ1-1	3.98E-05	06	MSI
3	CASSYDPGGAIGNEQFF	CSAYDPGAYEQYF	TRBV20-1	TRBJ2-7	3.85E-05	11	MSS
		CSAYDPGLQKETQYF	TRBV20-1	TRBJ2-5	1.20E-04	09	MSS
		CAIQSSGGGRQYF	TRBV6-2, TRBV6-3, TRBV6-5	TRBJ2-3	5.92E-05	15	MSS
		CASCSSGKQFF	TRBV6-5	TRBJ2-1	4.95E-05	05	MSI
		CAWQSSGKLF	TRBV30	TRBJ1-4	9.41E-05	01	MSI
4	CAIQSSGGGRQYF	CASSSSGKQFF	TRBV27	TRBJ2-1	1.39E-04	03	MSI
		CAISRQGINEQFF	TRBV10-3	TRBJ2-1	3.85E-05	11	MSS
5	CATSRSGVINEQYF	CASSRQGVINEQYF	TRBV7-9	TRBJ2-7	5.90E-05	10	MSS
		CATSRSGVINEQYF	TRBV15	TRBJ2-7	6.97E-05	04	MSI

Abbreviations: mCRPC, metastatic castration-resistant prostate cancer; MSI, microsatellite instable; MSS, microsatellite stable; TRB, T-cell receptor β locus

REFERENCES

1. Higano CS, Armstrong AJ, Sartor AO, et al: Real-world outcomes of sipuleucel-T treatment in PROCEED, a prospective registry of men with metastatic castration-resistant prostate cancer. *Cancer* 125:4172-4180, 2019
2. Gulley JL, Borre M, Vogelzang NJ, et al: Phase III Trial of PROSTVAC in Asymptomatic or Minimally Symptomatic Metastatic Castration-Resistant Prostate Cancer. *J Clin Oncol* 37:1051-1061, 2019
3. Le DT, Durham JN, Smith KN, et al: Mismatch repair deficiency predicts response of solid tumors to PD-1 blockade. *Science* 357:409-413, 2017
4. Abida W, Cheng ML, Armenia J, et al: Analysis of the Prevalence of Microsatellite Instability in Prostate Cancer and Response to Immune Checkpoint Blockade. *JAMA Oncol* 5:471-478, 2019
5. Robinson D, Van Allen EM, Wu YM, et al: Integrative clinical genomics of advanced prostate cancer. *Cell* 161:1215-1228, 2015
6. Kwon ED, Drake CG, Scher HI, et al: Ipilimumab versus placebo after radiotherapy in patients with metastatic castration-resistant prostate cancer that had progressed after docetaxel chemotherapy (CA184-043): a multicentre, randomised, double-blind, phase 3 trial. *The Lancet Oncology* 15:700-712, 2014
7. Beer TM, Kwon ED, Drake CG, et al: Randomized, Double-Blind, Phase III Trial of Ipilimumab Versus Placebo in Asymptomatic or Minimally Symptomatic Patients With Metastatic Chemotherapy-Naive Castration-Resistant Prostate Cancer. *J Clin Oncol* 35:40-47, 2017
8. Hansen AR, Massard C, Ott PA, et al: Pembrolizumab for advanced prostate adenocarcinoma: findings of the KEYNOTE-028 study. *Ann Oncol* 29:1807-1813, 2018
9. Antonarakis ES, Piulats JM, Gross-Goupil M, et al: Pembrolizumab for Treatment-Refractory Metastatic Castration-Resistant Prostate Cancer: Multicohort, Open-Label Phase II KEYNOTE-199 Study. *J Clin Oncol* 38:395-405, 2020
10. Wu YM, Cieslik M, Lonigro RJ, et al: Inactivation of CDK12 Delineates a Distinct Immunogenic Class of Advanced Prostate Cancer. *Cell* 173:1770-1782 e14, 2018
11. van Dessel LF, van Riet J, Smits M, et al: The genomic landscape of metastatic castration-resistant prostate cancers reveals multiple distinct genotypes with potential clinical impact. *Nat Commun* 10:5251, 2019
12. Quigley DA, Dang HX, Zhao SG, et al: Genomic Hallmarks and Structural Variation in Metastatic Prostate Cancer. *Cell* 175:889, 2018
13. Reimers MA, Yip SM, Zhang L, et al: Clinical Outcomes in Cyclin-dependent Kinase 12 Mutant Advanced Prostate Cancer. *Eur Urol*, 2019
14. van der Velden DL, Hoes LR, van der Wijngaart H, et al: The Drug Rediscovery protocol facilitates the expanded use of existing anticancer drugs. *Nature* 574:127-131, 2019
15. Simnica D, Akyüz N, Schliffke S, et al: T cell receptor next-generation sequencing reveals cancer-associated repertoire metrics and reconstitution after chemotherapy in patients with hematological and solid tumors. *Oncolimmunology*:1-11, 2019
16. Bolotin DA, Poslavsky S, Mitrophanov I, et al: MiXCR: software for comprehensive adaptive immunity profiling. *Nat Methods* 12:380-1, 2015

17. Nazarov VI, Pogorelyy MV, Komech EA, et al: tcR: an R package for T cell receptor repertoire advanced data analysis. *BMC Bioinformatics* 16:175, 2015
18. Glanville J, Huang H, Nau A, et al: Identifying specificity groups in the T cell receptor repertoire. *Nature* 547:94-98, 2017
19. Sethna Z, Elhanati Y, Callan CG, et al: OLGA: fast computation of generation probabilities of B- and T-cell receptor amino acid sequences and motifs. *Bioinformatics* 35:2974-2981, 2019
20. Elhanati Y, Sethna Z, Callan CG, Jr., et al: Predicting the spectrum of TCR repertoire sharing with a data-driven model of recombination. *Immunol Rev* 284:167-179, 2018
21. Pritchard CC, Morrissey C, Kumar A, et al: Complex MSH2 and MSH6 mutations in hypermutated microsatellite unstable advanced prostate cancer. *Nat Commun* 5:4988, 2014
22. Li B, Li T, Pignon JC, et al: Landscape of tumor-infiltrating T cell repertoire of human cancers. *Nat Genet* 48:725-32, 2016
23. Wooldridge L, Ekeruche-Makinde J, van den Berg HA, et al: A single autoimmune T cell receptor recognizes more than a million different peptides. *J Biol Chem* 287:1168-77, 2012
24. Mehra N, van Riet J, Smits M, et al: 798PD - In-depth assessment of metastatic prostate cancer with high tumour mutational burden. *Annals of Oncology* 29:viii274, 2018
25. Kim TM, Laird PW, Park PJ: The landscape of microsatellite instability in colorectal and endometrial cancer genomes. *Cell* 155:858-68, 2013
26. Yost KE, Satpathy AT, Wells DK, et al: Clonal replacement of tumor-specific T cells following PD-1 blockade. *Nat Med* 25:1251-1259, 2019
27. Sheikh N, Cham J, Zhang L, et al: Clonotypic Diversification of Intratumoral T Cells Following Sipuleucel-T Treatment in Prostate Cancer Subjects. *Cancer Res* 76:3711-8, 2016



PART IV

EPILOGUE



CHAPTER 7

SUMMARY

SUMMARY

Today prostate cancer is the fourth most common type of cancer and accounts for 6.8% of all cancer related deaths in men worldwide.

When cancer is diagnosed within the prostate, several foci of malignant cells are present with often different Gleason grades. Subsequently, metastatic sites can consist of different clones, e.g. clones with varying aggressiveness and hormone sensitivity. Androgen deprivation therapy (ADT) is the backbone for treatment of metastatic disease and suppresses outgrowth of hormone sensitive prostate cancer. But despite (complete) blockage of testosterone production, resistance always occurs leading to castration resistant state of disease by adaptive changes in androgen signaling and/or outgrowth of predominant hormone insensitive clones.

During the last two decades several new treatment modalities, both chemotherapy, androgen-receptor signaling inhibitors (ARSI) and radioligand therapies, were investigated in an extensive number of landmark trials. These drugs have improved quality of life and overall survival in men with metastatic castration resistant prostate cancer with a prolongation of survival of approximately 4 months. Although the addition of docetaxel and ARSIs to ADT in mHSPC setting seems to further improve overall survival, the modest effect of these new drugs is most likely the consequence of the fact that all cancer patients are treated in the same manner and not based on phenotypic or genetic characteristics.

Several next generation sequencing (NGS) studies have improved our understanding and knowledge about the genetic landscape of metastatic prostate cancer enormously, nevertheless there is still a gap in translating this knowledge into optimal sequencing and the development of new treatment strategies. Prostate cancer often solely or predominantly metastasizes to the bones and the success rate of obtaining sufficient tumor cells from bone metastases for these analyses is relatively low due to a tumor microenvironment which consists of a stromal cells mixture with mainly osteoclasts. This results in biopsies with lower tumor content when compared with lymph nodes or viscera.

The aim of this thesis was to improve our knowledge about the technical challenges of molecular analyses in prostate cancer patients and describes the potential clinical impact of unraveling the genomic landscape of metastatic prostate cancer.

In **part I** of this thesis we describe pre-biopsy blood and imaging variables which determine the success of metastatic bone biopsies and the role of PSMA/PET-CT in obtaining enough tumor yield for molecular analyses.

In **chapter 2** we evaluated the success rate of PSMA/PET-CT guided bone biopsies for molecular diagnostics in metastatic prostate cancer patients. A successful biopsy was defined as a tumor percentage of at least 30%. All prostate cancer patients who underwent a PSMA/PET-CT less than 12 weeks prior to the bone biopsy within the multicenter nationwide CPCT-02 study (NCT01855477) were included. A success rate of 70% was seen in this group of patients, which is remarkably higher than described in previous CT-guided bone biopsy studies. ^{68}Ga -PSMA uptake (SUV) was significantly higher in successful biopsies and in contrast, radiodensity (Hounsfield unit, HU) of the lesion was significantly lower on CT in successful biopsies, and appeared to be both strong predictors for a biopsy with high tumor fraction in multivariate analysis.

The success rate of PSMA/PET-CT guided bone biopsies was also investigated in **chapter 3** together with other imaging modalities used to guide bone biopsy sites. Furthermore, this study aimed to design a predictive model that could be used in daily clinical practice to increase the success of a bone biopsy for molecular characterization of a metastatic prostate cancer patient. A significantly higher success rate for both histological confirmation and molecular analysis were found when a prior PSMA/PET-CT was performed when compared to CT or MRI. In addition, we found that more homogenous lesions (low deviation) with low HU on CT imaging contained significantly more often tumor tissue suitable for molecular analyses. We developed a simple prediction model with these two variables. External validation of this model in a prospective study deems necessary before implementing is possible in daily practice.

In **part II** we take the next step by investigating in **chapter 4** the feasibility of the combination of PSMA/PET-CT and a diffusion-weighted MRI to determine the most optimal bone metastasis based on PSMA expression and diffusion restriction prior to a cone-beam CT guided biopsy and whether this new advanced target planning would lead to a higher success rate of bone biopsies for molecular analyses. We conducted a prospective pilot study with ten metastatic prostate cancer patients who underwent a bone biopsy for molecular analysis and received prior to the biopsy a PSMA/PET-CT and a diffusion-weighted MRI of the bone metastasis of interest. The histopathological diagnosis was confirmed in 90% and tumor yield was sufficient for molecular analyses in 80%. In two patients druggable targets were found. These results suggest that high diffusion restriction and PSMA uptake are indicative for high tumor yield and that the combination with cone-beam CT guidance could improve the success rate of a successful biopsy, potentially leading to the possibility of a more individualized choice of therapy.

In **part III** the potential clinical impact of molecular diagnostics is described in **chapter 5** and **6**. First, we present the identification of eight distinct genomic clusters within

metastatic castration resistant prostate cancer (mCRPC) in chapter 5. These clusters were found by unsupervised clustering based on genomic features, obtained by whole-genome sequencing (WGS) analysis of fresh frozen biopsies from 197 mCRPC patients within the nationwide Center for Personalized Cancer Treatment (CPCT)-02 trial (NCT01855477). These eight clusters contain a subgroup with a microsatellite instability (MSI) signature, a subgroup with a tandem duplication phenotype associated with biallelic loss of CDK12, a subgroup with homologous recombination deficiency or mutations in BRCA-associated genes and a subgroup with chromothripsis, a phenomenon leading to structural rearrangement, caused by random breakage and fusion at the level of DNA double-strand breaks of one or two chromosomes. The four other groups have signatures with currently unknown biological associations. Our cohort was compared to an unmatched WGS cohort of primary prostate cancer to further investigate whether the genetic aberrations found were metastatic specific. Tumor mutational burden is 3.8 times higher in our mCRPC cohort and frequency of structural variants is also higher in this group compared to the primary prostate cancer cohort. However, no striking primary-only nor mCRPC-derived genomic subgroups are revealed. The identification of these specific subgroups could be clinically relevant, both for prognostic and predictive reasons. Validation of clinical response and outcome on specific treatments in the discovered genomic subgroups will be further investigated in the near future.

In **chapter 6** results of T cell repertoire sequencing in peripheral blood of mCRPC patients, both microsatellite stable (MSS) and MSI, treated with immune checkpoint inhibitors (ICIs) are described. First, most pronounced clonal overlap is seen between patient-matched peripheral and tumor infiltrated T cells suggesting that peripheral blood T cell analyses mirror intratumorally T cell analyses. Secondly, our research showed a significantly higher T cell richness and diversity in the MSI subset, a group with a significantly higher response rate to ICIs when compared to the MSS cohort. Within the MSS cohort response to ICIs is less frequent, but a positive trend for correlation between T cell diversity and response to ICIs is seen. This specific T cell signature found in mCRPC patients with response to ICIs could help to identify a subgroup of MSS mCRPC patients that might also benefit from ICIs.

Finally in **part IV** we discuss the main findings of this thesis and provide our perspective on new developments in molecular characterization of mCRPC patients and its implementation in daily practice, which could lead to a more individualized treatment strategy and leading to an improvement in both quality and quantity of life for mCRPC patients.



CHAPTER 8

DISCUSSION & FUTURE PERSPECTIVES

DISCUSSION

In this thesis we first aimed to improve the success rate of next-generation sequencing in metastatic prostate cancer. Secondly we investigated the genomic landscape of metastatic castration resistant prostate cancer (mCRPC) patients and the potential prognostic and predictive value in daily practice.

Overcoming the technical challenges in obtaining an adequate bone biopsy for molecular characterization in metastatic prostate cancer

In daily practice the logistic path towards precision medicine in oncology can be arduous when fresh tissue is required. As described in **chapter 2** and **3** of this thesis (predominantly) bone metastatic prostate cancer patients are highly underrepresented in larger next-generation sequencing (NGS) studies. Furthermore, NGS studies in both primary prostate cancer (1, 2) metastatic prostate cancer (3-6) have given a comprehensive insight into the molecular landscape of prostate cancer, showing the evolution towards castration resistance mainly explained by aberrations in the androgen receptor (AR) signaling pathway. This evolution was also found in our whole-genome sequencing (WGS) study in mCRPC patients when compared to a cohort of primary prostate cancer patients as discussed in **chapter 5**. WGS has the advantage over targeted sequencing of giving a complete overview of molecular aberrations present, however it requires fresh frozen tissue with sufficient tumor yield/content, as discussed in **chapter 2** and **3**. Underrepresentation of bone metastatic prostate cancer patients in NGS studies, the partially treatment-driven evolution of prostate cancer and the preference for WGS to obtain a complete overview of molecular aberrations underlines the need for fresh frozen biopsies.

Nevertheless, obtaining fresh frozen tissue with sufficient tumor yield for NGS to guide precision medicine in metastatic prostate cancer can be a challenge. This has particularly been shown in large phase 3 precision medicine studies, where approximately 30% of efforts result in failure in acquiring a result (7). In particular, bone metastatic disease has proven a difficult site for acquiring sufficient tumor cell content. Therefore, we particularly sought out to improve on acquiring a bone biopsy for molecular analyses in metastatic prostate cancer by identifying clinical and imaging variables and investigating a new advanced target planning protocol in prostate cancer patients with solely bone metastases.

The predominantly sclerotic character of bone metastases in prostate cancer makes it difficult to distinguish active malignant bone metastases from nonmalignant osteosclerotic lesions (8) on conventional CT scan and bone scintigraphy. Previous studies (9, 10) investigating the image-guided bone biopsies in metastatic prostate cancer to guide molecular analyses, and aimed to identify clinical and imaging factors

that might influence biopsy outcome, including prostate specific antigen (PSA), lactate dehydrogenase (LDH), alkaline phosphatase (AF) and Hounsfield unit (HU) derived from a prior computed tomography (CT) scan. The most relevant variable, that may be used for clinical implementation, identified from CT imaging studies might be HU. A recent study confirmed that predominantly mild sclerosis and lower CT attenuation lesions result in significantly greater tumor-positive and NGS success rate, when compared with biopsies of dense sclerosis and higher attenuation lesions (11). Even though HU appears to be a relevant variable, prospective studies have not been performed and thus is not clearly implemented in daily practice.

We hypothesized that next-generation imaging (NGI) could overcome many technical pitfalls from the use of conventional imaging. Prostate-specific membrane antigen (PSMA) is highly expressed on prostate cancer cells and this expression is even higher in the majority of mCRPC patients (12, 13). We therefore focused on PSMA-PET to identify optimal bone lesions for biopsy, based on high level of PSMA-avidity, location and size of the lesion. After identification of the optimal lesion, this could be biopsied routinely through CT-guidance.

The value of use of the PSMA positron emission tomography (PET) /computed tomography (CT) scan has been proven in patients with de novo high risk, with higher rates of detection of metastases than routine imaging (14, 15). Particularly in patients with biochemical recurrence after therapy with curative intent (radical prostatectomy or salvage radiotherapy), usage of PSMA-PET/CT is now common practice (15-17).

Nevertheless, use of PSMA-PET-CT imaging has also increased in patients with castration-resistant prostate cancer. This is mainly due to predictive characteristics with regard to Lutetium-177-PSMA-617 treatment in mCRPC. The phase 3 randomized controlled VISION trial (18) showed an improved progression free survival (PFS) and overall survival (OS) when radioligand therapy with Lutetium-177-PSMA-617 was administered to heavily pretreated PSMA expressing metastatic prostate cancer patients compared to best supportive care and is therefore a promising new treatment modality for mCRPC patients. Currently ongoing clinical trials are investigating the response to Lutetium-177-PSMA-617 in an even earlier stage of metastatic disease (e.g. NCT04647526, NCT05204927, NCT04443062) and in combination with registered therapies (e.g. NCT05340374, NCT04419402, NCT03874884). However, to our knowledge PSMA/PET-CT is never investigated as an imaging tool to improve biopsy outcome for molecular characterization in a large group of solely or predominantly bone metastasized prostate cancer.

Based on the results of our studies described in **chapter 2** and **3** we can conclude that the chance of obtaining sufficient tumor yield for molecular analyses in a CT guided bone

biopsy can be improved by PSMA/PET-CT. Especially the uptake in PSMA expression (standard uptake value, SUV) and bone metastasis density (Hounsfield unit, HU) on CT were significantly associated with biopsy outcome.

Implementation of these imaging tools and taking the SUV and HU into account in the decision making with regard to biopsy location is feasible, as we showed in our prospective pilot study described in **chapter 4**. These results have already changed common practice for acquiring bone biopsies from bone (predominant) metastatic prostate cancer patients in the Radboud University Medical Center. All patients with mCRPC that are biopsied from bone metastases are discussed in the CRPC multidisciplinary tumor board, where a pre-biopsy PSMA-PET has become compulsory to guide the CT-guided biopsy of the bone lesion. Since 2020 the Radboud University Medical Center has regionalized biopsy for NGS in the PROMPT study (NCT04746300). Fresh frozen bone biopsy success with prior PSMA/PET-CT in this prospective trial is 65%, compared to 56% in biopsies with no prior PSMA/PET-CT (unpublished data).

Unfortunately PSMA/PET-CT is not yet available in every peripheral hospital and, even more relevant, not all lesions of patients with mCRPC express PSMA (13).

In **chapter 3** we described the results on biopsy outcome with prior MRI and found a similar success percentage compared to CT alone, however due to the retrospective nature of this study, diffusion restriction measurements on MRI weren't consequently taken into account in the decision of biopsy location. Also due to the retrospective nature of this study group sizes were very different (12 versus 62 for MRI and PSMA/PET-CT, respectively) and therefore we should interpret the results on outcome of bone biopsy with prior MRI with caution.

Previous studies have discussed the role of diffusion-weighted (DW) MRI in identifying malignant bone lesions (19, 20) and the correlation between DW- MRI and histological and molecular outcome of bone biopsies in prostate cancer patients (21, 22). In malignant bone lesions diffusion restriction (DR) is high and is corresponding with a lower apparent diffusion coefficient (ADC), which is a measurement for the rate of diffusion of water molecules in tissue (19, 21, 22). Based on these studies DR and corresponding ADC are likely to be useful parameters to use in predicting a successful biopsy. Unfortunately our prospective pilot study in **chapter 4** was not able to differentiate which influencing factor contributed most to the high success rate of bone biopsies, due to the similar introduction of prior PSMA/PET-CT and DW-MRI and a new innovative cone-beam CT-guided needle biopsy procedure. To our knowledge no other prospective study has been

conducted with the aim to evaluate correlation between DW-MR and the success rate of a successful bone biopsy for molecular analyses.

Therefore it could be suggested that a larger prospective trial, investigating the added value of prior DW MRI (DR and ADC) when compared to PSMA/PET-CT (SUV) in CT guided bone biopsies from metastases with HU below 450, with percentage successful molecular analyzed bone biopsies as primary outcome, would be advisable.

With the current knowledge DW-MRI could be considered prior to a bone biopsy when PSMA/PET-CT is not available or in the absence of PSMA expression in metastatic prostate cancer patients.

Unraveling the genomic landscape metastatic prostate cancer and its clinical and economic impact

During the last decade several next-generation sequencing (NGS) studies revealed a comprehensive insight into the different genetic aberrations in both primary and metastatic prostate cancer, leading to a better understanding of the development of prostate cancer in several stages of the disease. The identification of these genetic aberrations has also become paramount in the development of specific targeted therapies.

Robinson et al described the genomic landscape of mCRPC in a cohort of 150 patients, compared their findings to a primary prostate cancer cohort and revealed clinical relevance of their results (3). Most frequent aberrations in mCRPC were seen in AR (63%), TP53 (53%), ETS family (57%) and PTEN (41%). Possible actionable non-AR related alterations included aberrations in DNA repair pathway (14% BRCA1/2, 5% CDK12, 3% MMR), cell cycle control genes (7%) and PI3K pathway (49%) (3).

However, pathogenic druggable alterations are no guarantee for response to targeted therapy, for example due to heterogeneous rates of biallelic gene inactivation, and intrapatient tumor heterogeneity. Furthermore, targeted therapy could also benefit patients without a known druggable mutation as shown by Clarke et al for Olaparib (23). This could be explained by epigenetic alterations or interaction of pathways, such as the earlier mentioned interaction between AR signaling and DNA repair genes.

The complexity of the epigenetic and genomic landscape in metastatic prostate cancer underlines the need of a more extensive analysis for stratification of patients to improve selection for different targeted therapies.

Therefore we sought to utilize WGS to acquire mutational signatures that could have clinical impact. Our whole-genome sequencing (WGS) study in 197 mCRCP patients, described in **chapter 5**, is the first study that used unsupervised clustering of mutational characteristics to reveal eight distinct genomic clusters. Microsatellite instability (MSI) was found in all patients in cluster A with >90% of the patients harboring an alteration in MSH2, MSH6 and/or MLH1. Interestingly, in cohort B tandem duplications were predominantly caused by biallelic CDK12 loss, however in two patients no underlying genomic mechanisms were identified. Cohort D represents patients with homologous recombination deficiencies (HRD) or a high HR-deficiency prediction (CHORD) score. Biallelic inactivation of BRCA2 was most commonly found in this cluster (68%). Although in 4 out of 7 remaining patients at least one aberration in HRD genes was identified, in three patients high CHORD score could not be explained with current genomic knowledge. The results of our study underlines the clinical impact of WGS based clustering since currently used NGS panels in daily practice would miss several patients who could benefit from targeted therapy. In our current clinical practice we use a version of a large targeted gene panel True Sight Oncology 500 (TSO500), which does not incorporate signature detection in its design. Therefore, research is ongoing to implement low-pass WGS (LPWGS) to extract clinical relevant signatures, and in conjunction with TSO500, is more cost-effective compared to use of high-depth WGS.

Several clinical trials, including the phase 2 INSPIRE trial in the Radboud University Medical Center (NCT04717154), are conducted to evaluate the response to targeted therapy for patients in three identified clusters; microsatellite instability (MSI), homologous recombination deficiency (HRD) and tandem duplications predominantly caused by biallelic CDK12 loss.

However, these clusters contained only 24% of all mCRPC patients in our study. For the remaining clusters we are evaluating the clinical impact by analyzing WGS data from almost 300 biopsies of Dutch mCRPC patients within the nationwide CPCT02-study (NCT01855477), using the same unsupervised clustering as described in **chapter 5**. We aim to correlate this WGS data to multiple clinical outcomes and reveal the added prognostic and predictive value of unsupervised clustering in mCRPC patients. For the remaining patients in clusters with currently unknown genomic signatures, it remains necessary to assess the underlying oncogenic drivers, by assessing single-nucleotide variants, copy number variation, or structural variations for the majority of mCRPC patients to be able to match with targeted therapeutic options.

According to the Dutch Cancer Registration (IKNL) the incidence of cancer was 56.000 in the Netherlands in 1989. Within thirty years this number has increased to 118.000

new diagnoses and it has been predicted that in 2032 this the incidence will further rise to 156.000 new diagnoses (24). The rising incidence is mainly due to growth and aging of our society and lifestyle factors such as smoking, alcohol, obesity and the exposure to UV light (24).

This increase in cancer diagnoses leads to questions not only concerning clinical impact but also about the economic impact. First, in the working age population long term complications due to our systemic treatments such as neuropathy and fatigue can affect the ability to carry out work. Secondly, with the development of new treatment strategies during the last decade health costs are rising quickly.

Median overall survival from time of mCRPC diagnosis has improved from 17-19 months with only docetaxel (25, 26) to 32-36 months with the addition of chemotherapy and the androgen-receptor signaling inhibitors (ARSIs) in mCRPC setting between 2010 and 2013 (27, 28).

Although docetaxel seems to be beneficial in a subgroup of mCRPC patients, one could debate its clinical benefit for every mCRPC patient. The phase 3 trials investigating docetaxel in mCRPC patients showed a median overall survival of 19 months in patients receiving docetaxel (25, 26), which was three months longer than mitoxantrone. However, in the phase 3 trial investigating the addition of mitoxantrone versus prednisolone alone, the median overall survival of prednisolone alone was also 19 months (29). Since docetaxel was not compared to placebo and populations included in these clinical trials were not comparable, it is difficult to draw conclusions based on these trials about the role of docetaxel in mCRPC setting. Therefore, a network meta-analysis comparing effects of the different interventions in the previously mentioned docetaxel clinical trials, would be advisable to evaluate the benefit from docetaxel compared to placebo.

Cabazitaxel was registered as second line treatment option for mCRPC based on the results of the phase 3 trial when compared to mitoxantrone after progression on docetaxel (30), but the CAPRI trial, a Dutch real-world observational study, showed a less impressive median overall survival for cabazitaxel in second-line due to the treatment of patients with more aggressive disease characteristics and worse performance scores when compared to patients treated in clinical phase 3 trials (31). When administered in the third line, after docetaxel and ARSIs, cabazitaxel showed a significantly reduced risk of death when compared to another ARSI, however median overall survival was only 2.6 months longer (32). In addition, a cost-effectiveness analysis presented that cabazitaxel after docetaxel and ARSI is not likely to be a cost-effective treatment (33),

although it should be mentioned this analysis was performed at the time cabazitaxel was still patented.

Several landmark trials (34-39) have recently presented the dramatical improvement of overall survival when docetaxel or ARSIs were added to androgen-deprivation therapy (ADT) in metastatic hormone sensitive prostate cancer (mHSPC) when compared to ADT alone. Several cost-effectiveness analyses showed that both docetaxel and abiraterone are cost-effective (40-43) and with the price reduction of abiraterone and longer follow up data abiraterone might even be more cost-effective (42).

Taking all these considerations into account in combination with the increasing healthcare costs and an expected further decrease in healthcare staff that is needed to administer intravenously chemotherapy, it could be suggested that both docetaxel and cabazitaxel shouldn't be administered to all mCRPC patients. First, docetaxel seems to have a greater impact on overall survival when given in a mHSPC setting, based on the results of the CHAARTED trial especially in high volume disease, and should therefore be mainly considered in this setting. Secondly, molecular characterization could be very useful to identify the subgroups of mCRPC patients who would benefit from taxane-based chemotherapy, for example patients with AR gain or the presence of AR-V7 (44, 45).

As described in the general introduction of this thesis, the clinical phase 3 PEACE-1 (46, 47) and ARASENS trials showed an improved clinical outcome for triplet therapy in mHSPC with the addition of ARSIs to ADT and docetaxel.

Nevertheless, the real-world population is older and more fragile than patients included in these clinical trials and therefore we should consider whether triplet therapy would benefit every mHSPC patient. When docetaxel would be considered by the clinician, because of a high volume mHSPC patient with good clinical condition, one could suggest that the additional toxicity of ARSIs is acceptable taking the further improved overall survival with triplet therapy into account. However, when ARSIs are advised in mHSPC setting, due to low volume or in the more fragile patient, the addition of docetaxel should be reconsidered. Primarily for the well-being of the patient, but also because a decrease in cost-effectiveness could be expected due to higher risk of complications and shorter overall survival.

The clinical impact of molecular characterization in finding new targeted therapies has already been proven for two subgroups of mCRPC patients; the first targeted therapy for BRCA mutated metastatic prostate cancer, olaparib, was registered in 2020 and nivolumab was approved in 2022 by the Zorginstituut Nederland for MSI high or mismatch repair deficient (MMRd) metastatic solid tumors based on the results of the nationwide Drug

Rediscovery Protocol (DRUP) trial. Before the approval of nivolumab for this particular group of patients, a small group of heavily pretreated MSI high metastatic prostate cancer patients were treated with nivolumab in our hospital within the DRUP trial and showed a high response rate with durable responses to PDL1 inhibition as described in **chapter 6**.

Another emerging predictive biomarker, often accompanied by MSI high but also more frequently seen in DDRd mCRPC patients (3), also described in **chapter 5** of this thesis, is high tumor mutational burden (TMB), most frequently defined as >10 mutations per megabase. Contradictory results for response to PDL1 inhibitors in pan-cancer high TMB were presented in several retrospective studies (48-51) and indicate the need for a prospective trial in this particular group of patients.

A currently ongoing prospective BARCODE 2 trial aims to investigate the response to platinum-based chemotherapy in DNA repair deficient (DDRd) mCRPC patients, based on the rationale that platinum creates DNA crosslinks, which can't be repaired by a dysfunctional DNA repair pathway. Evidence for this rationale was already found in several retrospective studies (52-56).

The two subgroups of mCRPC patients for which targeted therapy is now available, described as cohort A and D in **chapter 5**, contain only 17.8% of all mCRPC patients and one could argue whether this molecular testing in all mCRPC patients is cost-effective. Two cost-effectiveness analyses have been conducted to evaluate olaparib in metastatic prostate cancer when compared to standard care, both studies using data from the proFOUND trial (57, 58). Although the study by Su et al suggests that olaparib is cost-effective, the study by Li et al shows the contrary. Differences between both analyses is that Su et al found that olaparib was cost-effective in the group with patients containing one of 15 altered genes in homologous recombination deficiency and this was less pronounced for the cohort with only BRCA1/BRCA2/ATM. This is probably partly due to a higher number needed to test in this cohort (57). Li et al focused on BRCA1, BRCA2 and ATM and found that treating with olaparib was not cost-effective (58). However, these cost-effectiveness studies were performed with expensive next-generation sequencing tests and analyses were performed on a group of patients with both BRCA1/2 and ATM mutations. The cost-effectiveness of olaparib in current daily practice would be much more pronounced for two reasons; sequencing can be focused only on BRCA1/2 and excluding patients with ATM mutations will increase the effect.

Although next-generation sequencing (NGS) might not yet be economic for the indication of olaparib alone in mCRPC patients, a retrospective study by Slootbeek et al described the potential of NGS in mCRPC patients in our tertiary referral center (59). Some of these

patients were also included in our WGS study described in **chapter 5**. NGS results of 215 metastatic prostate cancer patients were discussed in a molecular tumor board (MTB) and almost half of the patients received a genetically matched therapy advice. Most commonly recommended therapy was a PARP inhibitor (73%), but also PDL1-inhibitors (21%) and tyrosine kinase inhibitors (19%) were advised. An objective response rate was seen in almost 40% of the patients who started a genetically matched therapy. Median overall survival from the first mCRPC therapy was remarkably higher in patients receiving genetically matched therapy than patients who didn't (47.8 versus 27 months respectively) and suggests a survival benefit for patients with access to NGS and targeted therapy clinical trials (59).

These results have led to the design of a prospective observational trial within the Radboud University Medical Center, which aims to investigate both clinical and economic impact of NGS in early mCRPC setting (NCT04746300). Preliminary results of this trial were presented at the ASCO GU in 2022 (60), showing the feasibility of NGS in early stage mCRPC in a tertiary center with 89% success rate of performing NGS. In almost 40% of these patients an actionable target was identified. Results with regard to clinical responses with and without genetically matched therapies and its economic impact are expected in 2025.

While molecular profiling is extensively investigated in finding new targets, optimal sequencing of currently registered therapies for metastatic prostate cancer might also be guided by molecular characterization.

The randomized phase 3 ProBio trial is currently ongoing and aims to investigate the clinical effectiveness of treatment based on a biomarker signature compared to standard of care in both mHSPC and mCRPC patients (61). Predefined biomarker signatures are defined as presence of or alterations in specific genes or pathways; androgen receptor (AR), DDRd, TP53 and TMPRSS2-ERG fusion. Patients included in the experimental arm with AR and TP53 wildtype will receive either abiraterone or enzalutamide, when DDRd is present carboplatin or niraparib combined with abiraterone is administered and patients with TMPRSS2-ERG fusion will receive docetaxel. Results of this trial regarding clinical response, but also cost-effectiveness are expected in 2026.

An increasingly older and more frail population of metastatic prostate cancer patients on the one hand and on the other hand increasing healthcare costs accompanied by an expected rise of cancer diagnoses in the next decade, indicates the need of a more individualized care for our patients. Besides investigating new targets, molecular profiling should also be used to predict optimal sequencing of available treatment options and to predict resistance to therapy making it more rational to waive a particular treatment. For both the well-being of the individual patient as for sustainability of our healthcare system.

FUTURE PERSPECTIVES

(Adapted from ‘Molecular biomarkers to guide precision medicine in localized prostate cancer’ by Smits et al)

Although still a bit lost in translation, unraveling and defining molecular profiles within metastatic prostate cancer is the future for providing a more individualized treatment strategy with more durable responses, better quality of life and improved cost-effectiveness.

Today, the golden standard for performing molecular diagnostics in metastatic prostate cancer is on tumor tissue. However, analyses on tumor tissue come with its limitations.

First, it is not always possible to obtain a biopsy with sufficient tumor yield to allow for molecular analyses. This is in particular difficult for bone metastases due to technical challenges, leading to an underrepresentation of a large group of metastatic prostate cancer patients in NGS studies, as described in **chapter 2** and **3**.

Secondly from a patient perspective, a biopsy can be painful and is not without risks, such as infection or bleeding. Furthermore, to be able to guide treatment strategy in a most optimal manner at every stage of disease, repeated biopsies are necessary but not patient friendly.

Lastly, as we have shown in **chapter 5**, metastatic prostate cancer is a heterogeneous disease clustering into distinct genotypes, of which half is clinically relevant and highly druggable. This suggests that it is not necessary to focus research on identification of oncogenic drivers, but signature analyses could substitute for this. However, heterogeneity is not only seen between patients but also within the individual patient with several metastases (5, 62). Heterogeneity is not only established by molecular analyses but was also seen with PSMA/PET-CT imaging (13). This heterogeneity undermines the ability of a single metastasis biopsy to correctly identify main oncogenic drivers responsible for progression of disease.

A blood-based liquid biopsy, containing diverse tumor-derived products, could be a more patient friendly technique that has the ability to reflect polyclonality within one patient as a real-time assessment of the current disease state thereby overcoming the risk of missing treatment-associated dynamics after progression.

Circulating tumor cells (CTCs), circulating cell free tumor DNA (ctDNA) and exosomes are examples of these tumor-derived products that can be detected and have been investigated in metastatic prostate cancer.

ctDNA is currently the most extensively studied marker in liquid biopsies for metastatic prostate cancer. Cell-free DNA (cfDNA) can be detected in plasma of metastatic prostate cancer patients and comprises a mixture of ctDNA and cell-free nontumor DNA, which is the product of normal white cell blood cells turnover in healthy individuals. cfDNA contains coding and noncoding DNA and is composed of short double-stranded nucleosomal size DNA fragments. The mechanisms by which cfDNA is released into the circulation may include necrosis, apoptosis, and active secretion (63). The proportion of ctDNA of total cfDNA is expressed as ctDNA%.

During the last decade ctDNA and ctDNA fraction have been investigated as prognostic and predictive biomarkers by quantitative analyses. In addition ctDNA genotyping analyzed by different methods ranging from the focus on a region of interest with a targeted panel or providing a more comprehensive insight by performing whole-genome sequencing can be used to guide targeted therapy in metastatic prostate cancer.

At this moment US FDA-approved commercial platforms for ctDNA analyses are available (e.g. FoundationOne) but highly priced and ctDNA testing is currently mainly performed in clinical trial setting, where it is used alongside tumor tissue testing (61, 64-67).

Several trials have been investigating whether available techniques in liquid biopsies provide us with comparable information as our current tools for the evaluation of response and guidance in precision medicine.

Especially in the larger group of bone-only metastatic prostate cancer patients there is a need for new biomarkers to optimize treatment strategy. Feasibility of ctDNA analysis was investigated in a retrospective analysis in which 63 mCRPC patients were included (68). Almost half of the patients had bone-only disease and at least one pathogenic alteration was detected in more than 90%.

To guide precision medicine therapy targeted sequencing or whole-exome or genome sequencing (WES/WGS) can be performed on ctDNA.

A study by Wyatt et al was able to present a 75% success rate of finding >2% ctDNA in plasma samples taken from metastatic prostate cancer patients at the time a metastatic tissue biopsy was obtained. With targeted sequencing on ctDNA and exome sequencing

of tissue all somatic mutations found in tissue were also detected in ctDNA. Furthermore, in several patients clinically relevant alterations in oncogenic pathways were revealed by ctDNA and not present in paired tissue (69).

Several studies have shown the prognostic value of ctDNA in metastatic prostate cancer with higher levels of ctDNA found in high volume metastatic prostate cancer and higher ctDNA detected in mCRPC compared to mHSPC, corresponding with a worse median overall survival (70-74). One study suggested that baseline ctDNA in mCRPC patients is an even stronger predictor for overall survival than currently standard clinical prognostic factors, e.g. PSA, ECOG and presence of visceral metastases (74).

Presence of ctDNA has also proven to be predictive for treatment of metastatic prostate cancer. Decline of ctDNA just after the initiation of both taxane-based therapy or ARSIs was correlated with better PFS compared to patients with retaining high ctDNA (74-76).

While the abundance of ctDNA at baseline predict worse response to ARSIs, the development of resistance to ARSIs can also be detected by on-treatment sampling of ctDNA. Annala et al was able to display the predictive value of baseline ctDNA fraction and in addition, showed alterations in AR during treatment with ARSIs with a 50% increase in AR amplifications when progressing on ARSIs (72).

Since the feasibility of detecting ctDNA in metastatic prostate cancer has been proven and studies have shown its prognostic and predictive value, current and future research is and will be focused on next-generation sequencing of ctDNA to guide precision medicine.

ctDNA genotyping to guide precision medicine

To determine treatment strategy for the individual metastatic prostate cancer patient, sequencing of ctDNA can establish genomic drivers which can help us to predict resistance pre- and on-treatment and furthermore guide us in finding new druggable targets.

The introduction of olaparib in BRCA1 and BRCA2 mutated patients and nivolumab in MSI high patients were first steps in the era of precision medicine for mCRPC. Nevertheless, sequencing of tumor tissue has its limitations as discussed earlier in this thesis and therefore sequencing of ctDNA in liquid biopsies would further improve our quality of care for these patients.

Within the proFOUND trial tumor tissue was prospectively sequenced and in addition plasma ctDNA samples were collected and retrospectively sequenced to evaluate the

utility of ctDNA in identifying alterations in BRCA1, BRCA2 and ATM (66). This study showed the feasibility of ctDNA sequencing with a positive percentage agreement of 81% in finding BRCA and ATM alterations, using tissue as reference. This suggests that ctDNA genotyping complements tissue testing and that it can be used to identify mCRPC patients who are suitable for receiving olaparib. Concordance of BRCA mutations between tissue and plasma was also found in an additional analysis of the phase 2 TRITON2 study, investigating rucaparib in BRCA mutated mCRPC patients (77) and this concordance was confirmed in an ever larger group of patients of 3334 within the TRITON2/3 trial (67). Furthermore, an exploratory analysis of the proFOUND trial investigated within the cohort of tissue-confirmed BRCA1, BRCA2 or ATM alterations, the concordance of ctDNA sequencing and efficacy and safety of olaparib in patients with BRCA/ATM alterations identified by ctDNA NGS testing (78). Outcomes to olaparib in patients identified by ctDNA were comparable to the complete cohort of tissue confirmed BRCA/ATM alterations and supports the utility of ctDNA sequencing to identify patients with druggable targets, especially when tissue yield is insufficient for NGS.

The additional value of ctDNA sequencing was also shown by an exploratory analysis of the phase 2 trial investigating abiraterone with or without olaparib independent of homologous recombination repair (HRR) deficiency (79). Although results might be slightly biased due to no mandatory tissue collection in this trial, the addition of ctDNA sequencing led to an increase of assessing HRR status from 30% to 68% with an almost three-fold increase in identified HRR deficiencies.

Less studies have performed ctDNA sequencing for MSI in metastatic prostate cancer, but some studies suggest its feasibility and concordance with tissue testing (67, 80). Two case reports presented in both patients a reduction in somatic variant allele frequency at the time of response to pembrolizumab, suggesting that on-treatment liquid biopsies in these patients could detect response and progression when treated with PDL1-inhibitors (81).

At this moment, the main challenges of these analyses are on one hand the risk of missing druggable targets by targeted sequencing and on the other hand not being able to perform extensive sequencing due to low levels of ctDNA, which decreases sensitivity of detecting copy number alterations (CNA) and structural rearrangements (67, 71, 79, 82). Low-pass WGS (LPWGS) of ctDNA might be a cost-effective alternative to estimate ctDNA% and CNA. The utility of LPWGS was recently investigated in first-line mCRPC patients starting on ARSI's (83). At baseline both ctDNA% and high CNA burden (compared to low CNA burden) identified by LPWGS were both predictive and prognostic and the identified genotypes were comparable with the previously described studies of ctDNA in mCRPC patients. These results were confirmed by analysis in a validation cohort

(83). The predictive and prognostic value of LPWGS of ctDNA in metastatic prostate cancer was also found by Sumanasuriya et al who prospectively collected ctDNA at baseline and on treatment from patients included in two phase 3 prospective clinical trials receiving chemotherapy (73).

Today, tumor tissue is used for the development of prognostic and predictive biomarkers and finding new druggable targets in metastatic prostate cancer. Nevertheless, due to several limitations of testing on tissue, there is a need for new techniques and analysis of cfDNA in liquid promising is very promising in metastatic prostate cancer. Several studies have shown its feasibility and both qualitative and quantitative analyses of ctDNA could guide us to optimize treatment strategy for the individual patient. LPWGS could be a more cost-effective analysis of ctDNA and should therefore be included in future prospective clinical trials for further validation.

T cell repertoire sequencing as a new emerging biomarker in metastatic prostate cancer

The T-cell antigen receptor (TCR) is a complex found on the surface of T cells and is involved in the activation of specific T cells when they are presented to an antigen-derived peptide, bound to major histocompatibility (MHC) complexes on antigen-presenting cells (APCs), including macrophages, dendritic cells and B cells. If an antigen is engaged to the TCR complex, specific T cells get activated, proliferate and expand to a population of T cell clones with the same TCR sequences to induce an immune response. To acquire an effective specific immune response an enormously diverse repertoire of TCRs is necessary (84).

In cancer, cancer cell derived peptides, e.g. neo-antigens, can bind to MHC class I and this cancer specific peptide-MHC complex can activate a specific T cell response. However, this response rarely leads to a successful protection against cancer cell growth. This is partially due to the presence of negative regulators in TCR signaling, such as PDL1/PD1 and CTLA4, as previously described in the Cancer-Immunity cycle by Chen and Mellman (85). To overcome these negative regulators (checkpoints) to T cell response several therapies have been developed to target these inhibitory molecules, for example pembrolizumab (PD1 inhibitor), ipilimumab (CTLA4 inhibitor) and atezolizumab (PDL1 inhibitor).

While these immune checkpoint inhibitors (ICIs) provide high response rates with durable responses in melanoma (86), urothelial cancer (87) and lung cancer (88), only a subset of mCRPC respond to ICIs (89). MSI and MMR deficiency are known predictive biomarkers for response to ICIs (90-92) but response is not exclusively related to MSI or MMR

deficiency (89). Furthermore, the presence of PDL1 expression in mCRPC is, in contrast to other malignancies, not predictive for response as shown in the KEYNOTE-199 trial (89). However, the same clinical trial presented a subset of mCRPC responding to PD1 inhibitors despite the presence of currently known biomarkers, suggesting the need for further biomarker studies to identify other predictive biomarkers for ICI in mCRPC. In **chapter 6** of this thesis, we aimed to find immunologic signatures by next-generation sequencing of the TCR repertoire detected in liquid biopsies of our MSI cohort treated with PD1/PDL1 inhibitors and hereby identifying a possible new predictive biomarker for ICI in mCRPC. Our study showed the feasibility of TCR repertoire sequencing in peripheral blood with consistent clonal overlaps between patient-matched peripheral and intratumorally T-cell repertoires. Furthermore, a significantly higher T cell repertoire richness and diversity was seen in MSI patients and a positive trend for diversity was discovered in responding MSS patients. Lastly, T cell clusters with low generation probability were seen in our MSI cohort and MSS patients with this specific cluster signature had a significantly longer time to progression during treatment with ICI compared to non-responding MSS patients. These findings suggest the utility of TCR repertoire sequencing as a new predictive biomarker for response to ICI and could expand the group of patients who could benefit from ICI.

As earlier mentioned in this thesis, DDR deficient mCRPC patients seem to have a higher response rate to ICI compared to DDR proficient patients. To gain further insight in the immunogenicity of DDR deficient mCRPC patients, van Wilpe et al performed next-generation sequencing of T cell repertoire in peripheral blood in both DDR deficient and DDR proficient mCRPC patient and found a significantly higher T cell repertoire diversity in DDR deficient patients, as was also seen in our MSI cohort, strengthening the evidence for T cell repertoire sequencing in peripheral blood as a new predictive biomarker for response to ICI (93).

Interestingly, the utility of T cell repertoire sequencing as a predictive biomarker was also investigated for PARP inhibitors in ovarian cancer (94). Patients with maintenance PARP inhibitors had a significantly longer PFS if T cell repertoire diversity was rising after three months of treatment. This increased diversity was also in multivariate analysis associated with better response, even independent of BRCA1/2 mutation status and suggests that T cell repertoire diversity might also be a predictive biomarker for response to PARP inhibitors. Since PARP inhibitors are currently registered for only BRCA1/2 mutated mCRPC patients and clinical trials suggest that a subset of DDR proficient mCRPC patients also benefit from PARP inhibitors as described earlier in this thesis, it would be interesting to investigate whether TCR sequencing could guide us to, first, identify BRCA proficient

patients that would also benefit from PARP inhibition and secondly, predict response to PARP inhibitors while on treatment to prevent unnecessary toxicity and costs.

To summarize, unraveling the genomic landscape of metastatic prostate cancer will further help us to individualize treatment with better clinical outcome and less toxicity in a mainly older and fragile population of patients. Currently molecular testing on tumor tissue is the golden standard but has its limitations. Therefore techniques in liquid biopsies are developed and circulating tumor DNA is today the most extensively studied marker in metastatic prostate cancer. Studies have already shown the feasibility of detecting circulating tumor DNA and sequencing results are concordant with tissue testing. Furthermore, quantitative measurements of circulating tumor DNA have proven to be both prognostic and predictive and should be integrated in daily clinical practice.

T cell repertoire sequencing is a new emerging biomarker and seems to be predictive for response to immune checkpoint inhibitors. Our research in this thesis shows already promising results and further exploration of this biomarker is necessary to prove its utility and to expand the group of metastatic prostate cancer patients who could benefit from immune checkpoint inhibitors with often durable responses.

REFERENCES

1. Cancer Genome Atlas Research N. The Molecular Taxonomy of Primary Prostate Cancer. *Cell*. 2015;163(4):1011-25.
2. Taylor BS, Schultz N, Hieronymus H, Gopalan A, Xiao Y, Carver BS, et al. Integrative genomic profiling of human prostate cancer. *Cancer Cell*. 2010;18(1):11-22.
3. Robinson D, Van Allen EM, Wu YM, Schultz N, Lonigro RJ, Mosquera JM, et al. Integrative clinical genomics of advanced prostate cancer. *Cell*. 2015;161(5):1215-28.
4. Viswanathan SR, Ha G, Hoff AM, Wala JA, Carrot-Zhang J, Whelan CW, et al. Structural Alterations Driving Castration-Resistant Prostate Cancer Revealed by Linked-Read Genome Sequencing. *Cell*. 2018;174(2):433-47 e19.
5. Gundem G, Van Loo P, Kremeyer B, Alexandrov LB, Tubio JMC, Papaemmanuil E, et al. The evolutionary history of lethal metastatic prostate cancer. *Nature*. 2015;520(7547):353-7.
6. Quigley DA, Dang HX, Zhao SG, Lloyd P, Aggarwal R, Alumkal JJ, et al. Genomic Hallmarks and Structural Variation in Metastatic Prostate Cancer. *Cell*. 2018;174(3):758-69 e9.
7. de Bono J, Mateo J, Fizazi K, Saad F, Shore N, Sandhu S, et al. Olaparib for Metastatic Castration-Resistant Prostate Cancer. *N Engl J Med*. 2020;382(22):2091-102.
8. Coleman RE. Clinical features of metastatic bone disease and risk of skeletal morbidity. *Clin Cancer Res*. 2006;12(20 Pt 2):6243s-9s.
9. Holmes MG, Foss E, Joseph G, Foye A, Beckett B, Motamedi D, et al. CT-Guided Bone Biopsies in Metastatic Castration-Resistant Prostate Cancer: Factors Predictive of Maximum Tumor Yield. *J Vasc Interv Radiol*. 2017;28(8):1073-81 e1.
10. Lorente D, Omlin A, Zafeiriou Z, Nava-Rodrigues D, Perez-Lopez R, Pezaro C, et al. Castration-Resistant Prostate Cancer Tissue Acquisition From Bone Metastases for Molecular Analyses. *Clin Genitourin Cancer*. 2016;14(6):485-93.
11. Donners R, Fotiadis N, Figueiredo I, Blackledge M, Westaby D, Guo C, et al. Optimising CT-guided biopsies of sclerotic bone lesions in cancer patients. *Eur Radiol*. 2022;32(10):6820-9.
12. Sweat SD, Pacelli A, Murphy GP, Bostwick DG. Prostate-specific membrane antigen expression is greatest in prostate adenocarcinoma and lymph node metastases. *Urology*. 1998;52(4):637-40.
13. Paschalis A, Sheehan B, Riisnaes R, Rodrigues DN, Gurel B, Bertan C, et al. Prostate-specific Membrane Antigen Heterogeneity and DNA Repair Defects in Prostate Cancer. *Eur Urol*. 2019;76(4):469-78.
14. Hofman MS, Lawrentschuk N, Francis RJ, Tang C, Vela I, Thomas P, et al. Prostate-specific membrane antigen PET-CT in patients with high-risk prostate cancer before curative-intent surgery or radiotherapy (proPSMA): a prospective, randomised, multicentre study. *Lancet*. 2020;395(10231):1208-16.
15. Mottet N. EAU-EANM-ESTRO-ESUR-ISUP-SIOG Guidelines on prostate cancer. European Association of Urology. 2022.
16. Caroli P, Sandler I, Matteucci F, De Giorgi U, Uccelli L, Celli M, et al. (68)Ga-PSMA PET/CT in patients with recurrent prostate cancer after radical treatment: prospective results in 314 patients. *Eur J Nucl Med Mol Imaging*. 2018;45(12):2035-44.

17. Zacho HD, Nielsen JB, Dettmann K, Haberkorn U, Langkilde NC, Jensen JB, et al. 68Ga-PSMA PET/CT in Patients With Biochemical Recurrence of Prostate Cancer: A Prospective, 2-Center Study. *Clin Nucl Med*. 2018;43(8):579-85.
18. Sartor O, de Bono J, Chi KN, Fizazi K, Herrmann K, Rahbar K, et al. Lutetium-177-PSMA-617 for Metastatic Castration-Resistant Prostate Cancer. *N Engl J Med*. 2021;385(12):1091-103.
19. Mansour TMM, El-Barody MM, Tammam H, Okasha A. Role of diffusion-weighted MRI in differentiating between benign and malignant bone lesions: a prospective study. *Clin Radiol*. 2021;76(8):576-84.
20. Jacobs MA, Macura KJ, Zaheer A, Antonarakis ES, Stearns V, Wolff AC, et al. Multiparametric Whole-body MRI with Diffusion-weighted Imaging and ADC Mapping for the Identification of Visceral and Osseous Metastases From Solid Tumors. *Acad Radiol*. 2018;25(11):1405-14.
21. Perez-Lopez R, Nava Rodrigues D, Figueiredo I, Mateo J, Collins DJ, Koh DM, et al. Multiparametric Magnetic Resonance Imaging of Prostate Cancer Bone Disease: Correlation With Bone Biopsy Histological and Molecular Features. *Invest Radiol*. 2018;53(2):96-102.
22. Donners R, Figueiredo I, Tunariu N, Blackledge M, Koh DM, de la Maza M, et al. Multiparametric bone MRI can improve CT-guided bone biopsy target selection in cancer patients and increase diagnostic yield and feasibility of next-generation tumour sequencing. *Eur Radiol*. 2022;32(7):4647-56.
23. Clarke N, Wiechno P, Alekseev B, Sala N, Jones R, Kocak I, et al. Olaparib combined with abiraterone in patients with metastatic castration-resistant prostate cancer: a randomised, double-blind, placebo-controlled, phase 2 trial. *Lancet Oncol*. 2018;19(7):975-86.
24. J. Praagman ES, L. van Disseldorp, V. Lemmens. Kanker in Nederland; trends en prognoses tot en met 2032. IKNL. 2022.
25. Tannock IF, de Wit R, Berry WR, Horti J, Pluzanska A, Chi KN, et al. Docetaxel plus prednisone or mitoxantrone plus prednisone for advanced prostate cancer. *N Engl J Med*. 2004;351(15):1502-12.
26. Petrylak DP, Tangen CM, Hussain MH, Lara PN, Jr., Jones JA, Taplin ME, et al. Docetaxel and estramustine compared with mitoxantrone and prednisone for advanced refractory prostate cancer. *N Engl J Med*. 2004;351(15):1513-20.
27. Westgeest HM, Uyl-de Groot CA, van Moorselaar RJA, de Wit R, van den Bergh ACM, Coenen J, et al. Differences in Trial and Real-world Populations in the Dutch Castration-resistant Prostate Cancer Registry. *Eur Urol Focus*. 2018;4(5):694-701.
28. Bandini M, Pompe RS, Marchioni M, Zaffuto E, Gandaglia G, Fossati N, et al. Improved cancer-specific free survival and overall free survival in contemporary metastatic prostate cancer patients: a population-based study. *Int Urol Nephrol*. 2018;50(1):71-8.
29. Berry W, Dakhil S, Modiano M, Gregurich M, Asmar L. Phase III study of mitoxantrone plus low dose prednisone versus low dose prednisone alone in patients with asymptomatic hormone refractory prostate cancer. *J Urol*. 2002;168(6):2439-43.
30. de Bono JS, Oudard S, Ozguroglu M, Hansen S, Machiels JP, Kocak I, et al. Prednisone plus cabazitaxel or mitoxantrone for metastatic castration-resistant prostate cancer progressing after docetaxel treatment: a randomised open-label trial. *Lancet*. 2010;376(9747):1147-54.

31. Westgeest HM, Kuppen MCP, van den Eertwegh AJM, de Wit R, Coenen J, van den Berg HPP, et al. Second-Line Cabazitaxel Treatment in Castration-Resistant Prostate Cancer Clinical Trials Compared to Standard of Care in CAPRI: Observational Study in the Netherlands. *Clin Genitourin Cancer*. 2019;17(5):e946-e56.
32. de Wit R, de Bono J, Sternberg CN, Fizazi K, Tombal B, Wulfing C, et al. Cabazitaxel versus Abiraterone or Enzalutamide in Metastatic Prostate Cancer. *N Engl J Med*. 2019;381(26):2506-18.
33. Zhang PF, Xie D, Li Q. Cost-effectiveness analysis of cabazitaxel for metastatic castration resistant prostate cancer after docetaxel and androgen-signaling-targeted inhibitor resistance. *BMC Cancer*. 2021;21(1):35.
34. Sweeney CJ, Chen YH, Carducci M, Liu G, Jarrard DF, Eisenberger M, et al. Chemohormonal Therapy in Metastatic Hormone-Sensitive Prostate Cancer. *N Engl J Med*. 2015;373(8):737-46.
35. James ND, Clarke NW, Cook A, Ali A, Hoyle AP, Attard G, et al. Abiraterone acetate plus prednisolone for metastatic patients starting hormone therapy: 5-year follow-up results from the STAMPEDE randomised trial (NCT00268476). *Int J Cancer*. 2022;151(3):422-34.
36. Davis ID. Updated overall survival outcomes in ENZAMET (ANZUP 1304), an international, cooperative group trial of enzalutamide in metastatic hormone-sensitive prostate cancer (mHSPC). *Journal of Clinical Oncology*. 2022;40.
37. Fizazi K, Tran N, Fein L, Matsubara N, Rodriguez-Antolin A, Alekseev BY, et al. Abiraterone plus Prednisone in Metastatic, Castration-Sensitive Prostate Cancer. *N Engl J Med*. 2017;377(4):352-60.
38. Armstrong AJ, Szmulewitz RZ, Petrylak DP, Holzbeierlein J, Villers A, Azad A, et al. ARCHES: A Randomized, Phase III Study of Androgen Deprivation Therapy With Enzalutamide or Placebo in Men With Metastatic Hormone-Sensitive Prostate Cancer. *J Clin Oncol*. 2019;37(32):2974-86.
39. Chi KN, Agarwal N, Bjartell A, Chung BH, Pereira de Santana Gomes AJ, Given R, et al. Apalutamide for Metastatic, Castration-Sensitive Prostate Cancer. *N Engl J Med*. 2019;381(1):13-24.
40. Pelloux-Prayer R, Schiele P, Oudard S, Gravis G, Kleinclauss F, Crehange G, et al. Cost-effectiveness Analysis of Innovative Therapy for Patients with Newly Diagnosed Hormone-Sensitive Metastatic Prostate Cancer. *Clin Genitourin Cancer*. 2021;19(5):e326-e33.
41. Barbier MC, Tomonaga Y, Menges D, Yebyo HG, Haile SR, Puhan MA, et al. Survival modelling and cost-effectiveness analysis of treatments for newly diagnosed metastatic hormone-sensitive prostate cancer. *PLoS One*. 2022;17(11):e0277282.
42. Sung WWY, Choi HCW, Luk PHY, So TH. A Cost-Effectiveness Analysis of Systemic Therapy for Metastatic Hormone-Sensitive Prostate Cancer. *Front Oncol*. 2021;11:627083.
43. Wang L, Hong H, Alexander GC, Brawley OW, Paller CJ, Ballreich J. Cost-Effectiveness of Systemic Treatments for Metastatic Castration-Sensitive Prostate Cancer: An Economic Evaluation Based on Network Meta-Analysis. *Value Health*. 2022;25(5):796-802.
44. Scher HI, Lu D, Schreiber NA, Louw J, Graf RP, Vargas HA, et al. Association of AR-V7 on Circulating Tumor Cells as a Treatment-Specific Biomarker With Outcomes and Survival in Castration-Resistant Prostate Cancer. *JAMA Oncol*. 2016;2(11):1441-9.
45. Antonarakis ES, Lu C, Luber B, Wang H, Chen Y, Nakazawa M, et al. Androgen Receptor Splice Variant 7 and Efficacy of Taxane Chemotherapy in Patients With Metastatic Castration-Resistant Prostate Cancer. *JAMA Oncol*. 2015;1(5):582-91.

46. Fizazi K, Foulon S, Carles J, Roubaud G, McDermott R, Flechon A, et al. Abiraterone plus prednisone added to androgen deprivation therapy and docetaxel in de novo metastatic castration-sensitive prostate cancer (PEACE-1): a multicentre, open-label, randomised, phase 3 study with a 2 x 2 factorial design. *Lancet*. 2022;399(10336):1695-707.
47. Smith MR, Hussain M, Saad F, Fizazi K, Sternberg CN, Crawford ED, et al. Darolutamide and Survival in Metastatic, Hormone-Sensitive Prostate Cancer. *N Engl J Med*. 2022;386(12):1132-42.
48. Marabelle A, Fakih M, Lopez J, Shah M, Shapira-Frommer R, Nakagawa K, et al. Association of tumour mutational burden with outcomes in patients with advanced solid tumours treated with pembrolizumab: prospective biomarker analysis of the multicohort, open-label, phase 2 KEYNOTE-158 study. *Lancet Oncol*. 2020;21(10):1353-65.
49. Cristescu R, Aurora-Garg D, Albright A, Xu L, Liu XQ, Loboda A, et al. Tumor mutational burden predicts the efficacy of pembrolizumab monotherapy: a pan-tumor retrospective analysis of participants with advanced solid tumors. *J Immunother Cancer*. 2022;10(1).
50. Graf RP, Fisher V, Weberpals J, Gjoerup O, Tierno MB, Huang RSP, et al. Comparative Effectiveness of Immune Checkpoint Inhibitors vs Chemotherapy by Tumor Mutational Burden in Metastatic Castration-Resistant Prostate Cancer. *JAMA Netw Open*. 2022;5(3):e225394.
51. McGrail DJ, Pilie PG, Rashid NU, Voorwerk L, Slagter M, Kok M, et al. High tumor mutation burden fails to predict immune checkpoint blockade response across all cancer types. *Ann Oncol*. 2021;32(5):661-72.
52. Schmid S, Omlin A, Higano C, Sweeney C, Martinez Chanza N, Mehra N, et al. Activity of Platinum-Based Chemotherapy in Patients With Advanced Prostate Cancer With and Without DNA Repair Gene Aberrations. *JAMA Netw Open*. 2020;3(10):e2021692.
53. Slootbeek PHJ, Duizer ML, van der Doelen MJ, Kloots ISH, Kuppen MCP, Westgeest HM, et al. Impact of DNA damage repair defects and aggressive variant features on response to carboplatin-based chemotherapy in metastatic castration-resistant prostate cancer. *Int J Cancer*. 2021;148(2):385-95.
54. Mota JM, Barnett E, Nauseef JT, Nguyen B, Stopsack KH, Wibmer A, et al. Platinum-Based Chemotherapy in Metastatic Prostate Cancer With DNA Repair Gene Alterations. *JCO Precis Oncol*. 2020;4:355-66.
55. Cheng HH, Pritchard CC, Boyd T, Nelson PS, Montgomery B. Biallelic Inactivation of BRCA2 in Platinum-sensitive Metastatic Castration-resistant Prostate Cancer. *Eur Urol*. 2016;69(6):992-5.
56. Pomerantz MM, Spisak S, Jia L, Cronin AM, Csabai I, Ledet E, et al. The association between germline BRCA2 variants and sensitivity to platinum-based chemotherapy among men with metastatic prostate cancer. *Cancer*. 2017;123(18):3532-9.
57. Su D, Wu B, Shi L. Cost-Effectiveness of Genomic Test-Directed Olaparib for Metastatic Castration-Resistant Prostate Cancer. *Front Pharmacol*. 2020;11:610601.
58. Li Y, Lin S, Zhong L, Luo S, Huang X, Huang X, et al. Is olaparib cost effective in metastatic castration-resistant prostate cancer patients with at least one favorable gene mutation in BRCA1, BRCA2 or ATM? *Pharmacogenomics*. 2021;22(13):809-19.

59. Slootbeek PHJ, Kloots ISH, Smits M, van Oort IM, Gerritsen WR, Schalken JA, et al. Impact of molecular tumour board discussion on targeted therapy allocation in advanced prostate cancer. *Br J Cancer*. 2022;126(6):907-16.
60. I.S.H. Kloots PHJS, M. Smits, S. van Helvert, L. Kroeze, M. Kets, K. Grünberg, J. van Ipenburg, M. Ligtenberg, J.A. Schalken, I.M. van Oort, H. Bloemendal, W.R. Gerritsen, N. Mehra. First results of the PROMPT trial: Precision oncology allocation in patients with early castration-resistant prostate cancer following routine molecular profiling. *Journal of Clinical Oncology*. 2022.
61. Crippa A, De Laere B, Discacciati A, Larsson B, Connor JT, Gabriel EE, et al. The ProBio trial: molecular biomarkers for advancing personalized treatment decision in patients with metastatic castration-resistant prostate cancer. *Trials*. 2020;21(1):579.
62. Haffner MC, Mosbrugger T, Esopi DM, Fedor H, Heaphy CM, Walker DA, et al. Tracking the clonal origin of lethal prostate cancer. *J Clin Invest*. 2013;123(11):4918-22.
63. Stroun M, Lyautey J, Lederrey C, Olson-Sand A, Anker P. About the possible origin and mechanism of circulating DNA apoptosis and active DNA release. *Clin Chim Acta*. 2001;313(1-2):139-42.
64. Clarke N. Abiraterone and Olaparib for Metastatic Castration-Resistant Prostate Cancer. *New England Journal of Medicine Evidence*. 2022.
65. Chi K. Phase 3 MAGNITUDE study: First results of niraparib (NIRA) with abiraterone acetate and prednisone (AAP) as first-line therapy in patients (pts) with metastatic castration-resistant prostate cancer (mCRPC) with and without homologous recombination repair (HRR) gene alterations. *Journal of Clinical Oncology*. 2022.
66. Chi KN, Barnicle A, Sibilla C, Lai Z, Corcoran C, Barrett JC, et al. Detection of BRCA1, BRCA2, and ATM Alterations in Matched Tumor Tissue and Circulating Tumor DNA in Patients with Prostate Cancer Screened in PROfound. *Clin Cancer Res*. 2023;29(1):81-91.
67. Tukachinsky H, Madison RW, Chung JH, Gjoerup OV, Severson EA, Dennis L, et al. Genomic Analysis of Circulating Tumor DNA in 3,334 Patients with Advanced Prostate Cancer Identifies Targetable BRCA Alterations and AR Resistance Mechanisms. *Clin Cancer Res*. 2021;27(11):3094-105.
68. Shaya J, Nonato T, Cabal A, Randall JM, Millard F, Stewart T, et al. Analysis of the Prognostic Significance of Circulating Tumor DNA in Metastatic Castrate Resistant Prostate Cancer. *Clin Genitourin Cancer*. 2021;19(6):564 e1- e10.
69. Wyatt AW, Annala M, Aggarwal R, Beja K, Feng F, Youngren J, et al. Concordance of Circulating Tumor DNA and Matched Metastatic Tissue Biopsy in Prostate Cancer. *J Natl Cancer Inst*. 2017;109(12).
70. Reichert ZR, Morgan TM, Li G, Castellanos E, Snow T, Dall'Olio FG, et al. Prognostic value of plasma circulating tumor DNA fraction across four common cancer types: a real-world outcomes study. *Ann Oncol*. 2023;34(1):111-20.
71. Kohli M, Tan W, Zheng T, Wang A, Montesinos C, Wong C, et al. Clinical and genomic insights into circulating tumor DNA-based alterations across the spectrum of metastatic hormone-sensitive and castrate-resistant prostate cancer. *EBioMedicine*. 2020;54:102728.
72. Annala M, Taavitsainen S, Khalaf DJ, Vandekerkhove G, Beja K, Sipola J, et al. Evolution of Castration-Resistant Prostate Cancer in ctDNA during Sequential Androgen Receptor Pathway Inhibition. *Clin Cancer Res*. 2021;27(16):4610-23.

73. Sumanasuriya S, Seed G, Parr H, Christova R, Pope L, Bertan C, et al. Elucidating Prostate Cancer Behaviour During Treatment via Low-pass Whole-genome Sequencing of Circulating Tumour DNA. *Eur Urol.* 2021;80(2):243-53.
74. Annala M, Fu S, Bacon JVW, Sipola J, Iqbal N, Ferrario C, et al. Cabazitaxel versus abiraterone or enzalutamide in poor prognosis metastatic castration-resistant prostate cancer: a multi-centre, randomised, open-label, phase II trial. *Ann Oncol.* 2021;32(7):896-905.
75. Jayaram A, Wingate A, Wetterskog D, Wheeler G, Sternberg CN, Jones R, et al. Plasma tumor gene conversions after one cycle abiraterone acetate for metastatic castration-resistant prostate cancer: a biomarker analysis of a multicenter international trial. *Ann Oncol.* 2021;32(6):726-35.
76. S.H. Tolmeijer EB, T. Sumiyoshi, S. Ng, E.M. Kwan et al. On-treatment plasma ctDNA fraction and treatment outcomes in metastatic castration-resistant prostate cancer. *Journal of Clinical Oncology.* 2022.
77. Loehr A, Patnaik A, Campbell D, Shapiro J, Bryce AH, McDermott R, et al. Response to Rucaparib in BRCA-Mutant Metastatic Castration-Resistant Prostate Cancer Identified by Genomic Testing in the TRITON2 Study. *Clin Cancer Res.* 2021;27(24):6677-86.
78. Matsubara N, de Bono J, Olmos D, Procopio G, Kawakami S, Urun Y, et al. Olaparib Efficacy in Patients with Metastatic Castration-resistant Prostate Cancer and BRCA1, BRCA2, or ATM Alterations Identified by Testing Circulating Tumor DNA. *Clin Cancer Res.* 2023;29(1):92-9.
79. Carr TH, Adelman C, Barnicle A, Kozarewa I, Luke S, Lai Z, et al. Homologous Recombination Repair Gene Mutation Characterization by Liquid Biopsy: A Phase II Trial of Olaparib and Abiraterone in Metastatic Castrate-Resistant Prostate Cancer. *Cancers (Basel).* 2021;13(22).
80. Mayrhofer M, De Laere B, Whittington T, Van Oyen P, Ghysel C, Ampe J, et al. Cell-free DNA profiling of metastatic prostate cancer reveals microsatellite instability, structural rearrangements and clonal hematopoiesis. *Genome Med.* 2018;10(1):85.
81. Ravindranathan D, Russler GA, Yantorni L, Drusbosky LM, Bilen MA. Detection of Microsatellite Instability via Circulating Tumor DNA and Response to Immunotherapy in Metastatic Castration-Resistant Prostate Cancer: A Case Series. *Case Rep Oncol.* 2021;14(1):190-6.
82. Annala M, Vandekerckhove G, Khalaf D, Taavitsainen S, Beja K, Warner EW, et al. Circulating Tumor DNA Genomics Correlate with Resistance to Abiraterone and Enzalutamide in Prostate Cancer. *Cancer Discov.* 2018;8(4):444-57.
83. Norgaard M, Bjerre MT, Fredsoe J, Vang S, Jensen JB, De Laere B, et al. Prognostic Value of Low-Pass Whole Genome Sequencing of Circulating Tumor DNA in Metastatic Castration-Resistant Prostate Cancer. *Clin Chem.* 2023.
84. Shah K, Al-Haidari A, Sun J, Kazi JU. T cell receptor (TCR) signaling in health and disease. *Signal Transduct Target Ther.* 2021;6(1):412.
85. Chen DS, Mellman I. Oncology meets immunology: the cancer-immunity cycle. *Immunity.* 2013;39(1):1-10.
86. Hodi FS, O'Day SJ, McDermott DF, Weber RW, Sosman JA, Haanen JB, et al. Improved survival with ipilimumab in patients with metastatic melanoma. *N Engl J Med.* 2010;363(8):711-23.
87. Bellmunt J, Bajorin DF. Pembrolizumab for Advanced Urothelial Carcinoma. *N Engl J Med.* 2017;376(23):2304.

88. Herbst RS, Baas P, Kim DW, Felip E, Perez-Gracia JL, Han JY, et al. Pembrolizumab versus docetaxel for previously treated, PD-L1-positive, advanced non-small-cell lung cancer (KEYNOTE-010): a randomised controlled trial. *Lancet*. 2016;387(10027):1540-50.
89. Antonarakis ES, Piulats JM, Gross-Goupil M, Goh J, Ojamaa K, Hoimes CJ, et al. Pembrolizumab for Treatment-Refractory Metastatic Castration-Resistant Prostate Cancer: Multicohort, Open-Label Phase II KEYNOTE-199 Study. *J Clin Oncol*. 2020;38(5):395-405.
90. Abida W, Cheng ML, Armenia J, Middha S, Autio KA, Vargas HA, et al. Analysis of the Prevalence of Microsatellite Instability in Prostate Cancer and Response to Immune Checkpoint Blockade. *JAMA Oncol*. 2019;5(4):471-8.
91. Graham LS, Montgomery B, Cheng HH, Yu EY, Nelson PS, Pritchard C, et al. Mismatch repair deficiency in metastatic prostate cancer: Response to PD-1 blockade and standard therapies. *PLoS One*. 2020;15(5):e0233260.
92. van der Velden DL, Hoes LR, van der Wijngaart H, van Berge Henegouwen JM, van Werkhoven E, Roepman P, et al. The Drug Rediscovery protocol facilitates the expanded use of existing anticancer drugs. *Nature*. 2019;574(7776):127-31.
93. van Wilpe S, Simnica D, Sloombeek P, van Ee T, Pamidimarri Naga S, Gorris MAJ, et al. Homologous recombination repair deficient prostate cancer represents an immunologically distinct subtype. *Oncoimmunology*. 2022;11(1):2094133.
94. Shu T, Zhou Z, Bai J, Xiao X, Gao M, Zhang N, et al. Circulating T-cell receptor diversity as predictive biomarker for PARP inhibitors maintenance therapy in high grade serous ovarian cancer. *Gynecol Oncol*. 2023;168:135-43.



PART V

APPENDICES

LIST OF ABBREVIATIONS

LIST OF PUBLICATIONS

RESEARCH DATA MANAGEMENT

PHD PORTFOLIO

CURRICULUM VITAE

NEDERLANDSE SAMENVATTING

DANKWOORD

LIST OF ABBREVIATIONS

mCRPC	metastatic castration resistant prostate cancer	EMA	European Medicine Agency
mHSPC	metastatic hormone sensitive prostate cancer	FDA	Food and Drug Administration
PSA	prostate specific antigen	LDH	lactate dehydrogenase
NGS	next-generation sequencing	AF	alkaline phosphatase
WGS	whole-genome sequencing	HU	Hounsfield unit
LH	luteinizing hormone	SUV	standard uptake value
LHRH	luteinizing releasing hormone	NGI	next-generation imaging
ADT	androgen deprivation therapy	LPWGS	low-pass WGS
AR	androgen receptor	CTC	circulating tumor cell
ARSI	androgen receptor signaling inhibitor	ctDNA	circulating cell-free tumor DNA
PFS	progression-free survival	cfDNA	circulating cell-free DNA
OS	overall survival	TCR	T-cell antigen receptor
rPFS	radiographic progression-free survival	CBCT	cone-beam CT
HR	homologous repair	PCa	prostate cancer
HRR	homologous recombination repair	PARP	poly(ADP-ribose) polymerase
HRD	homologous recombination deficiencies	CNA	copy number alteration
DDR	DNA damage repair	ICB	immune checkpoint blockade
MSI	microsatellite instability	PDL1	programmed cell death ligand 1
MSS	microsatellite stability	IHC	immunohistochemistry
MMR	mismatch repair	ROI	region of interest
TMB	tumor mutational burden	Dev	deviation
MTB	molecular tumor board		
PSMA	prostate-specific membrane antigen		
PET	positron-emission tomography		
CT	computed tomography		
MRI	magnetic resonance imaging		
DWI	diffusion-weighted		
DR	diffusion restriction		
ADC	apparent diffusion coefficient		
ICI	immune checkpoint inhibitor		

LIST OF PUBLICATIONS

de Jong AC*, **Smits M***, van Riet J, Futterer JJ, Brabander T, Hamberg P, et al. (68) Ga-PSMA-Guided Bone Biopsies for Molecular Diagnostics in Patients with Metastatic Prostate Cancer. *J Nucl Med.* 2020;61(11):1607-14.

Smits M*, Ekici K*, Pamidimarri Naga S, van Oort IM, Sedelaar MJP, Schalken JA, et al. Prior PSMA PET-CT Imaging and Hounsfield Unit Impact on Tumor Yield and Success of Molecular Analyses from Bone Biopsies in Metastatic Prostate Cancer. *Cancers (Basel).* 2020;12(12).

van Steenberg TRF*, **Smits M***, Scheenen TWJ, van Oort IM, Nagarajah J, Rovers MM, et al. (68)Ga-PSMA-PET/CT and Diffusion MRI Targeting for Cone-Beam CT-Guided Bone Biopsies of Castration-Resistant Prostate Cancer Patients. *Cardiovasc Intervent Radiol.* 2020;43(1):147-54.

van Dessel LF*, van Riet J*, **Smits M**, Zhu Y, Hamberg P, van der Heijden MS, et al. The genomic landscape of metastatic castration-resistant prostate cancers reveals multiple distinct genotypes with potential clinical impact. *Nat Commun.* 2019;10(1):5251.

Simnica D*, **Smits M***, Willscher E, Fanchi LF, Kloots ISH, van Oort I, et al. Responsiveness to Immune Checkpoint Inhibitors Is Associated With a Peripheral Blood T-Cell Signature in Metastatic

Castration-Resistant Prostate Cancer. *JCO Precis Oncol.* 2020;4:1374-85

Slootbeek PHJ, Kloots ISH, **Smits M**, van Oort IM, Gerritsen WR, Schalken JA, et al. Impact of molecular tumour board discussion on targeted therapy allocation in advanced prostate cancer. *Br J Cancer.* 2022;126(6):907-16.

Rivello F*, Matula K*, Piruska A, **Smits M**, Mehra N, Huck WTS. Probing single-cell metabolism reveals prognostic value of highly metabolically active circulating stromal cells in prostate cancer. *Sci Adv.* 2020;6(40).

Smits M, Mehra N, Sedelaar M, Gerritsen W, Schalken JA. Molecular biomarkers to guide precision medicine in localized prostate cancer. *Expert Rev Mol Diagn.* 2017;17(8):791-804.

Smits M, Gerritsen W, Mehra N. Future therapeutic strategies for metastatic prostate cancer. *Tijdschrift voor Urologie.* 2019;9(6):117-30.

Merit Award recipient for a poster at the ASCO GU February 2018; Immunological and genomic correlates of response to anti-PD1 checkpoint therapy in mismatch proficient and deficient patients with metastatic CRPC

*both authors contributed equally

RESEARCH DATA MANAGEMENT

This thesis is based on the results of human studies, which were conducted in accordance with the principles of the Declaration of Helsinki. The medical and ethical review board Committee on Research Involving Human Subjects Region Arnhem Nijmegen, Nijmegen, The Netherlands has given approval to conduct these studies. In addition, the collaborative studies (chapter 2 and chapter 5) published in this thesis were also approved by the institutional review boards and local committees on research involving human subjects at the ErasmusMC (Rotterdam, the Netherlands) and the Antoni van Leeuwenhoek Hospital (Amsterdam, The Netherlands).

In all studies we made use of the WGS data from samples that were collected as part of the CPCT-02 study and in chapter 6 we made use of samples that were collected as part of the ROBUST biobank.

Research data were initially collected on paper case report forms or directly entered in CastorEDC. For chapter 2 we entered all clinical data in ALEA Clinical. All paper data were also entered in CastorEDC or ALEA Clinical. The privacy of the participants is warranted by use of encrypted and unique individual subject codes. The code was stored separately from the study data.

The data were managed and monitored within CastorEDC or ALEA Clinical and the database was locked after ending of the study.

Data were converged from CastorEDC or ALEA Clinical to SPSS for data analysis and manipulation. An audit trail which tracks every manipulation is included in SPSS.

The patients samples and data, including the written informed consents, are stored at the Medical Oncology apartment archive at the Radboudumc or archived on the site, depending on the site of participant inclusion. Digital data is stored on the servers of CastorEDC and ALEA Clinical and on the Medical Oncology department server of the Radboudumc.

The data analyzed can only be used for future research after renewed permission by the patient as recorded in the informed consent. The datasets analyzed in this thesis are available from the corresponding author on reasonable request.

PHD PORTFOLIO OF MINKE SMITS

Department: Urology and Medical Oncology

PhD period: 01/01/2017 – 01/06/2023

PhD Supervisor(s): Prof. Dr. J.A. Schalken, Prof. Dr. W.R. Gerritsen

PhD Co-supervisor(s): Dr. N. Mehra, Dr. J.P.M. Sedelaar

Training activities	ECTS
Courses	
Introduction day Radboudumc 2017	0.5
Graduate school specific introductory course (RIMLS) 2017	0.8
BROK course 2017	1.5
Opfriscursus statistiek 2017	2.0
FACS course 2017	0.8
Scientific Integrity course 2018	1.0
Scientific writing 2018	2.0
Within sight of my PhD course 2018	0.8
Presentation skills course 2019	1.5
Seminars	
Radboud Frontiers 2017	1.0
Radboud Frontiers 2018	1.0
PhD retreat + poster 2018	0.5 + 0.25
PhD retreat + poster 2019	0.5 + 0.25
DUOS jaarsymposium 2018	0.25
Prostate cancer academy 2017	0.25
Prostate cancer academy + presentation 2018	0.25 + 0.25
ESMO preceptorship Immuno-oncology 2018	0.5
Radboudumc Lecture Dr. K. Fizazi + presentation 2018	0.1+0.25
Radboudumc Lecture Dr. G. Attard 2018	0.1
Conferences	
Nederlandse internistendagen 2017	0.5
ASCO GU + poster 2018	0.75 + 0.5
Tour d'Europe 2018	0.5
Other	
RIMLS committee member (2017-2019)	0.5+0.5+0.25
Organizing Meet-the-Expert (2017-2019)	0.5+0.5+0.25
Co-organizing 2 day PhD retreat 2018	2.0
CPCT meetings 2018-2019	0.4 + 0.4
Weekly MDO tumorboard 2017-2019	3.0+3.0+3.0
Weekly MDO mCRPC 2017-2019	4.0+4.0+4.0
Teaching activities	
Lecturing	
Journal club fellows medical oncology 2018	1.0
Supervision of internships / other	
Supervision of medical student during his research internship 2019	1.0
Weekly supervision of medical students in a research team (biopsy team) 2018-2019	1.5+1.5
Total	49.9

CURRICULUM VITAE

Minke Smits werd op 10 mei 1988 geboren te Arnhem. In 2006 voltooide zij het atheneum op het Arentheem college, locatie Thomas à Kempis en begon zij datzelfde jaar met de studie geneeskunde aan de Radboud Universiteit te Nijmegen. Zowel haar senior coschap als haar onderzoeksstage deed zij op de afdeling medische oncologie in het Radboudumc.

Na het behalen van haar artsentitel in 2013, startte zij direct met de opleiding tot internist in het Tweesteden Ziekenhuis te Tilburg (opleider dr. Thomas Wierema), waarna zij deze vanaf 2016 vervolgde in Radboudumc te Nijmegen (opleider prof. dr. J. van der Graaf en nadien Dr. G.M.M. Vervoort).

Vanaf 1 januari 2017 heeft Minke haar opleiding onderbroken voor een promotietraject bij de afdeling urologie en medische oncologie, onder leiding van (co)promotoren prof. dr. J.A. Schalken, prof. dr. W.R. Gerritsen, dr. N Mehra en dr. J.P.M. Sedelaar.

Tijdens haar promotieonderzoek includeerde zij patiënten voor nationale en internationale studies, verrichtte zij poliklinische zorg voor de prostaatkanker patiënten, die zowel regulier als in studies werden behandeld en stuurde zij het biopten team van de research medische oncologie aan voor het waarborgen van de logistiek van het afnemen van biopten.

In 2018 ontving zij een Conquer Cancer Foundation Merit Award tijdens de ASCO GU in San Francisco, Verenigde Staten voor werk dat in dit proefschrift is beschreven.

In augustus 2020 hervatte zij de opleiding en startte zij met de specialisatie tot internist-oncoloog, welke eind november 2023 zal worden afgerond.

NEDERLANDSE SAMENVATTING

Op dit moment is wereldwijd prostaatkanker nummer vier van meest voorkomende vormen van kanker en ondanks dat het grootste deel van de mannen die hiermee gediagnosticeerd wordt geneest, is er nog steeds een gedeelte die helaas komt te overlijden aan uitgezaaide prostaatkanker.

Bij uitgezaaide prostaatkanker is er op dit moment met de bestaande behandelingen geen mogelijkheid tot genezing en is het doel van de behandeling het optimaliseren van de kwaliteit van leven en het verlengen van de duur van het leven.

Androgeen is een hormoon die door binding aan een receptor (androgeen receptor, AR) op de prostaatkankercel zorgt voor deling van de kankercel, waardoor de kanker groeit. De belangrijkste behandeling ten tijde van de diagnose van uitgezaaide prostaatkanker bestaat dan ook uit het blokkeren van de binding van androgeen aan deze androgeen receptor en noemen we antiandrogeen deprivatie therapie (ADT). Door het blokkeren van AR kan de kankercel niet groeien en zal hij dood gaan. We noemen de ziekte in deze fase hormoongevoelig (HSPC).

Helaas zal de prostaatkanker uiteindelijk resistent worden voor deze ADT en zal de kanker weer toenemen in omvang. We noemen dit castratie-resistent prostaatkanker (CRPC).

Sinds 2004 kennen we chemotherapie, docetaxel, als een vorm van behandeling voor uitgezaaide hormoonongevoelige prostaatkanker (mCRPC) en sinds 2010 zijn een andere soort chemotherapie, cabazitaxel, en twee soorten tweede generatie antiandrogenen therapie, abiraterone en enzalutamide, hieraan toegevoegd. Deze tweede generatie antiandrogenen hebben primair een effect op de aanmaak van androgeen in ons lichaam of een blokkerend effect op de binding van androgeen aan de receptor op de prostaatkankercel. Deze middelen hebben een sterkere werking dan het effect van ADT bij uitgezaaid hormoongevoelig prostaatkanker (mHSPC).

In de afgelopen jaren heeft men onderzocht in hoeverre het toevoegen van chemotherapie of een zogenoemd tweede generatie antiandrogeen aan ADT bij mHSPC een verbetering zou geven van kwaliteit van leven en levensduur. De resultaten van grote internationale studies hebben geleid tot de registratie van zowel docetaxel als tweede generatie antiandrogenen aan ADT bij mHSPC, waarbij in de studies een gemiddelde levensduur van ongeveer vijf jaar werd bereikt.

Er ontbreekt vooralsnog een meer geïndividualiseerde vorm van behandeling voor de prostaatkanker patiënten, zowel met betrekking tot de volgorde van het geven van verschillende behandelopties, als ook de ontwikkeling van therapie specifiek gericht op DNA afwijkingen die zijn ontstaan in de prostaatkankercel.

In de afgelopen jaren zijn enkele grote studies verricht die onderzoek hebben gedaan naar DNA veranderingen door middel van next-generation sequencing (NGS) in de prostaatkankercel om hiermee een beter beeld te kunnen krijgen van het biologisch gedrag van prostaatkanker in verschillende stadia van de ziekte, zowel bij niet uitgezaaide prostaatkanker, bij mHSPC, als bij mCRPC. Daarnaast hebben deze studies inzicht gegeven in voorspelling van zowel respons op therapie als inschatting van de levensduur en heeft het tevens geleid tot de ontwikkeling van inmiddels twee typen doelgerichte therapie; olaparib (PARP remmer) voor mCRPC patiënten die een BRCA1 of BRCA2 gen afwijking blijken te hebben in de prostaatkankercel en een zogenaamde immune checkpoint remmer (immuuntherapie) voor mCRPC patiënten met aanwezigheid van microsatelliet instabiliteit (MSI) in het DNA van de prostaatkankercellen. Deze ontwikkelingen bevestigen het nut van het verrichten van DNA en moleculair onderzoek van prostaatkanker voor iedere patiënt met uitgezaaide prostaatkanker.

Helaas is het verrichten van dit moleculaire onderzoek niet eenvoudig. Het overgrote deel van de patiënten met uitgezaaide prostaatkanker heeft alleen (43%) of vooral (73%) uitzaaiingen in de botten. Het verkrijgen van weefsel voor moleculair onderzoek van een uitzaaiing uit de botten wordt met de huidige conventionele beeldvorming, bestaande uit een CT scan en een botscan, voornamelijk bemoeilijkt door het slecht kunnen onderscheiden van een uitzaaiing met actieve kankercellen en een uitzaaiing die eerder door de effecten van behandeling nu verlittekening laat zien. Het overgrote deel van de prostaatkanker patiënten is daarom onderbelicht in eerder genoemde grote NGS studies wat kan leiden tot een gemis in therapeutische opties voor deze groep en zowel een overschatting als onderschatting van voorspelling van respons op therapie en levensduur. Daarom is het van belang dat het verkrijgen van weefsel van een botuitzaaiing door middel van een biopsie wordt geoptimaliseerd.

In het eerste deel van dit proefschrift hebben we ons gefocust op het onderzoeken van mogelijke factoren die de uitkomst van een biopsie van een botuitzaaiing kunnen beïnvloeden.

Sinds enige jaren is de prostate membrane specific antigen (PSMA) PET/CT scan beschikbaar gekomen als diagnosticum bij prostaatkanker. PSMA komt bij veel patiënten met prostaatkanker tot expressie op de kankercel en kan hiermee als aangrijpingspunt

dienen voor het aantoonbaar maken van kankercellen op beeldvorming. Deze scan kan dus veel beter inzichtelijk maken waar actieve kankercellen aanwezig zijn en wij hebben de hypothese gesteld in **hoofdstuk 2** dat het maken van deze scan voorafgaand aan een biopsie van positieve invloed kan zijn op een succesvol verrichte biopsie van een botuitzaaiing. In dit onderzoek hebben we retrospectief gekeken naar de uitkomst van botbiopten en de correlatie met de mate van PSMA uptake (SUV) op de PSMA-PET/CT scan op de locatie waar de CT geleide biopsie was uitgevoerd. Allereerst hebben wij vastgesteld dat een succesvolle biopsie werd uitgevoerd bij 70% van alle biopten, wat een stuk hoger is dan de in de literatuur beschreven gemiddelde van 40% bij een CT scan. Tevens hebben wij met dit onderzoek vastgesteld dat een hoge SUV een goede voorspeller is van een succesvolle biopsie. Ten slotte heeft dit onderzoek aangetoond dat de hoge mate van aanwezigheid van osteoblasten in een uitzaaiing, op een CT te meten als een lage Hounsfield unit (HU), ook een goede voorspeller is voor het verkrijgen van voldoende kankercellen voor moleculair onderzoek. De beperking van deze studie was de afwezigheid van een vergelijking met andere vormen van beeldvorming voorafgaande aan een biopsie en dus hebben wij in **hoofdstuk 3** een onderzoek beschreven die groepen patiënten vergelijkt die voorafgaand aan de biopsie een PSMA-PET/CT scan, dan wel een CT scan of een MRI scan hebben gehad. Biopten die voorafgegaan waren aan een PSMA-PET/CT scan waren in ruim 72% ook succesvol voor moleculair onderzoek, wat ongeveer 15% hoger was dan voor de biopten die voorafgegaan waren door een CT of MRI in dit onderzoek. Ook in deze studie werd een hoge SUV waarde als belangrijke voorspeller voor een succesvolle biopsie bevonden en ook een lage HU waarde op CT werd als voorspeller bevestigd. In deze studie hebben we tevens kunnen aantonen dat ook een meer homogene botuitzaaiing (lage deviatie) op de CT een voorspeller is voor de uitkomst van een biopsie. Ten slotte hebben we op basis van deze resultaten een model gemaakt op basis van HU en deviatie, waarmee de grootste kans op een succesvolle biopsie voor moleculair onderzoek voorspeld kan worden. Dit model zal in een prospectieve studie onderzocht moeten worden alvorens het in de dagelijkse praktijk geïmplementeerd kan worden.

In het **tweede deel** van dit proefschrift, in **hoofdstuk 4**, hebben we onderzocht in hoeverre het implementeren van een PSMA-PET/CT scan in combinatie met een MRI scan zou kunnen leiden tot een nog betere inschatting van de locatie van een biopsie van een botuitzaaiing. Tevens hebben we onderzocht of vervolgens het verrichten van een cone-beam CT-geleide biopsie de kans op een succesvolle biopsie nog verder zou vergroten. Deze prospectieve pilot studie met tien prostaatkanker patiënten heeft laten zien dat de combinatie van voorafgaand zowel een PSMA-PET/CT scan als een MRI met vervolgens een cone-beam CT geleid biopsie het succes percentage van botbiopten voor moleculair onderzoek heeft vergroot tot 80%. De combinatie van PSMA uptake (SUV) en

een hoge diffusie-restrictie meting op de MRI, zijn indicatief voor de aanwezigheid van veel kankercellen en kan dus leiden tot een nog hogere kans op een succesvolle biopsie voor prostaatkanker patiënten met (vooral) botuitzaaiingen.

Het **derde deel** van dit proefschrift heeft zich gericht op de klinische consequenties van moleculair onderzoek van prostaatkanker.

In **hoofdstuk 5** hebben we 197 mCRPC patiënten geïnccludeerd voor onderzoek naar de uitkomsten van het DNA onderzoek (whole-genome sequencing, WGS) van de bipten die waren verricht in het kader van de Nederlandse Center for Personalized Cancer Treatment (CPCT)-02 studie. Op basis van dit onderzoek hebben we acht subgroepen prostaatkanker patiënten kunnen vaststellen, die specifieke overeenkomende genetische veranderingen hebben. Van drie van de acht groepen weten we inmiddels ook meer over de klinische relevantie hiervan. Eén subgroep bevat patiënten die DNA veranderingen hebben in DNA reparatie genen. Deze genen zorgen normaal gesproken voor reparatie van fouten in DNA die kunnen ontstaan bij de celdeling. Als er een mutatie ontstaat in één van deze genen, kan het voorkomen dat een fout bij de celdeling niet wordt herkend en dus niet wordt gerepareerd. Dit kan vervolgens leiden tot ongeremde celgroei, wat kan leiden tot vorming van kanker. BRCA1 en BRCA2 zijn DNA reparatie genen en behoren onder andere tot deze door ons vastgestelde subgroep. Inmiddels weten we ook dat deze specifieke patiënten een grote kans hebben op respons middels doelgerichte therapie in de vorm van een PARP-remmer, waaronder olaparib. Een andere door ons vastgestelde subgroep bestaat uit patiënten met de aanwezigheid van microsatelliet instabiliteit (MSI) in de kankercel. We weten inmiddels dat het geven van immuuntherapie in deze specifieke groep een grote kans geeft op (langdurig) respons. Ten slotte is een derde subgroep geïdentificeerd met de (gedeeltelijke) afwezigheid van het gen CDK12, welke ook een rol heeft in de reparatie van DNA fouten bij celdeling en op basis van eerste onderzoeken lijken ook deze patiënten met immuuntherapie een grotere kans te hebben op respons.

Deze bevindingen tonen het belang van moleculair onderzoek aan met betrekking tot voorspellen van respons op specifieke therapie. Tevens zullen we in de nabije toekomst onderzoeken wat de predictieve waarde (voorspelling van respons op therapie) en prognostische waarde (voorspelling van levensduur) is van het verdelen van de prostaatkanker patiënten in deze acht verschillende subgroepen.

Inmiddels weten we op basis van klinische studies dat niet alleen patiënten met MSI (langdurig) kunnen responderen op immuuntherapie, maar is er ook een andere kleine subgroep die ook baat lijkt te hebben van deze therapie. Momenteel weten we nog

niet welke specifieke patiënten dit zijn en zijn we op zoek naar biomarkers die kunnen helpen in het identificeren van deze subgroep. In **hoofdstuk 6** hebben we in het bloed onderzoek gedaan van prostaatkanker patiënten met MSI en patiënten zonder MSI die allen immuuntherapie hebben gekregen met wisselend effect hiervan op de groei van de ziekte. We hebben in deze studie kunnen aantonen door middel van DNA onderzoek, dat specifieke T-cellen, een type afweercel, die rondom de kankercellen bij de patiënt aanwezig zijn, ook in het bloed van de patiënt terug te vinden zijn. Hiermee is het dus mogelijk om informatie te verkrijgen van de kankercel van de patiënt door middel van bloedonderzoek. Ten tweede hebben we met dit onderzoek laten zien dat er bij de MSI patiënten meer T cellen aanwezig zijn en daarnaast ook een grotere diversiteit aan soorten T cellen. Dit was significant verschillend ten opzichte van de groep van patiënten zonder MSI. Daarnaast zagen we in de groep patiënten zonder MSI die wel respondeerden op de immuuntherapie ook een positieve trend naar meer diversiteit in T cellen, zoals zichtbaar bij de MSI patiënten. Deze specifieke T cel kenmerken zouden dus kunnen bijdragen in het identificeren van niet MSI prostaatkanker patiënten, die potentieel wel zouden kunnen responderen op immuuntherapie.

In het **vierde deel** van dit proefschrift geven we een samenvatting van de bevindingen van dit proefschrift en bediscussiëren we de implicaties van de uitkomsten van onze onderzoeken. Tevens zullen we ons perspectief geven op wat in de (nabije) toekomst belangrijke ontwikkelingen kunnen en zullen zijn met betrekking tot het verrichten en interpreteren van moleculair onderzoek bij prostaatkanker patiënten met als doel het verbeteren van de zorg voor deze patiëntengroep.

DANKWOORD

Als eerste wil ik mijn dankwoord graag richten aan alle prostaatkanker patiënten die hebben deelgenomen aan de verschillende onderzoeken die zijn beschreven in dit proefschrift. Zonder hun deelname hadden wij niet deze kennis kunnen verkrijgen en zou de ontwikkeling naar een meer geïndividualiseerde vorm van therapie nog minder ver zijn. Ik bewonder de enorme drive die u allen heeft om de kennis over prostaatkanker te vergroten in de hoop hiermee de zorg te kunnen verbeteren. Veel dank hiervoor!

Vervolgens wil ik graag mijn promotieteam bedanken, bestaande uit vier man sterk.

Prof. dr. Schalken, beste Jack. Als AIOS interne kwam ik bij jou op het lab praten over een mogelijk promotietraject. Waar tot die tijd vooral biomedische wetenschappers en urologen in spe onder jou promoveerden, werd het nu tijd voor een AIOS interne geneeskunde. Toegegeven, de eerste gesprekken duizelde het mij van de technische termen en werd ik al enigszins nerveus van het zien van een pipet, maar al snel bleek ik vooral de brug tussen de kliniek en het lab te kunnen gaan slaan en voelde ik mij tussen de patiëntenzorg en de logistiek naar het lab als een vis in het water. Dank voor het overdragen van al jouw kennis, het bediscussiëren van nieuwe hypotheses, jouw soms ook hele nuchtere kijk op de dingen en tussendoor het bekijken van de foto's van jouw (inmiddels al niet meer zo) nieuwe auto.

Prof. dr. Gerritsen, beste Winald. En toen ging ik promotieonderzoek doen bij de internist-oncoloog die internationaal bekend was om alle mooie onderzoeksresultaten op het gebied van prostaatkanker en immunologie. Twee dingen waar het aan mijn kennis toch nog wel enigszins ontbrak. Gelukkig nam je me snel mee in de wereld van prostaatkanker en met alle nieuwe ideeën en hypotheses kwam er al snel genoeg materiaal voor een proefschrift. Dank voor de tijd die je nam om mijn kennis bij te spijkeren. Ook na jouw pensioen bleef je betrokken waarvoor extra dank.

Dr. Sedelaar, beste Michiel. Jouw relativerende vermogen bracht veel rust als ik onrustig werd van de dingen die niet lukten of ik simpelweg even het overzicht kwijt was. Met een kop koffie en een half uur samen kletsen kon ik vervolgens daadwerkelijk weer met een frisse blik verder. Jouw persoonlijke betrokkenheid, zoals een kraambezoekje in het CWZ, kan ik enorm waarderen en ook nu nog ben je geïnteresseerd hoe ook dingen buiten onderzoek gaan. Enorm veel dank daarvoor.

Dr Mehra, beste Niven. Van drie jaar lang dagelijkse begeleider tot met de collega's een biertje drinken in de kroeg tot vrijwel gelijktijdig ouder worden. Het waren drie hele

leuke, intense en leerzame jaren. Je hebt me enorm veel geleerd zowel over het doen van onderzoek als over de zorg van de prostaatkanker patiënten. Je hebt me geholpen tijdens de gebruikelijke hobbels tijdens een promotietraject en jouw enorme wetenschappelijke drive is aanstekelijk. Heel veel dank voor al die wijze lessen en ik hoop dat er nog vele zullen komen.

Vervolgens wil ik graag mijn paranimfen danken dat zij beiden naast mij willen staan tijdens mijn verdediging van dit proefschrift. Anouk en Sarah, jullie zijn fantastische collega's die zowel voor de patiënt als voor de directe collega oog hebben. Ik bewonder jullie 'alles kunnen' wat zonder enige moeite lijkt te gaan. Jullie zijn er voor mij en de collega fellows oncologie bij de leuke en soms ook minder leuke momenten en juist bij het werk wat wij doen is dat extra belangrijk. Ik hoop dat we nog lang zulke fijne collega's mogen blijven.

Een promotietraject doe je niet zonder de collega onderzoekers. De momenten van even koffie drinken, sparren over welke kant je discussie nu op moet en samen gezellig naar een congres gaan, zijn onmisbaar. Vicky, Martine, Sarah, Eline en Wim, dank voor de gezellig tijd zowel tijdens onze onderzoekers tijd als tijdens de opleiding tot internist-oncoloog nadien. Jullie zijn geweldige collega's en ik bewonder jullie enorm om jullie doorzettingsvermogen en ambities. Maarten, als toch beetje buitenbeentje tussen al die A(N)IOS interne heb jij je staande gehouden en je inmiddels ontwikkeld tot wat mij betreft een internist-uroloog. Jij was mijn onderzoekers maatje op het gebied van prostaatkanker, wat ik als een hele leuke en goede samenwerking heb ervaren. Dank voor alle hulp en de gezelligheid. Harm, dank voor alle hulp met de MSI patiënten, jouw kennis over deze groep patiënten heeft bijgedragen aan dit proefschrift. Iris, jij bent na mij aan de slag gegaan met het verbeteren van zorg voor de prostaatkanker patiënt. Je bent al een heel eind en zult straks een prachtig boekje gaan neerzetten. Heel veel succes met de afronding hiervan.

Ten slotte natuurlijk ook dank aan alle andere collega onderzoekers!

Ik wil graag de urologen en internist-oncologen bedanken voor de hulp met inclusie van patiënten in de studies, ook jullie bijdrage heeft gezorgd voor het kunnen verrichten van de onderzoeken beschreven in dit proefschrift. Dr. van Oort, Inge. Jij bent dan wel geen onderdeel van mijn promotieteam, je hebt echter wel enorm bijgedragen aan het tot stand komen van dit proefschrift. Heel veel dank daarvoor.

Speciaal dank aan Dr. Desar, Ingrid, Dr. Timmer-Bonte, Anja, en Prof. dr. van Herpen, Carla, voor de hulp die ik van jullie heb gekregen tijdens mijn opleiding tot internist-oncoloog voor het afronden van dit proefschrift.

Tevens wil ik graag alle medewerkers van de polikliniek medische oncologie, urologie en het de verpleegafdeling medische oncologie bedanken voor hun hulp bij alle bloedafnames, het geven van de verschillende behandelingen en het bieden van een luisterend oor aan de patiënten.

De organisatie van het aanvragen van een biopsie tot aan het op de juiste manier verwerken van het verkregen materiaal was niet mogelijk zonder de hulp van de vele studenten die hierbij hebben geholpen. Daarnaast hebben jullie ook andere taken op jullie genomen zoals het bijhouden van de database en het meehelpen in het beoordelen van scan uitslagen. Jullie waren van alle markten thuis, een prettige aanspreekpunt voor de patiënt en jullie enorme enthousiasme was zeer aanstekelijk. Kortom, een perfect team om mee samen te werken en een belofte voor de (voornamelijk dokters-) toekomst. Nogmaals veel dank!

Dank tevens aan de collega's van het researchteam medische oncologie. Jullie begeleiding van de studenten was perfect en bij jullie kon ik terecht met mijn vragen over de verschillende studies.

De afdeling radiologie en nucleaire geneeskunde heeft een grote rol gehad in de uitvoering en analyses van verschillende onderzoeken die in dit proefschrift zijn beschreven. De logistiek was af en toe uitdagend dus veel dank voor de organisatie hiervan. Graag wil ik Prof. dr. Fütterer, Jurgen, en Prof. dr. Nagarajah, James, danken voor hun hulp bij het uitvoeren van de MITEC studie en hun hulp bij de analyses van de resultaten in de andere beeldgeleide bipten studies.

Dank aan alle medewerkers op het urologisch laboratorium en in het bijzonder Marion en Elze, jullie hielpen met het verwerken van alle bloedsamples en als ik weer eens iets wilde komen verzamelen voor een onderzoek zorgden jullie dat het al helemaal klaar stond. Daarnaast een speciaal dank aan Tilly. Jij probeerde mij wat bij te brengen over het maken van organoïds en nam mij mee in lab technische termen die soms als een razende voorbij kwamen tijdens onze research besprekingen.

Tevens wil ik de collega onderzoekers op het tumor immunologisch lab hartelijk danken voor de hulp bij analyses die in dit proefschrift vermeldt staan.

Ik wil alle coauteurs hartelijk danken voor hun bijdrage aan dit proefschrift. Een speciaal dank aan Thomas, Anouk, Kamer en Donjete met wie ik als gedeeld eerste auteur deze mooie artikelen heb kunnen maken.

Aan alle lieve vrienden en vriendinnen; enorm dank voor alle leuke vriendenweekenden, etentjes, festivals en andere uitjes. Samen is het altijd gezellig. Deze afleiding heeft enorm geholpen in tijden van de bij het promotietraject behorende frustraties als het even niet lukte, om daarna weer met frisse moed verder te gaan. Boy, hierbij nog een speciale dank aan jou voor de introductie aan Jack.

Lieve Hans en Wilma, Jasper en Eline. Ik had mij geen betere schoonfamilie kunnen wensen. Jullie staan altijd voor ons klaar, zijn geïnteresseerd in wat ons bezig houdt en bovenal zijn onze meiden dol op jullie liefde en gekkigheid.

Lieve Ilja en Jora, met drie meiden in huis was er geen moment stilte. Ik denk met veel plezier terug aan onze jeugd samen en bewonder jullie keuzes en ambities. Ondanks of juist doordat we alle drie een andere kant op gingen, blijft het nooit stil als we 'thuis' zijn.

Lieve Tim en Thijs, jullie zijn een mooie aanvulling op ons gezin. Lieve Lize, jij bent een geweldig nichtje en liefste speelmaatje van Anna en Julia.

Lieve paps en mams, jullie hebben mij altijd gestimuleerd 'je best te doen, meer dan je best is niet mogelijk'. Jullie liefde en interesse is groot en zorgen ervoor dat thuis stiekem soms nog gewoon thuis is. Jullie helpen ons bij vele dingen, van het oppassen op onze meiden (met de grootste verwennerij) tot het bouwen van kasten en het maken van jurkjes. Heel veel dank!

Lieve, lieve Anna en Julia. Met twee tegelijk zijn jullie het meest uitdagende maar vooral het meest geweldige wat mij is overkomen. Samen ontdekken jullie de wereld en nemen jullie mij mee in jullie heerlijke fantasie. Jullie onvoorwaardelijke liefde en plezier in de kleine dingen relateert enorm en doet des te meer beseffen wat belangrijk is in het leven.

Niek, mijn allerliefste. Jij haalt het beste in mij naar boven en stimuleert mij voor het hoogst haalbare te gaan zonder mijzelf uit het oog te verliezen. Hoe tegenstrijdig onze karakters op vele vlakken ook zijn, juist deze tegenstrijdigheden maken ons de perfecte match. Jij hebt mij het allermooiste gegeven wat mogelijk was, namelijk onze twee prachtige dochters. Ik hoop dat wij ooit samen oud en grijs op een bankje terug mogen kijken op wat nu al een fantastisch rijk leven samen is.

